System Engineering Study of Electrodynamic Tether as a Spaceborne Generator and Radiator of Electromagnetic Waves in the ULF/ELF Frequency Band

NASA Grant NAG8-551

Final Report

For the period 1 September 1985 through 30 November 1986

Principal Investigator

Dr. Robert D. Estes

February 1987

Prepared for
National Aeronautics and Space Administration
Marshall Space Flight Center, Alabama 35812

Smithsonian Institution
Astrophysical Observatory
Cambridge, Massachusetts 02138

The Smithsonian Astrophysical Observatory
is a member of the
Harvard-Smithsonian Center for Astrophysics

The NASA Technical Officer for this Grant is
Dr. Georg F. von Tieshenausen, Code PS01 and
Mr. Chris Rupp, Code PS04, Advanced Systems
Office, Marshall Space Flight Center, Alabama 35812

System Engineering Study of Electrodynamic Tether as a Spaceborne Generator and Radiator of Electromagnetic Waves in the ULF/ELF Frequency Band

NASA Grant NAG8-551

Final Report

For the period 1 September 1985 through 30 November 1986

Principal Investigator

Dr. Robert D. Estes

Co-Investigators

Dr. Mario D. Grossi
Dr. Enrico C. Lorenzini

February 1987

Prepared for

National Aeronautics and Space Administration
Marshall Space Flight Center, Alabama 35812

Smithsonian Institution
Astrophysical Observatory
Cambridge, Massachusetts 02138

CONTENTS

CONTENTS (Cont.)

Acknowledgements

This report has been written by Dr. Robert D. Estes, PI, and by Dr. Mario D. Grossi, Co-I, with inputs from the various members of the project team.

Summary

An electrodynamic tether deployed from a satellite in low-earth orbit can perform, if properly instrumented, as a partially self-powered generator of electromagnetic waves in the ULF/ELF band, potentially at power levels high enough to be of practical use.

Electrodynamic drag compensation is accomplished along with signal generation by operating the system alternately in two different modes. In the first phase of the cycle the motion-induced electromotive force $(\vec{v} \times \vec{B} \cdot \vec{\ell})$ drives the tether current. In this, the "natural" mode, electrodynamic drag acts on the system. An on-board electrical power source then provides the voltage necessary to drive the tether current in the opposite sense, utilizing the electrodynamic thrust to compensate for the drag of the first phase.

Alfvén wing currents of alternating polarity would be excited in the ionosphere at the tether end and would carry electromagnetic energy along the geomagnetic field lines. Information could potentially be transmitted by varying the relative duration of the "natural" and thruster phases, or with other suitable approaches.

On-board power requirements can be minimized by lowering tether length and electrical resistance. However, both dynamic stability and wave generation efficiency concerns place limits on how short the tether can be made. If there is more than enough power available to generate sufficiently intense electromagnetic waves in the "natural" phase, then the extra energy can be stored in batteries and utilized to help drive the current in the reversed, or thruster, phase.

The on-board power source must make up for the ohmic losses in the tether, the power into the waves, and the losses in the tether power transfer process. A 25 m^2 solar array should suffice to keep a 5 km tether ULF radiator system operating for many months with a 10 ampere tether current and ULF wave power levels of tens of watts.

The report is divided in two main parts. A first part illustrates the project's theoretical developments and includes a physical explanation of the tether's e.m. wave generation by the Alfvén Wings mechanism, with important practical consequences. It is shown that the wave impedance for an electrodynamic tether terminated with electrodes at each end does not limit drastically the intensity of the current that can flow in it at ULF/ELF, as other authors had claimed.

Having cleared the ground from this fundamental objection that had put in doubt the very feasibility of a tether system as generator of DC power and as radiator of ULF/ELF waves, we could proceed to perform the system study. This is the second part of the report. We show that a vertical tether as long as 100 km and with a current as large as 30 A performs rather marginally as a spaceborne transmitter at ULF/ELF in a link of operational use. Its applicability depends on noise abatement techniques that are still under development at this time. On the contrary, we found exceptionally promising the use, as spaceborne antennas, of two-dimensional tethered structures. These can perform as magnetic dipoles with very large moments. The system study includes an initial definition of a system configuration, with an estimate of size and mass of the various subsystems and components.

1.0 INTRODUCTION

This is a systems study of an orbiting electrodynamic tethered satellite system for ULF/ELF* wave transmission. Since the technology involved is advanced and of necessity largely untested, while the application is specific, the study has a certain hybrid quality. It should be noted, however, that the technology and feasibility of environmentally acceptable ground-based ELF communications transmitters are not well-established either. In any case the present study has had to deal with fundamental issues more than would be the case for the usual study based on an extrapolation of established results and technology to new domains of applicability.

The most predictable conclusion of this study is that an actual test should be made in space of a system like the one studied here. There is absolutely no substitute for this. In the meantime, however, studies like the present one are valuable in guiding the design of prototype systems and in building a case for carrying out such experiments. The physics underlying the operation of the system has to be made manifest if the argument to build an expensive (as all space systems are) experimental system is to be convincing, given that the concepts are novel and often meet with initial scepticism. We have tried to accomplish this throughout our report, although the physical models we have used do not take into account all factors. The interactions between the tethered system and the ionosphere are far too complicated, and the theoretical understanding -- in the absence of any experimental results -- too limited for us to be able to give definitive answers to all the questions of feasibility relevant to the system studied.

*According to ITU Radio Regulations (July 1965), the ELF band extends from 300 Hz down to 30 Hz; informally, the ULF band extends from 30 Hz down to 3 Hz, although communication practitioners call "ULF" also the frequencies below 3 Hz, without establishing a precise lower boundary for the band.

We have focussed our attention on two basic problems. The first is that of the level of wave power that the system can be expected to generate in the ULF/ELF radiation band. It is the peculiar nature of the electrodynamic tethered satellite system that its very functioning depends on its ability to exchange electrical charge with the plasma medium in which it moves, and that this ability is in part governed by the ionospheric plasma's ability to carry charge away from the system by means of electromagnetic plasma waves. Since the system under study is specifically designed to generate electromagnetic waves, understanding the mechanism by which this is accomplished has to be one of the primary goals of the study. Obtaining a satisfactory answer to this problem became especially urgent during the course of the study when two separate papers on the subject were published, each of them calling into question (from different standpoints) the ability of an electrodynamic tethered satellite system to generate substantial radiation in the ULF/ELF band. After a careful analysis of the problem we have concluded that one of these studies is incorrect and that the results of the other study do not apply to a real tethered system, but to an unrealistic orbiting wire. This is not to say that we have been able to demonstrate exhaustively that waves would be transmitted at easily detectable levels to the Earth's surface. What we have shown is that previous estimates of the wave impedance for ULF/ELF waves from a tethered system, i.e., on the order of an ohm or a few ohms, are reasonable, and that the radiation resistance of other frequency bands should not be a limiting factor in the tether current attainable. Since these propositions had been called into question we feel that it was necessary to justify them in some detail.

The second major question that our study attempts to answer is whether an electrodynamic tethered satellite system for transmitting waves can be made

partially self-powering so that power requirements for drag compensation can be met within economical constraints of mass, cost, and complexity.

The study began with a candidate system, one that we refer to as the "self-driven" system, because it stores part of the electrical energy generated by the tether motion in the natural current phase and then utilizes that energy to help drive the current in the reversed, electrodynamic thrust, phase of operation.

Section 2 presents the theoretical developments worked out by our project. It shows that the wave impedance for the electrodynamic tethered satellite system will not be a major limiting factor to the current that flows in the system, as some authors had indicated it would. The results of Section 2 leave open the possibility of tethered systems applications such as electrical power generation, electrodynamic drag compensation (by the thrust that comes when a power source is used to drive the current in the direction opposite to that induced by the system's motion), and ULF/ELF wave generation at power levels that are adequate for useful applications.

Specific topics covered in Section 2 are the theory of the Alfvén waves generated and radiated by the electrodynamic tether, the derivation of the basic equations and the source current distribution, the calculation of the "Alfvén Wing" current, and the Alfvén wave impedance.

Section 3 reports on our system application study, that concentrated on the investigation of the potential use of the electrodynamic tether in strategic communications at ULF/ELF. We found that a vertical tether, even with 100 km length and a current of 31.8 Amp, is rather marginal in terms of its ability to provide a large Signal-to-Noise Ration (SNR) at ULF/ELF over an area of sufficient extension, unless noise abatement is adopted, following recent findings by

other groups that show the potential of applicable least-squares linear predictors.

What we found, on the contrary, to be exceptionally promising, was the use, as magnetic dipoles, of spaceborne two-dimensional structures made with tethers, and stabilized by electrodynamic forces. There is here a reserve of SNR that can be used in a variety of ways, such as to simplify the system, to extend its coverage to larger areas, to increase the data rate, etc.

Specific topics covered in Section 3 are basic design criteria, the drag-compensation method (that is perhaps the highlight of our study), the effects on the propagation paths from orbit to Earth surface of high-altitude nuclear debris patches (these had been considered to be potential show stoppers, but our study did show that it is not so), the illustration of a proposed system configuration, inclusive of discussion of the possible modulation schemes, the working out of a system block diagram and of a mechanization of the tethered satellite, the first-cut breakdown of the major subsystems, and the estimate of masses and sizes involved.

To conclude, Section 4 contains an outline of recommended analytical work, to be performed as a follow-on to the present study, aimed at further strengthening the theoretical understanding of the e.m. wave phenomena associated with the electrodynamic tether, and at the better definition of the hardware instrumentation to be used in the spaceborne system.

2.0 THEORETICAL DEVELOPMENTS*

2.1 Alfvén Waves From The Electrodynamic Tether -- Introductory Remarks

Within the next few years, the first full-scale deployment of a tethered satellite from the U.S. Space Shuttle will take place. The 20 km cable connecting the Shuttle to the vertically deployed subsatellite will be a dielectric-coated copper wire, permitting a $\vec{v} \times \vec{B}$ induced electric current to flow through the tether, the terminating orbiter and subsatellite, and the ionosphere.

Anticipation of this initial flight and of future applications of electrodynamic tethered satellite systems has been the main stimulus to recent interest in the problem of electromagnetic wave generation by a large, electrically conducting body moving through a magnetized plasma. All of the recent research on this topic [Rasmussen et al., 1985; Dobrowolny and Veltri, 1986; Barnett and Olbert, 1986] has its roots in the 1965 publication of Drell et al. in which the phenomenon of the "Alfvén wings" was first described.

All of the authors cited above calculate the wave impedance associated with motion-induced Alfvén waves. As Table 2-1 illustrates, the results are not mutually consistent. Part of this apparent inconsistency, as demonstrated in the present work, turns out to be due to the authors' having considered different limiting cases (explicitly or implicitly). None of the previous analyses really take into account the peculiar "dumbbell" shape of the tethered satellite system. The present analysis is a step toward a more realistic model of the tethered system current distribution and the ionospheric waves and currents associated with it. There is no restriction to system dimensions much larger than the satellite velocity

*Contributed by R.D. Estes

divided by the ion cyclotron frequency. Alfvén wing currents along the magnetic field lines are explicitly calculated and are seen to extend well beyond the system's dimensions along the line of flight for the case where these dimensions are not larger than the system's velocity divided by the ion cyclotron frequency.

The basic principles of the electrodynamic tether are as follows. A long, electrically conducting cable, insulated from the ionosphere along its length, stretches along the vertical to connect two terminating masses, thus forming a single orbiting system. By virtue of its motion through the geomagnetic field, the system experiences an induced emf between the tether ends, whose value is (in Gaussian units) $(\vec{v} \times \vec{B}) \cdot \vec{L}/c$, where $\vec{v}$ is the system's velocity, $\vec{B}$ the geomagnetic field vector, and $\vec{L}$ the vector along the vertical with magnitude L, the tether length. (For simplicity we are approximating the system's motion as uniform linear motion with velocity $\vec{v}$ through a uniform field $\vec{B}$.) The tether is in electrical contact with the system's terminating masses, which have conducting surfaces exposed to the ambient plasma.

The motion-induced emf produces a current flow in the tether. Since the terminal masses can exchange charge with the ambient plasma, the current is not merely a short-lived flow to redistribute charge within the system; it continues to flow indefinitely, as charge is transferred from one vertical layer of the ionosphere to another by means of the conducting tether. The ability of the terminal masses to exchange charge with the ionospheric plasma is an obvious limiting factor in the system's ability to draw current. If current collection is insufficient, most of the motion-induced emf will go into charging the terminal masses to large potentials.

In order to increase the current-collecting capability of the terminals, it has been proposed to utilize hollow cathode devices, which emit a neutral plasma cloud that is supposed to expand into the ionosphere, increasing the effective charge-exchanging surface of the system and dramatically lowering the impedance of the interface between the system and the ionosphere.

The analysis presented here is not concerned with the details of the charge-exchange mechanism between the system and the ionosphere. The system/ionosphere interface is viewed in a highly idealized way, but one that hopefully keeps the essential features necessary to study electromagnetic wave generation. It is assumed that charge-exchange is in a steady state, i.e. that no effects that cause a time variation in the tether current are present.

As noted by Drell et al., a system such as the one described above can be likened to a moving generator that sequentially delivers a voltage pulse to a series of geomagnetic field line pairs which function as transmission lines to carry away current pulses of opposite polarity at the upper and lower ends of the tether. The net charge left in a region of the plasma due to current flow from the plasma into the tethered system travels away from the system along the geomagnetic field lines as an Alfvén wave packet. These regions of flowing net charge are called the Alfvén wings, since they extend out from the ends of the tether like the (slightly swept back) wings of a biplane. This is the simplified picture. The picture that emerges from the present analysis is somewhat more complicated.

The purpose of the analysis reported here is to study the Alfvén wings and the wave impedance associated with them for the case of a tethered satellite system, hopefully resolving discrepancies between previous analyses and obtaining

results useful to the planning of future experiments. Since the functioning of an electrodynamic tethered system depends on the ionospheric plasma's ability to carry away charge — to "complete the circuit," in the somewhat misleading phrase — and, since this is done through current carrying electromagnetic waves, the subject is of more than academic interest.

2.2 Basic Equations And The Source Current Distribution

Faraday's and Ampere's laws can be combined in the usual way to obtain the general expression for the Fourier transform of the electric field vector $\vec{E}_k$:

$$-k^2\vec{E}_k + \vec{k}\,(\vec{k}\cdot\vec{E}_k) = -\frac{\omega^2}{c^2}\,\vec{D}_k - \frac{4\pi i\omega}{c^2}\,\vec{j}_k \qquad (1)$$

where the plasma is treated as a linear dielectric medium, and

$$\vec{D}_k = \epsilon(\omega)\cdot\vec{E}_k \qquad (2)$$

with $\epsilon(\omega)$ the plasma dielectric tensor.

The current $\vec{j}_k$ is the "external" current, as distinguished from the plasma current $\vec{J}$, which is determined self-consistently with the electromagnetic field and given by

$$\vec{J}_k = \frac{-i\omega}{4\pi}\,(\vec{D}_k - \vec{E}_k) \qquad (3)$$

The basic approach here is the same as that taken in previous work on the problem. We take the external (or source) current to be the current flowing in the tethered system. The tethered system current distribution is specified, based on physical reasoning, with the total current in the tether being an undetermined multiplicative constant. Equation (1), with the appropriate dielectric tensor ϵ, is then used to obtain the plasma fields and currents in terms of an arbitrary total tether current. After the ionospheric impedance has been calculated utilizing the obtained electromagnetic field, the tether current can then be determined self-consistently for given tether and tether/plasma interface impedances.

It should be noted that there is a subtle and perhaps unjustified assumption hidden in the procedure outlined above. It assumes that a steady state with constant tether current has been achieved in the distant past. A real tethered system will have to be "turned on" at some time. Since the tethered system current depends upon the plasma response, there is no *a priori* guarantee a constant tether current would ever be achieved, even excluding nonlinear effects. The determination of the tether current should ideally be made as part of a self-consistent analysis of the tether/plasma system as a whole. This, however, will be an extremely complicated analysis, which is why everyone so far has approached the problem in more or less the same way as the present analysis.

The present analysis differs from previous work first of all in its choice of the tethered system current distribution. None of the recent studies have attempted to model the problem with a current distribution that takes into account the system's dumbbell shape, i.e. a thin tether connecting satellites with dimensions much greater than the tether's diameter. They have all considered vertically aligned cylindrical structures. Either one extreme — an orbiting wire — or the other — an orbiting cylinder with dimension in the direction of flight measuring

tens of meters — has been considered. And these models do not allow for asymmetry between the upper and lower terminations of the system, such as will exist in the case of the TSS-1 mission, where a subsatellite with a radius of 1 meter will be deployed from the much larger Space Shuttle.

In their model of a tethered system, Barnett and Olbert consider an orbiting wire (a long narrow cylinder with circular cross-section), whose areas of contact with the ionospheric plasma are just the terminating cross-sections of the wire. They obtain an extremely high radiation impedance (10,000 Ω) for a band of frequencies between the lower hybrid and electron cyclotron frequencies.

Such high wave impedances would imply low current values even for long, high-voltage tethers and would require a re-evaluation of many proposed electrodynamic tether applications. Of course, such an orbiting wire would also be severely restricted in its ability to exchange charge with the ionosphere by the very small area of contact.

A real tethered satellite system would be quite different, however. The ends of the tether will be connected to metallic satellites with dimensions far greater than the tether's diameter. Plasma clouds emitted from hollow-cathode devices might extend the effective dimensions at the ends of the tethered system many meters into the ionosphere.

The present analysis demonstrates that the critical dimension is that of the system's electrical contact with the ionosphere along the direction of motion across the geomagnetic field lines.

Rasmussen et al., approached the problem of modeling the tethered system somewhat differently. In their model, the tethered system is like a long cylinder

whose cross section is elongated along the direction of motion to reach tens or hundreds of meters. While this is clearly not a realistic model of the actual tether current distribution, it should in principle give the same results for the Alfvén wing currents and radiation as a thin tether terminated by an equivalent source of external charge to the ionospheric plasma, at least for the case of a constant d.c. current flowing through the tether. For an oscillating tether current, the current distribution in the tether would become more important.

The Rasmussen model also assumes the system is identical at the two ends. The model used in the present analysis allows for possible top/bottom asymmetry in the system dimensions. Even in the symmetric case, however, our results differ from those of Rasmussen et al.

The period of time it takes for the charge-exchanging surfaces of the system to pass by a geomagnetic field line determines the frequencies associated with the disturbance; so the critical dimension is the one along the direction of motion. For simplicity (and following the practice of most previous analyses) we are assuming the motion is perpendicular to the magnetic field.

We idealize our system to be a vertical line current (representing the tether) terminated at each end by line currents projecting backward and forward along the line of motion and linearly falling off to zero at the limits of the system ($x = \pm L_x/2$). Extension of the terminating part of the system beyond the tether's dimensions necessarily implies an x-component to the system current. The choice of j_x used here means that the tethered system injects "external charge" uniformly along its x-dimensions at each end of the tether (with opposite signs at the two ends). The model illustrated in Figure 2.1, where the x, y, and z axes are defined. The motion is assumed to be eastward, so that the current flows up the tether.

The mathematical expressions for the components of $\vec{j}$ are as follows:

$$j_z\ (\vec{x},t)\ =\ \frac{I\delta(z)}{L_x}\ \left[\delta(y+L/2)-\delta(y-L/2\right]\bullet \tag{4a}$$

$$\left\{(x'+L_z/2)\left[H(x'+L_z/2)-\overline{H}(x')\right]+(x'-L_z/2)\left[H(x')-H(x'-L_z/2)\right]\right\}$$

$$j_y\ (\vec{x},t)\ =\ I\ \delta(z)\ \left[H(y+L/2)-H(y-L/2)\right]\ \delta(x'), \tag{4b}$$

where $x'\ =\ x\ -\ v_x t$, and

$$H\ (x)\ =\ \left\{\begin{matrix}1,\ x\ \geq\ 0\\0,\ x\ <\ 0\end{matrix}\right\}$$

$$\overline{H}\ (x)\ =\ \left\{\begin{matrix}1,\ x\ >\ 0\\0,\ x\ \leq\ 0\end{matrix}\right\}$$

This distribution has top/bottom ($y = L/2,\ y = -L/2$) symmetry in the L_x dimension, but the generalization to two different values of L_x is obvious.

From now on we suppress the k subscript used to indicate Fourier transformed quantities. Any quantity in an expression involving $\vec{k}$ and ω can be assumed to be a Fourier transform. The Fourier transformed current components of $\vec{j}$ are given by

$$j_x\ =\ \frac{I}{\pi}\ \delta(\omega-k_x v_x)\sin\left(\frac{k_y L}{2}\right)\ \left[\frac{2\sin(k_x L_x/2)}{k_x^2 L_x}-\frac{1}{k_x}\right] \tag{5a}$$

$$j_y = \frac{I}{\pi}\,\delta(\omega - k_z v_z)\frac{\sin(k_y L/2)}{k_y} \qquad (5b)$$

We later have need for

$$\vec{k}\cdot\vec{j} = \frac{2I}{\pi}\,\delta(\omega - k_z v_z)\,\sin\left(\frac{k_y L}{2}\right)\frac{\sin\,(k_z L_z/2)}{k_z L_z} \qquad (6)$$

since it determines all of the electromagnetic wave quantities. Expression (6) is exactly what an orbiting ribbon (all current in the y-direction) of width L_z and length L would give, a consequence of the fact that the tether current divergence is the same in the two cases, since the region in which they exchange charge with the plasma and the rate at which they do it is the same. It will be seen that the wave fields and plasma currents associated with these two current distributions are identical, because it is the time derivative of the tether current divergence that excites the waves.

2.3 Calculation Of The "Alfvén Wing" Current

Despite the good physical description of the Alfvén wing currents (albeit for a special case and based on physical reasoning more than explicit calculations) found in the 1965 paper of Drell et al., confusion has persisted on "how the current loop is completed" in the ionosphere. Thus Dobrowolny and Veltri fault Drell et al. for using J_z, the plasma current along the field lines, to calculate the magnetic field of the Alfvén wave packet. They state that J_z is a "d.c. current (in the z direction) and has nothing to do with Alfvén waves."

The results of this section will clearly show that what Dobrowolny and Veltri call "the main component of the wing current J_z which is the continuation of the conductor's current into the medium" is in fact strictly a plasma wave phenomenon. The results further show that, J_z is not just the extension of tether current into the medium, since the Alfvén wings extend beyond the dimensions of the system along the line of flight, well beyond them for $L_x \leq v_x/\Omega_{ci}$. Other striking features demonstrate the wave nature of this phenomenon.

Barnett and Olbert show that the condition $\omega = k_x v_x$ (which holds for fields due to an unmodulated, motion-induced source current) places stringent conditions on the possible radiation, conditions which can be satisfied only for $\omega < \Omega_{ci}$, $\omega_{LH} < \omega < \omega_{ce}$, and $\omega_{pe} < \omega < \omega_{UH}$, where ω_{LH} is the lower hybrid frequency, ω_{ce} the ion cyclotron frequency, ω_{pe} the electron plasma frequency, and ω_{UH} the upper hybrid frequency.

The maximum frequency associated with the motion of the system is $\omega \sim \frac{\pi v_x}{L_x} \simeq 3 \times 10^4$ rad/sec for $L_x = 1m$, which is about the minimum effective L_x likely for an operating tethered system. The subsatellite for the first tethered satellite mission has a radius of around 1 meter ($L_x \geq 2m$). As noted before, large charge-collecting terminals or hollow cathode plasma clouds might lead to L_x values in the tens or even hundreds of meters.

The lower hybrid frequency in the F layer, taking the ion to be 0^+, is $\omega_{LH} \simeq 5 \times 10^4$ rad/sec. Thus we should not expect the contribution of Barnett's and Olbert's lower hybrid band to be significant for a real tethered satellite system operating in the d.c. mode, and it is ignored in the calculations that follow. This point is discussed in more detail in the section that compares the present results with previous ones.

The cold plasma dielectric tensor may be expressed as

$$\epsilon = \begin{pmatrix} \epsilon_\perp & ig & 0 \\ -ig & \epsilon_\perp & 0 \\ 0 & 0 & \epsilon_z \end{pmatrix}$$

where the ambient magnetic field lies along the $z-axis$.

For $\omega < \Omega_{ci} \ll \omega_{ce}$ and ${\omega_{ce}}^2 \ll {\omega_{pe}}^2$, the following approximations apply:

$$\epsilon_z = \infty \tag{7}$$

$$\epsilon_\perp = \frac{c^2}{{v_A}^2} \frac{1}{1-(\omega/\Omega_{ci})^2} \tag{8}$$

$$g = \epsilon_\perp(\omega/\Omega_{ci}) \tag{9}$$

where

$$v_A \simeq c(\Omega_{ci}/\omega_{pi})$$

Expression (7) just means that E_z (but not J_z) can be ignored. Then expressions (1) and (3) yield

$$J_z = -\frac{ic^2}{4\pi\omega} k_z \ (\vec{k}_\perp \cdot \vec{E}) \tag{10}$$

$$\vec{k}_\perp \cdot \vec{E} = \frac{4\pi i\omega}{c^2} \frac{\left[(\vec{k}_\perp \cdot \vec{j})(k^2 - \omega^2\epsilon_\perp/c^2) + ig \ (\omega^2/c^2)(\vec{k}\times\vec{j})_z\right]}{(k^2 - \omega^2\epsilon_\perp/c^2)({k_z}^2 - \omega^2\epsilon_\perp/c^2) - g^2\omega^4/c^4} \tag{11}$$

The condition $k_z = (\omega/v_z)$, implies $k \geq (\omega/v_z)$. Taking $(v_A/v_z) \simeq 40$, which applies to the F-layer in sunlight (v_A minimum), this condition gives, for $\omega = 0.99\ \Omega_{ci}$: $|g| \simeq \epsilon_\perp \leq 0.03(kc/\omega)^2$. Thus, except for $\omega \simeq \Omega_{ci}$, expression (11) is closely approximated by

$$\vec{k}_\perp \cdot \vec{E} = \frac{4\pi i\omega}{c^2} \frac{(\vec{k}_\perp \cdot \vec{j})}{(k_z^2 - \omega^2\epsilon_\perp/c^2)} \tag{12}$$

In the low frequency limit, this corresponds to a particularly revealing equation for the divergence of the electric field in the plasma [Drell et al., 1965].

$$\frac{\partial^2(\vec{\nabla} \cdot \vec{E})}{\partial z^2} - \frac{1}{v_A^2}\frac{\partial^2(\vec{\nabla} \cdot \vec{E})}{\partial t^2} = \frac{4\pi}{c^2}\frac{\partial(\vec{\nabla} \cdot \vec{j})}{\partial t}$$

$$= -\frac{4\pi}{c^2}\frac{\partial^2(\rho_{ext})}{\partial t^2} \tag{13}$$

where ρ_{ext} is the charge density due to the system's charge exchange with the plasma. The system is injecting "external" charge (i.e. not determined by the plasma response) into the plasma. Expression (13) is just the one-dimensional wave equation for the net charge density in the plasma. Thus the tether source drives waves of net charge down the field lines. These regions of net charge are the Alfvén wings. The situation is more complicated when higher frequency components are taken into account, but the basic physics is the same. The circuit completion in the ionosphere is a wave phenomenon.

Since waves with $\omega \simeq \Omega_{ci}$ are known to be strongly damped and can therefore be ignored, expression (12) is taken to apply throughout the region of interest $\omega < \Omega_o$, where Ω_o is slightly less than Ω_{ci}.

Thus equation (6) gives

$$J_x = \frac{-2I}{\pi} \frac{k_x \delta(\omega - k_x v_x)}{\left(k_Z^2 - \omega^2 \epsilon_\perp(\omega)/c^2\right)} \sin\left(\frac{k_y L}{2}\right) \frac{\sin(k_x L_x/2)}{k_x L_x} \tag{14}$$

The problem is now to find the inverse Fourier transform of (14). The integral over ω is trivial and confines the k_x range of integration to $|k_x| \leq K_o = \Omega_o/v_x$. Since $\epsilon_\perp$ depends only on k_x, the k_y integration is also trivial. The integration path for k_x is chosen as in Figure 2.2, based on physical reasoning that selects Alfvén wings that are swept back (rather than forward), since excited lines of force are being left behind. For $z > 0$ the k_x integral can be closed in the upper half-plane and evaluated using Cauchy's theorem. This leaves

$$J_x(x', y, z > 0) = \frac{I}{2\pi L_x} \left[\delta(y - L/2) - \delta(y + L/2)\right] \bullet \int_{-K_o}^{K_o} dk_x \frac{\sin(k_x L_x/2) e^{ik_x(x' + z'(k_x))}}{k_x} \tag{15}$$

$$\text{where } z'(k_x) = \left(\frac{v_x}{v_A}\right) \frac{z}{\left[1 - (k_x v_x/\Omega_{ci})^2\right]^{1/2}}$$

The integral in (15) becomes

$$\int_0^{K_0} dk_x \frac{\left[\sin\left(k_x\left[L_x/2 + \tilde{x}\ (k_x)\right]\right) + \sin\left(k_x\left[L_x/2 - \tilde{x}\ (k_x)\right]\right)\right]}{k_x} \tag{16}$$

where $\tilde{x}(k_z) = x' + z'(k_z)$.

This expression reduces to a familiar form as the line-of-flight ($z = 0$) is approached. As $z \to 0$, $\tilde{x} \to x' = x - v_x t$, which is independent of k_z. In this case

$$J_z(x', y, z > 0) = \frac{I}{2\pi L_z}\left[Si\Big(K_o\big[x' + L_z/2\big]\Big) - Si\Big(K_o\big[x' - L_z/2\big]\Big)\right] \cdot\big[\delta(\text{y-L/2}) - \delta(\text{y+L/2})\big] \quad (17)$$
$$z \to 0$$

where $\mathrm{Si}(v) = \int_o^v \frac{\sin u}{u}\, du$, the sine-integral function.

The picture of the field line currents that emerges from the preceding analysis is different from the one that has prevailed until now. The Alfvén wings have previously been described (e.g. in Drell et al.) as regions of unidirectional z current with x-dimension equal to L_x, the moving conductor system's x-dimension. These are the "perfect Alfvén wings" shown in Figure 2.3. The sheet current density is $(I/2L_z)$ on each side of the $z = 0$ line. As equation (17) shows, this case really corresponds to infinite L_z or Ω_{ci}. For very large L_z, Figure 2.3 is a pretty good approximation. This is illustrated in Figure 2.4, which shows J_z (plotted in units of $(I/2L_z)$) near the system ($z \to 0$) on the positive side of the upper end of the tethered system for the case $L_z = 32(v_x/\Omega_{ci})$, which would correspond to an enormous system for the F-region ($L_z \simeq 800m$). J_z is symmetric in x', so only the positive x' half is shown. The perfect Alfvén wing would correspond to $J_z = 1$ out to $\bar{x}' = 16$ and $J_z = 0$ beyond. The field-line current density in Figure 2.4, though concentrated (and close to unity) in the region of the system, is not exactly confined to $|x'| \leq L_z/2$, and the direction of the current oscillates (with decreasing amplitude) as $|x'|$ increases beyond $L_z/2$.

The central portion of the wings extends beyond the dimensions of the system for a distance $d \sim v_x/\Omega_{ci}$ (around 25m for the central F-region case).

This phenomenon may be viewed in the following way. The plasma, in its response to the travelling disturbance represented by the tethered satellite system, is limited (by the physical reasons already discussed) to frequencies below the ion cyclotron frequency or, equivalently, to wavelengths in the x-direction greater than v_x/Ω_{ci}. For a system with L_x (the x-dimension of the charge-exchanging portion of the system — the terminating metallic satellite or plasma contactor cloud) much greater than v_x/Ω_{ci}, as in Figure 2.4, this means that the Alfvén wings are well-approximated by a "boxcar function" that coincides with the system's charge-exchange dimensions, except for ripples at the edges, a physical analogy of the Gibbs phenomenon familiar from Fourier analysis.

For systems with L_x less than v_x/Ω_{ci} the plasma is forced to "represent" the disturbance with wavelengths greater than its actual size, and the Alfvén wings necessarily extend beyond the dimensions of the system along the line-of-flight. This is evident for the case $L_x = 0.4(v_x/\Omega_{ci})$ seen in Figure 2.5. The intermediate case $L_x = 2(v_x/\Omega_{ci})$ is shown in Figure 2.6, where the symmetry of J_z is displayed. The sheet current density in the central "wing" is less than $(I/2L_x)$ in these cases (less than unity in the chosen units) because the current extends beyond the dimensions of the system, while the total z-current in the ionosphere is still I/2 on each side of the system. This phenomenon strikingly demonstrates the wave nature of the ionospheric field-line currents.

The tethered system current distribution utilized in the calculations contracts the y and z dimensions of the charge-exchange region of the system at each end down to a line, and this in turn confines the J_z currents to the planes

defined by $y = \pm L/2$. The J_z currents are then sheet currents. This restriction of J_z to the sheets ($y = \pm L/2$) even beyond the dimensions of the system (i.e. for $| x' | > L_x/2$) occurs because of the discontinuities in E_y, and hence J_y, which exist at $y = \pm L/2$.

Let us consider these results from the standpoint of the constant tether current assumption, which is really an assumption about a steady state of the whole system, including the ionosphere. Clearly we must hypothesize a transition period during which the steady state with constant tether current is established. The analysis reported here assumes that a steady state with constant tether current has been achieved, which necessarily means, within the context of our model, that the Alfvén wings have assumed the form described by equation (15).

When expression (15) is evaluated for higher values of z, i.e. away from the system, the symmetry of the J_z distribution about the center of the wing (defined by the line $z = -x'(v_A/v_x)$) is destroyed. This is seen in Figures 2.7-2.9 for the three different cases considered previously. One unit of z in the figures corresponds to around 1 km for the F-layer parameters that we have been considering. The general behavior as z increases is the same in all three cases. The boundary of the leading edge of the wing becomes progressively sharper with increasing z, while the "wake" region sees larger oscillations in J_z that persist for hundreds of meters. The peak of the current distribution is displaced from $x' = 0$ in the negative x' direction.

The asymmetry of the distribution is evidently due to frequency components out of the Alfvén range. Figures 2.10 and 2.11 show how the distribution changes when the upper limit of integration in expression (15) is reduced to $0.7K_0$. Since the higher frequency components contributing to the wings correspond to lower

phase velocities along z, thermal effects will be more important for them. Therefore the specific features of the sheet current distribution's changing shape with increasing z seen in the present analysis (which uses cold plasma theory) cannot be applied with confidence to an actual ionospheric tethered satellite system.

Let us examine the other components of the plasma current (J_x, J_y) in the Alfvén wing region in order to get a clearer picture of the physics. It should be noted that the calculations of electromagnetic field quantities and plasma currents presented in this section are for the waves and currents that travel to infinity. Evanescent waves have not been included, but this does not mean that their contribution to the fields and currents in the vicinity of the system is necessarily zero.

Expressions (1), (2), (9) and (12) yield the wave field components

$$E_{x,y} = \frac{4\pi i\omega}{k_\perp{}^2 c^2} \frac{(\vec{k}_\perp \cdot \vec{j})}{[k_z{}^2 - (\omega^2/c^2)\epsilon_\perp]} \quad k_{x,y} \tag{18}$$

$$J_{x,y} = \frac{\omega^2}{k_\perp{}^2 c^2} \frac{(\vec{k}_\perp \cdot \vec{j})}{[k_z{}^2 - (\omega^2/c^2)\epsilon_\perp]} \epsilon_\perp \left[k_{x,y} \pm i k_{y,x}(\omega/\Omega_{ci})\right] \tag{19}$$

In the low frequency limit $\omega \ll \Omega_{ci}$, this corresponds to $\vec{J}_\perp = -\frac{i\omega\epsilon_\perp \vec{E}_\perp}{4\pi}$, as it should. Hall current terms contribute to higher frequency components of the plasma current.

The expressions for E_z and J_z corresponding to the region previously considered for J_z (i.e., $z > 0$, $y = L/2$) are:

$$E_x = \frac{-2I}{L_x}\left(\frac{v_A}{c^2}\right)\int_0^\kappa \frac{\left(e^{-k\bar{L}}-1\right)}{k}\sqrt{1-k^2}\ \sin k[\bar{x}+\bar{z}\,'(k)]\ \sin\left(\frac{k\bar{L}_z}{2}\right)dk \qquad (20)$$

$$J_x = \frac{I}{2\pi L_x}\left(\frac{\Omega_{ci}}{v_A}\right)\int_0^\kappa \sqrt{\frac{1-k}{1+k}}\ (1-e^{-k\bar{L}})\ \cos k[\bar{x}+\bar{z}\,'(k)]\ \sin\left(\frac{k\bar{L}_z}{2}\right)dk \qquad (21)$$

where $\bar{L} = L\left(\frac{\Omega_{ci}}{v_x}\right)$, $\bar{x} = x'\left(\frac{\Omega_{ci}}{v_x}\right)$, etc., and $\kappa = \Omega_o/\Omega_{ci}$.

These quantities are shown in Figures 2.12-2.19 for the L_x cases previously considered for J_x. Note that, for $z \to 0$, E_x changes sign at $x' = 0$, as it should since the charge-exchange region is symmetric (and E_x is antisymmetric) about $x' = 0$. The time derivative of E_x, drives the Alfvén components of J_x, so J_x has its maximum value at $x' = 0$ where E_x is varying most rapidly.

The plots of J_x and E_x for $\bar{L}_z = .4$ and $\bar{L}_z = 2.0$ (Figures 2.14-2.17) are virtually identical. Thus J_x and E_x scale with the inverse of $\bar{L}_z$ in this region, i.e. the integrals in expressions (20) and (21) depend weakly on $\bar{L}_z$. This is also true for the corresponding J_y and E_y (Figures 2.22-2.25).

The y-component of the electric field is discontinuous across the planes of the charge-exchange regions at each end of the system because the external charge density is confined to lie along the lines traced by the charge-exchange regions in the model used here. The expressions for E_y and J_y for $|y| < L/2, z > 0$ are given by:

$$E_y = \frac{-4Iv_A}{c^2 L_x}\int_0^\kappa \frac{\sqrt{1-k^2}}{k}\ \sin\left(\frac{k\bar{L}_z}{2}\right)\ \cos k(\bar{x}+\bar{z}\,')\cosh(k\bar{y})e^{-k\bar{L}/2}\,dk \qquad (22)$$

$$J_y = \frac{I}{\pi L_z}\left(\frac{\Omega_{ci}}{v_A}\right)\int_o^\kappa \sin\left(\frac{k\bar{L}_z}{2}\right)\sqrt{\frac{1-k}{1+k}}\,\sin k(\bar{x}+\bar{z}\,')\cosh(k\bar{y})e^{-k\bar{L}/2}\,dk \qquad (23)$$

Since $L \gg (v_z/\Omega_{ci})$, i.e. $\bar{L} \gg 1$, these quantities basically just change sign at the discontinuities. E_y and J_y for y approaching $L/2$ from above are shown for several cases in Figures 2.20-2.27. J_y has its peak values at the edges of the "wing" (with opposite signs at the two edges). This makes sense, since those are the places where the time derivative of E_y is largest.

2.4 The Alfvén Wave Impedance

The wave impedance of the electrodynamic tether operating in its constant current mode can be found by calculating the power lost in the form of electromagnetic waves and dividing the result by the square of the current. This power is just the negative of the dot product of the tether current density and the wave electric field integrated over the tethered satellite system. The contribution due to the x-component of the current is negligible, so there is no need to worry about effects due to the specific functional form of the current density in the terminating parts of the system.

The wave impedance Z_A (using (4b) and (22)) is then given by

$$Z_A = -\int_{-L/2}^{L/2} E_y(x'=0,y,z=0)j_y\;dy/I^2 \qquad (24)$$

$$= \frac{4v_A}{\bar{L}_z c^2} \int_o^\kappa dk(1 - e^{-k\bar{L}}) \frac{\sin\left(k\bar{L}_z/2\right)\sqrt{1-k^2}}{k^2}$$

where $\bar{L}_z = L_z(\Omega_{ci}/v_z)$, etc., and $\kappa = \Omega_o/\Omega_{ci}$.

This is the general result. Figure 2.28 shows the variation of the Alfvén wave impedance over a wide range of values of $L_z(\Omega/v_z)$ for fixed tether length $L = 20km$. The Alfvén wave impedance is seen to slowly fall off with increasing values of $L_z(\Omega/v_z)$. Figure 2.29 shows the variation with tether length for fixed L_z ($\bar{L}_z = .4$). As some previous analyses had indicated in various limits, the Alfvén wave impedance is a slowly varying function of the system dimensions. Even the inclusion of higher frequencies (up to the ion cyclotron frequency) is a secondary effect.

By far the most important parameter is v_A, the Alfvén speed. The results presented here find a linear dependence on v_A, in agreement with all previous analyses of this problem, with the exception of that carried out by Dobrowolny and Veltri [1986], which found that the Alfvén wave impedance varied inversely with v_A. These authors also obtained an (L/L_z) dependence for the wave impedance, which is at odds with the present results and all others except for the original paper on the subject by Drell, et al. [1965]. Rasmussen, et al. [11985] pointed out that the Drell results correspond to the case of a system with $L_z \gg L$, although they did not explicitly compute the wave impedance in this limit. Dobrowolny and Veltri [1986], however, are considering a very long and infinitely thin tether, which is at the opposite extreme. After obtaining their results, these authors attempt to justify them by physical reasoning. First of all, they maintain that J_z, the plasma current along the magnetic field lines, is not a wave

phenomenon at all. The present analysis clearly shows that it is. Then they claim that the energy flow due to this "d.c. moving current" is mainly along the x-axis (i.e., moving with the system). They compute the supposed z-component of this energy flow and find it to be in agreement with their calculation. This is taken as an argument in favor of their results, even though the authors had already stated J_z had nothing to do with Alfvén waves. The true Alfvén magnetic field component is then asserted to lie along the z-direction. The authors advanced their arguments to justify the deviation of their results (roughly by a factor $(v_z/v_A)^2$) from those of Drell et al., which should not apply to the case they considered anyway, if Rasmussen et al. are correctly stating the domain of applicability of the Drell analysis. It is shown below, in fact, that expression (24) reduces to the result of Drell, et al. in the limiting case $L_z \gg L$.

The previous results for the Alfvén wave impedance are summarized in Table 2-1. The analysis presented here will now be shown to agree with some of these results in the appropriate limits. First of all, let us consider the case $\bar{L}_z \ll 1$, $\bar{L} \gg 1$. Then expression (24) becomes approximately

$$Z_A^{(1)} = \frac{2v_A}{c^2} \int_0^1 dk(1 - e^{-k\bar{L}}) \frac{\sqrt{1-k^2}}{k} \tag{25}$$

$$\simeq \frac{2v_A}{c^2} \left[\ell n(2\bar{L}) + \gamma - 1 \right] ,$$

where $\gamma = 0.577$ is the Euler constant.

This is exactly the result obtained by Barnett and Olbert in the limit $b \ll v_z/\Omega_{ci}$, where b is the radius of the wire. This agreement is just a special case of the general result that it is only the dimensions of the charge-exchange region and the

amount of change-exchange per unit time that matter. Of course $\bar{L}_z$ must still be much greater than (v_z/ω_{LH}) for comments made previously about the relative unimportance of the lower hybrid band radiation to be valid.

For $\bar{L}_z \gg, \bar{L} \gg 1$ (the "MHD" limit) expression (24) yields

$$Z_A^{MHD} \simeq \frac{4v_A}{\bar{L}_z c^2}\left[\bar{L}\,\cot^{-1}\left(\frac{2\bar{L}}{\bar{L}_z}\right) + \left(\frac{\bar{L}_z}{4}\right)\ell n\left(\frac{\bar{L}^2+(\bar{L}_z/2)^2}{(\bar{L}_z/2)^2}\right)\right] \tag{26}$$

For the case $L_z \gg L$ this gives

$$Z_A^{(2)} = \frac{2\pi v_A}{c^2}\,\frac{L}{L_z} \tag{27}$$

the result obtained by Drell et al., just as Rasmussen et al. said it should.

In the opposite limit (the tethered system limit) $L \gg L_z$ expression (26) goes to

$$Z_A^{(3)} = \frac{2v_A}{c^2}\left(1+\ell n\left(\frac{2L}{L_z}\right)\right) \tag{28}$$

The logarithmic term, which dominates for a long tether, corresponds to the impedance of two infinite bi-filar transmission lines in parallel immersed in a dielectric ($\epsilon = c^2/v_A{}^2$), where the radius of the wire is $L_z/2$ and the separation between the wires is L. The transmission line analogy, which goes all the way back to Drell et al. is seen to be a pretty good one. Expression (27), in fact,

corresponds to the case of two parallel plate transmission lines electrically in parallel. Williamson and Banks, in an unpublished report (see Table 2-1) noted the bifilar line similarity and obtained twice the logarithmic term in (28), evidently forgetting that each "wing" is a separate transmission line, the two wings being in parallel with respect to the tether source.

Expression (26), a general result, has been seen to agree with some previously obtained results in the (quite different) limits considered by different investigators. No attempt has been made to compare the results to the Barnett and Olbert expression beyond the narrow region considered in (25), but on the basis of the reasoning already presented one might expect good agreement everywhere.

The results of Dobrowolny and Veltri have already been discussed. That leaves only the value of Rasmussen et al. of those included in Table 2-1, as yet undiscussed. They obtained approximations to the wave fields valid only for $| y | \ll L/2$, $| x' | \ll L/2$, but then applied these expressions throughout an $L \times L$ area when they estimated Z_A, which probably accounts for the difference between their results and expression (28), which should correspond to their case.

Let us now return to the question of radiation in the "lower hybrid band" of Barnett and Olbert. The present analysis (in agreement with that of Barnett and Olbert, it should be noted) found that the wave fields were determined by $\vec{k}_\perp \cdot \vec{j}$, which corresponds to the divergence of the tethered system current density, to which the constant current along the tether contributes not at all.

It is at the ends of the tethered system that the system's current density becomes non-solenoidal, where the tethered system exchanges charge with the

ambient plasma, i.e. acts as a source or sink of external charge to the plasma. In the constant current mode of tethered system operation, it is the time-varying fields generated by these moving charge sources at the ends of the system which drive the waves that carry away the net charge density created by the charge-exchange between the system and the ionospheric plasma. Thus it is very important to model the current distribution in the tethered system in a way that correctly takes into account the essential dimension of the charge-exchange region at the ends of the system.

The model used in the present analysis ignores the y and z extent of this region, collapsing the ends of the system to a line along the direction of flight. While this may miss some secondary effects, the wave fields at long distances from the system should be well-approximated by the model, since the time-variation of the disturbance is due only to the motion of the system along the x-direction.

It has been seen that the expression for Z_A obtained here agrees with the Barnett and Olbert result in the limit of very small L_z, if the radius b is equated to $L_z/2$. This should be expected from the argument given above. Indeed, there is no reason to doubt that an orbiting wire would excite waves with frequencies above the lower-hybrid frequency or that the calculations of Barnett and Olbert accurately give the corresponding wave impedance (for a cold plasma). The problem is that such a system would seem to be of only academic interest, given that it does not adequately model the essential charge-exchange region dimension of a real tethered satellite system.

The analysis reported here indicates that applying the expression obtained by Barnett and Olbert for a cylindrical system's lower-hybrid band wave impedance to a system with the radius equal to $L_z/2$ should be a reasonable way

to proceed even for radii much greater than any conceivable tether's. When this is done (by numerical integration), a dramatic drop in the wave impedance for this band is observed as the radius increases beyond a meter. By ten meters it is only a few percent of the Alfvén wave impedance.

2.5 Summary And Conclusions Of The Theoretical Work

The ionospheric plasma currents associated with the operation of an orbiting, constant-current electrodynamic tethered satellite system have been calculated using linear cold plasma theory and a tethered system current distribution model that takes into account the peculiar dumbbell shape of the system. It has been noted that the assumption of a constant tether current is also an assumption about a steady state of the whole current system, including the ionosphere. No attempt has been made to analyze the transition to this steady state. The field-line currents are carried by electromagnetic plasma wave packets. If the terminating, charge-exchanging portions of the system have dimensions as large as a few meters (for low earth orbit) these wave packets are composed primarily of plane waves whose frequencies are below the ion-cyclotron frequency. This is because there is a frequency band between the ion cyclotron and lower hybrid frequencies for which no waves that travel to infinity are excited by a constant-current electrodynamic tethered system [Barnett and Olbert, 1986]; and the frequencies excited by the system as it moves through the ionosphere are roughly bounded by v_x/L_x, where v_x is the system's velocity across the geomagnetic field lines and L_x is the dimension of the charge-exchange region along the x-direction.

The analysis reported here has emphasized that L_z is the crucial dimension of the system for determining the spectrum of excited waves. This is because it is the time-varying fields (as seen by the plasma) due to the tethered system's injection and extraction of charge from the plasma that drive the waves. Modeling the tethered system as an orbiting wire (as was done by Barnett and Olbert) grossly underestimates L_z and leads to incorrect conclusions about the importance of the radiation band above the lower hybrid frequency. This is an important result, because the very high wave impedances calculated by Barnett and Olbert would severely limit currents attainable in a tethered satellite system, thus precluding the use of such systems as power generators of ELF wave transmitters.

The field-line current calculations show plasma sheet currents at each end of the tethered system. The basic structure of these current sheets is roughly that of the previously described "Alfvén wings," which really correspond to the limiting case of infinite L_z or Ω_{ci}. A number of new features, due to the wave nature of the phenomenon have been noted, however. The disturbance caused by the moving tethered system extends beyond its dimensions along the line-of-flight. For systems with v_z/L_z not far less than Ω_{ci} this implies that the sheet current J_z extends well beyond the dimensions of the system. Furthermore, J_z changes sign (and oscillates with decreasing amplitude) as the distance from the system increases along the x-direction. The model used in the present analysis, which has sharp spatial boundaries for the regions of non-zero $\frac{\partial \rho_{ext}}{\partial t}$, exaggerates this effect, but the phenomenon of Alfvén wing extension beyond the system's charge-exchange x-dimension is a result of the existence of the excluded band noted by Barnett and Olbert, which in effect places an upper limit on the frequency of the plasma's response to the moving disturbance represented by the electrodynamic tethered

system. This frequency limit, coupled with the $k_z v_z = \omega$ condition (constant tether current), limits the k_z values. Thus the phenomenon does not depend on the specific model for the tethered system current distribution.

The form of the "wings" are seen to alter as they travel away from the system, i.e., their shape depends on z. The "front" boundary becomes sharper, while the ripples in J_z in the "wake" extend to greater distances with larger amplitudes. Since this effect depends on the interference of wave packet components beyond the MHD limit, components for which thermal effects should be especially important, this result should be taken with a grain of salt.

The wave impedance has been calculated for a wide range of system dimension values and shown to agree with some prior calculations in the appropriate limits. The expression obtained is in sharp disagreement with a recently published result by Dobrowolny and Veltri. While no effort has been made to find an error in the calculations of these authors, flaws in the reasoning they used to justify their results have been pointed out. It is concluded that the linear dependence of the wave impedance on the Alfvén speed found in the present analysis and all others, save that of Dobrowolny and Veltri, is correct. The wave impedance is found to be weakly dependent on the system dimensions (both tether length and L_z), being basically a logarithmic dependence.

In the middle of the F-layer (around 300 km altitude) during the daytime, the calculated wave impedance is around 0.4Ω. At nighttime, or at different altitudes, the impedance could be significantly higher, since the value given above was computed where the Alfvén speed is at its minimum in the ionosphere. At nighttime, low-latitude ionization level minima, the impedance might be an order of magnitude greater, even at the same altitude.

It is important to keep in mind some of the limitations of the model at this point. The calculations have assumed an infinite, homogeneous plasma medium immersed in a uniform magnetic field. There is nothing to reflect the waves in this model: thus the infinite transmission line result. Nor is there dissipation of the wave energy or even Landau (collisionless) damping in the cold plasma model used. The inclusion of spatial variations in ionospheric quantities, in particular the plasma and neutral particle density (and collision frequencies), will complicate the problem a great deal, but a more complicated model will have to be developed if the fundamental problems of wave propagation from an electrodynamic tethered satellite system are to be realistically treated.

Perhaps the main justification for making the usual oversimplifications is that a couple of recent publications (using the same assumptions) had presented results that in one case [Barnett and Olbert, 1986] called into question the very functioning of an electrodynamic tethered satellite system at current levels above a few mA and in the other case [Dobrowolny and Veltri, 1986] claimed a completely different dependence on the Alfvén speed and system dimensions for the wave impedance.

It is concluded that the wave impedance for the electrodynamic tethered satellite system will not be a major limiting factor to the current that can flow in the system, which leaves open the possibility of tethered system applications such as electrical power generation, electrodynamic drag compensation (by the thrust that comes when a power source is used to drive the current in the direction opposite to that induced by the system's motion), and ELF wave generation.

The system's ability to exchange charge with the ionosphere would seem to be the really critical factor in current flow through the system. The TSS-1

mission and a number of other space and laboratory-based experiments should be shedding light on this question over the next few years.

Table 2-1

ALFVEN WING IMPEDANCE CALCULATIONS

		Z_A/Z_o	COMMENTS
1965	DRELL, FOLEY AND RUDERMAN JGR 70, 3131	$\pi\left(\frac{L}{D}\right)$	BASICALLY THE PARALLEL PLATE TRANSMISSION LINE CASE
1976	WILLIAMSON AND BANKS NOAA REPORT 03-5-022-60	$2 \ln\left(\frac{L}{R_B}\right)$	TWO-WIRE TRANSMISSION LINE
1985	RASMUSSEN, BANKS AND HARKER, JGR 90, 505	$\frac{4}{\pi}$	RESULT IS INDEPENDENT OF L; $D \gg \frac{v_x}{\Omega_i}$; POINT OUT DRELL RESULT CORRESPONDS TO $D \gg L$
1986	DOBROWOLNY AND VELTRI N.C. 9C, 27	$\frac{1}{3}\left(\frac{L}{D}\right)\left(\frac{v_x}{v_A}\right)^2$	CLAIM TO HAVE CAUGHT ERROR OF DRELL, ET AL.; ORBITING WIRE
1986	BARNETT AND OLBERT JGR 91, 10117	$\left[\ln\left(\frac{L\Omega_i}{v_x}\right) + 0.27\right]$	$D \ll \frac{v_x}{\Omega_i}$

$Z_o = \frac{2v_A}{C^2}$, L = TETHER LENGTH, D = DIMENSION ALONG SATELLITE VELOCITY

v_x = SATELLITE VELOCITY, v_A = ALFVEN SPEED

2.6 References For Section 2

1. Barnett, A. and S. Olbert, 1986. "Radiation of Plasma Waves by a Conducting Body Moving Through a Magnetized Plasma." Journal Geophys. Research 91, 10117.

2. Dobrowolny, M. and P. Veltri, 1986. "MHD Power Radiated by a Large Conductor in Motion Through a Magnetoplasma." Nuovo Cimento 9C, 27.

3. Drell, S.P., H.M. Foley and M.A. Ruderman, 1965. "Drag and Propulsion of Large Satellites in the Ionosphere: An Alfvén Engine in Space." Journal Geophys. Research 70, 3131.

4. Rasmussen, C.E., P.M. Banks and K.J. Harker, 1985. "The Excitation of Plasma Waves by a Current Source Moving in a Magnetized Plasma: The MHD Approximation." Journal Geophys. Research 90, 505.

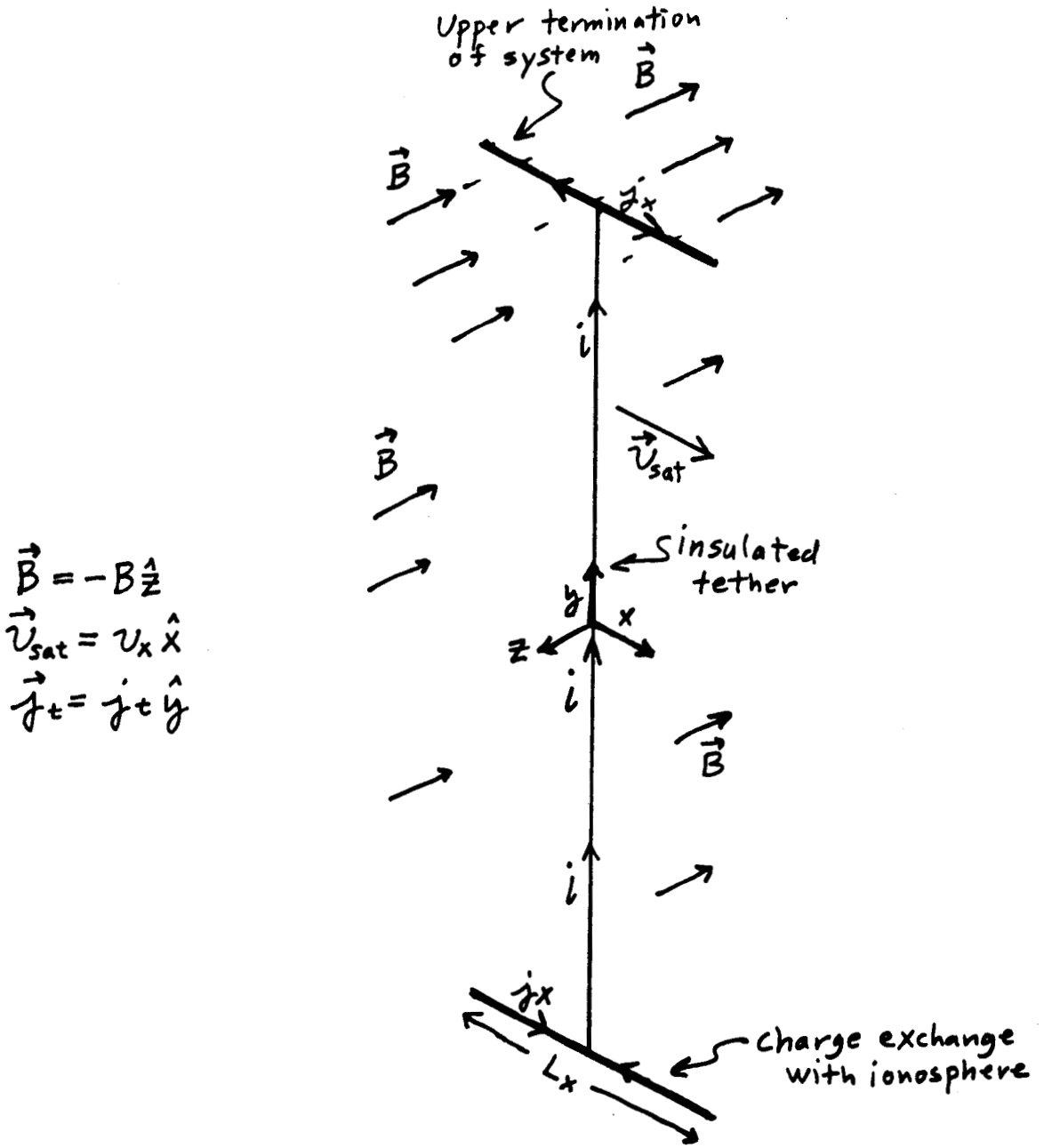

Figure 2.1. The tethered satellite system model used in the calculations.

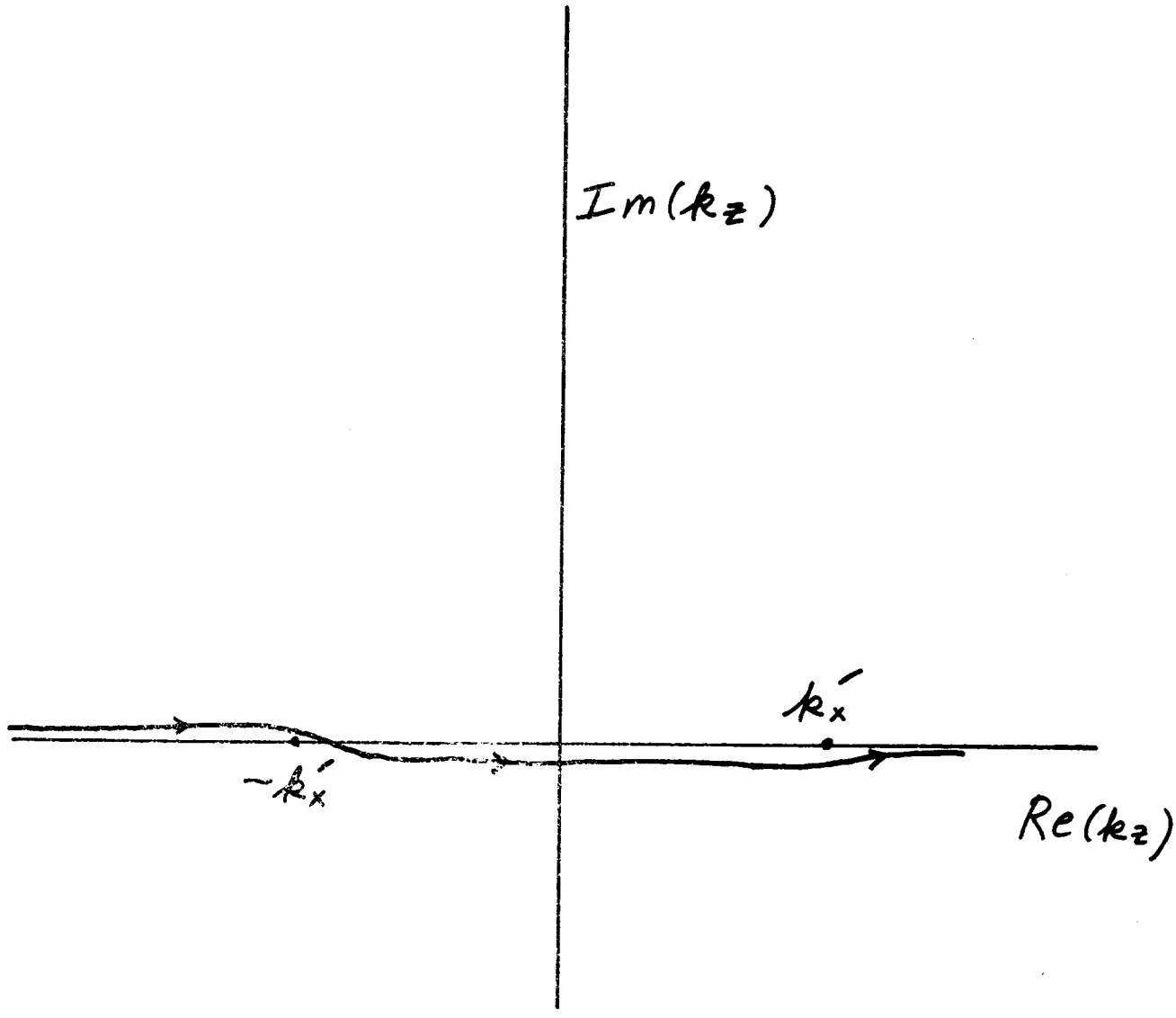

Figure 2.2. Integration path for k_z integration around poles at $\pm\ k'_z = \pm\ \frac{k_x v_x \sqrt{\epsilon_\perp}}{c}$.

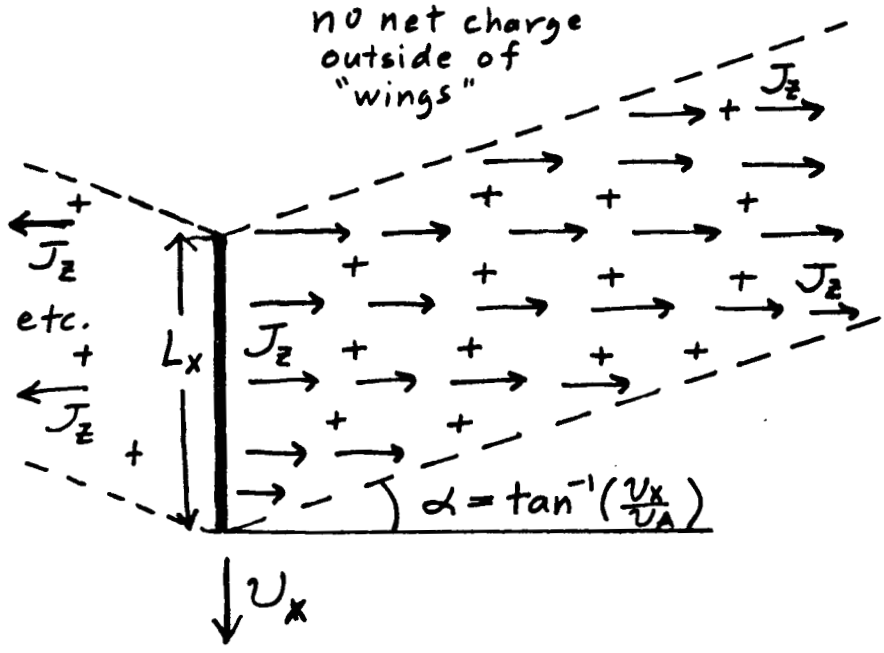

Figure 2.3. "Perfect Alfvén wings": top of system viewed from above by an observer at rest with respect to the ionosphere.

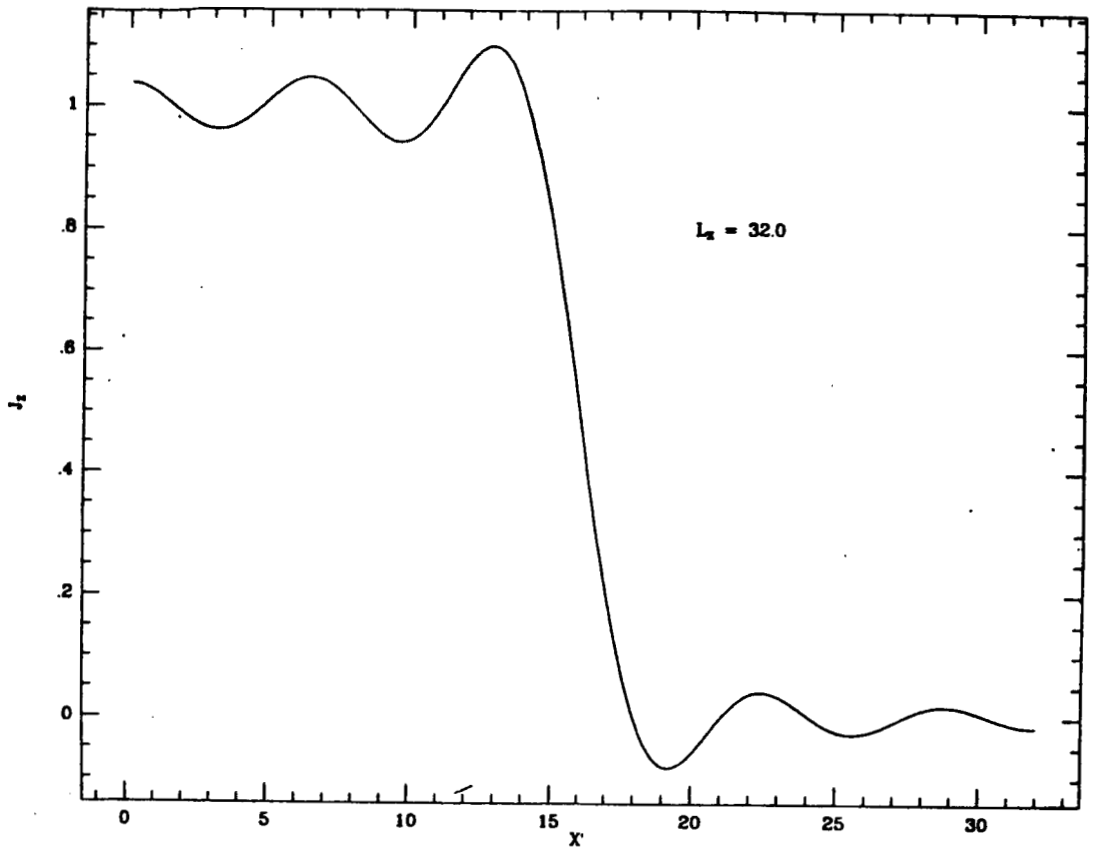

Figure 2.4. J_z sheet current density (in units of $I/2L_z$) for $\overline{L}_z = 32$ ($L_z = 800m$ at F-region plasma density maximum) versus $\overline{x}$ (one unit $\simeq$ 25m) very near system ($z \rightarrow 0$).

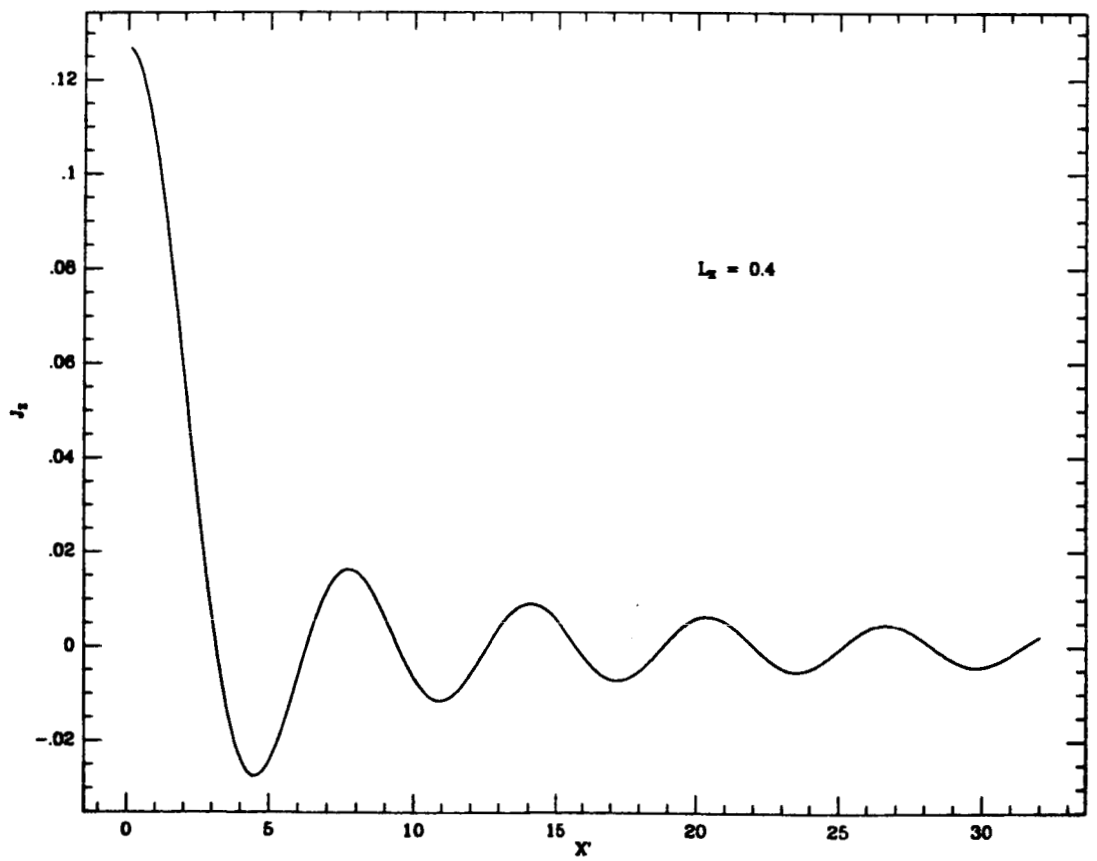

Figure 2.5. J_z for $\overline{L}_z = 0.4$ ($L_z \simeq 10m$) versus $\overline{x}$ for $z \rightarrow 0$.

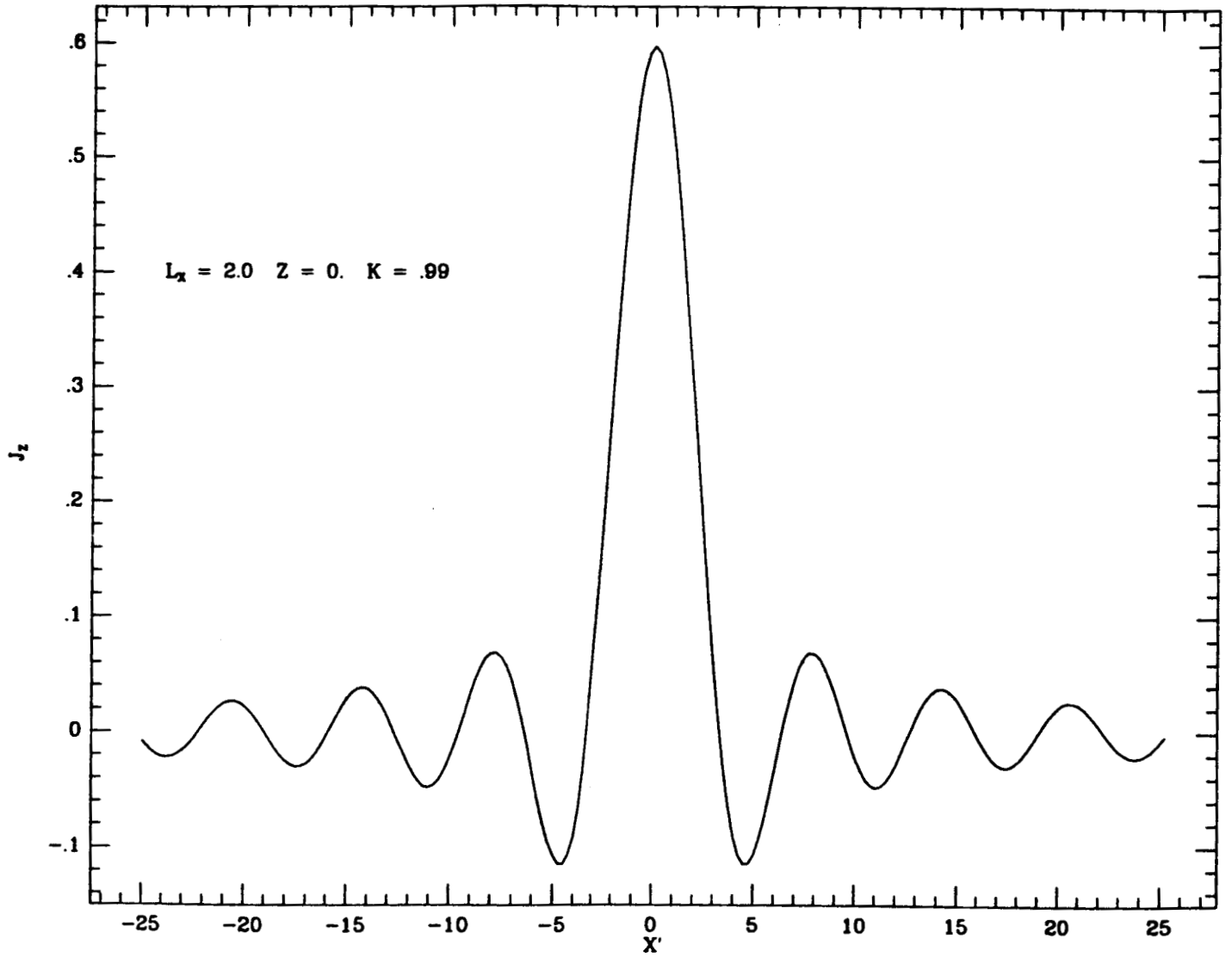

Figure 2.6. J_z for $\overline{L}_x = 2.0$ $(L_x \simeq 50m)$ versus $\overline{x}$ for $z \to 0$.

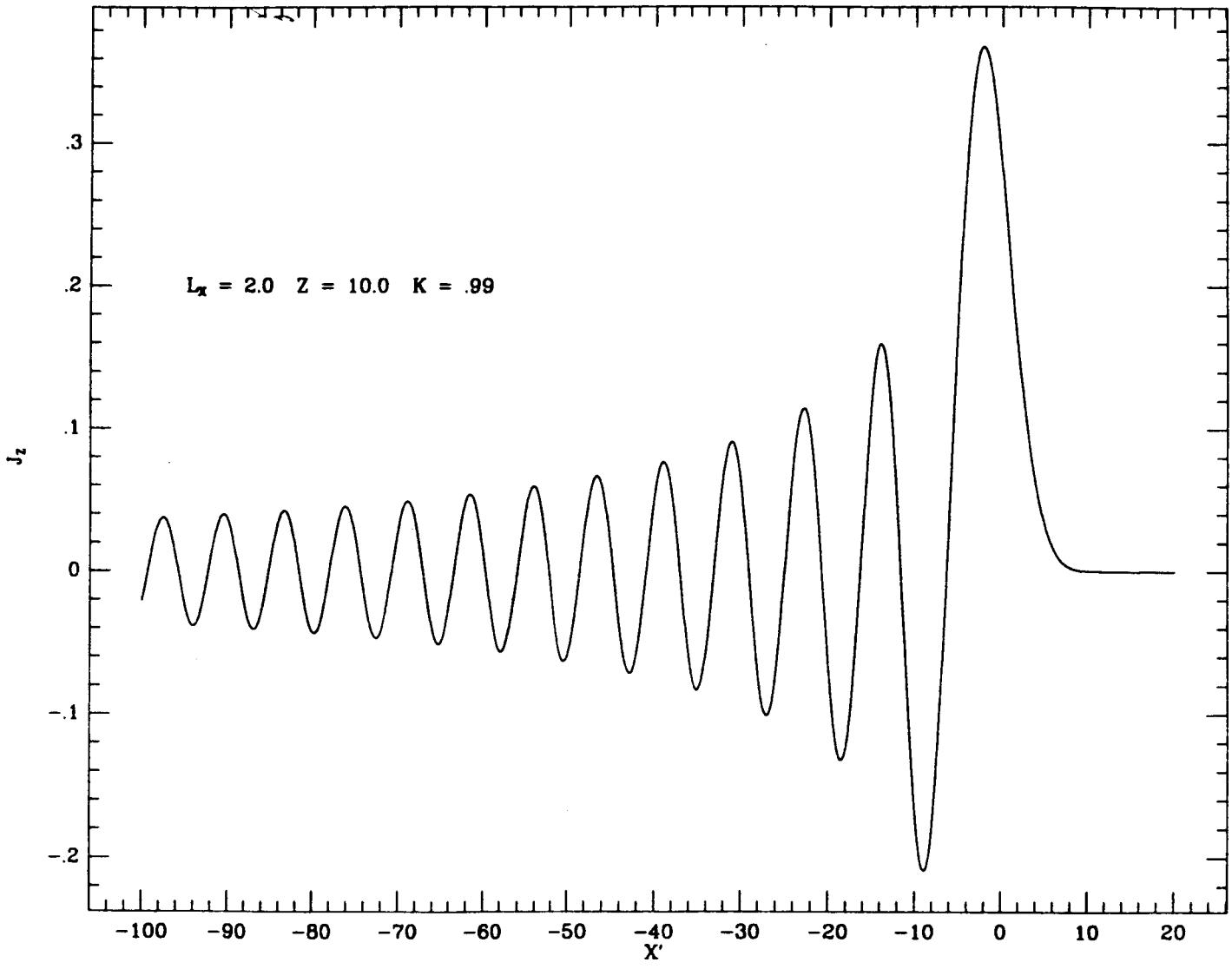

Figure 2.9. J_z for $\overline{L}_x = 2.0$ and $\widetilde{z} = 10$.

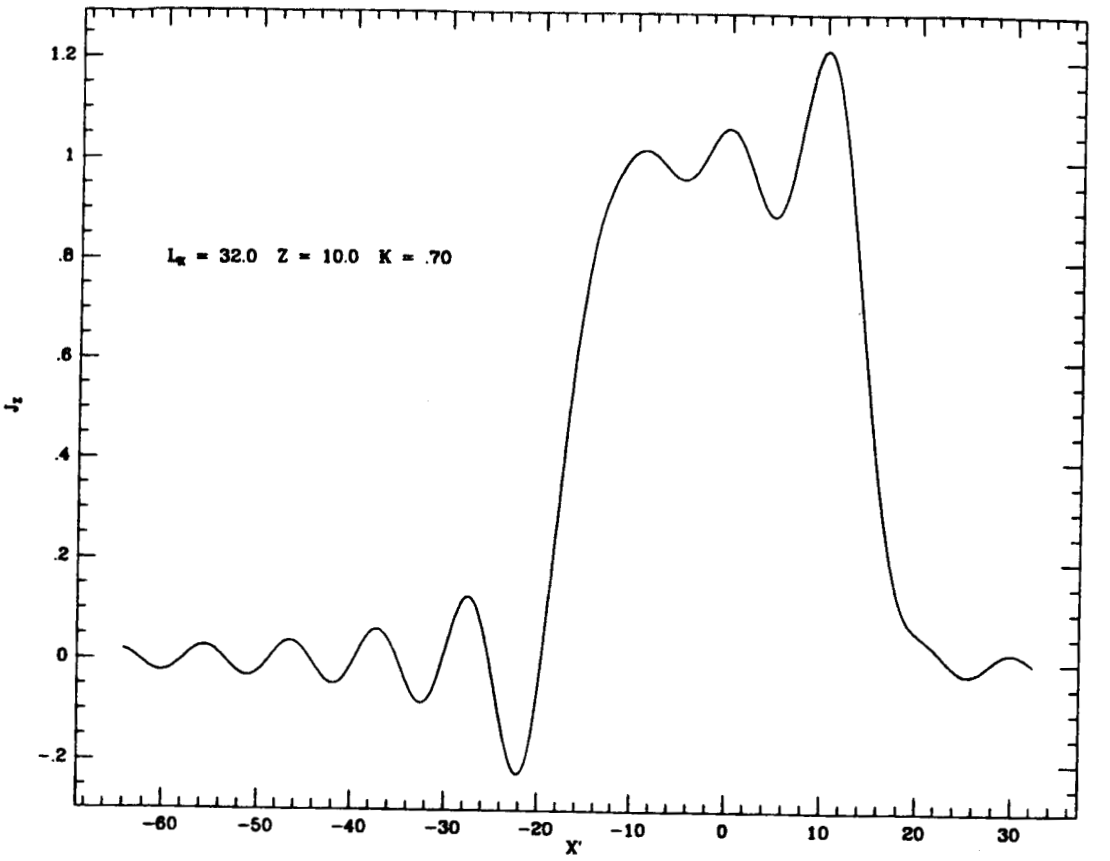

Figure 2.10. J_z for $\overline{L}_x = 32$ and $\widetilde{z} = 10$, $\Omega_o = .7\Omega_{ci}$.

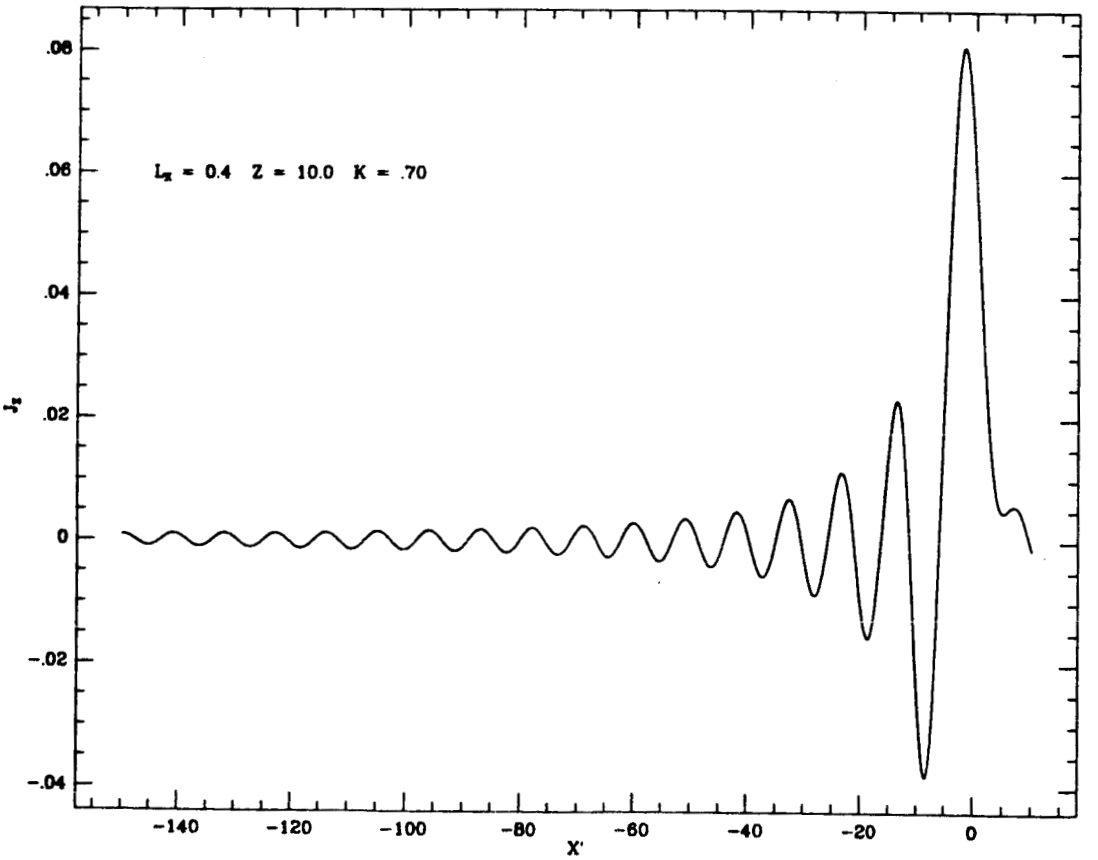

Figure 2.11. J_z for $\overline{L}_x = 0.4$ and $\widetilde{z} = 10$, $\Omega_o = 7\Omega_{ci}$.

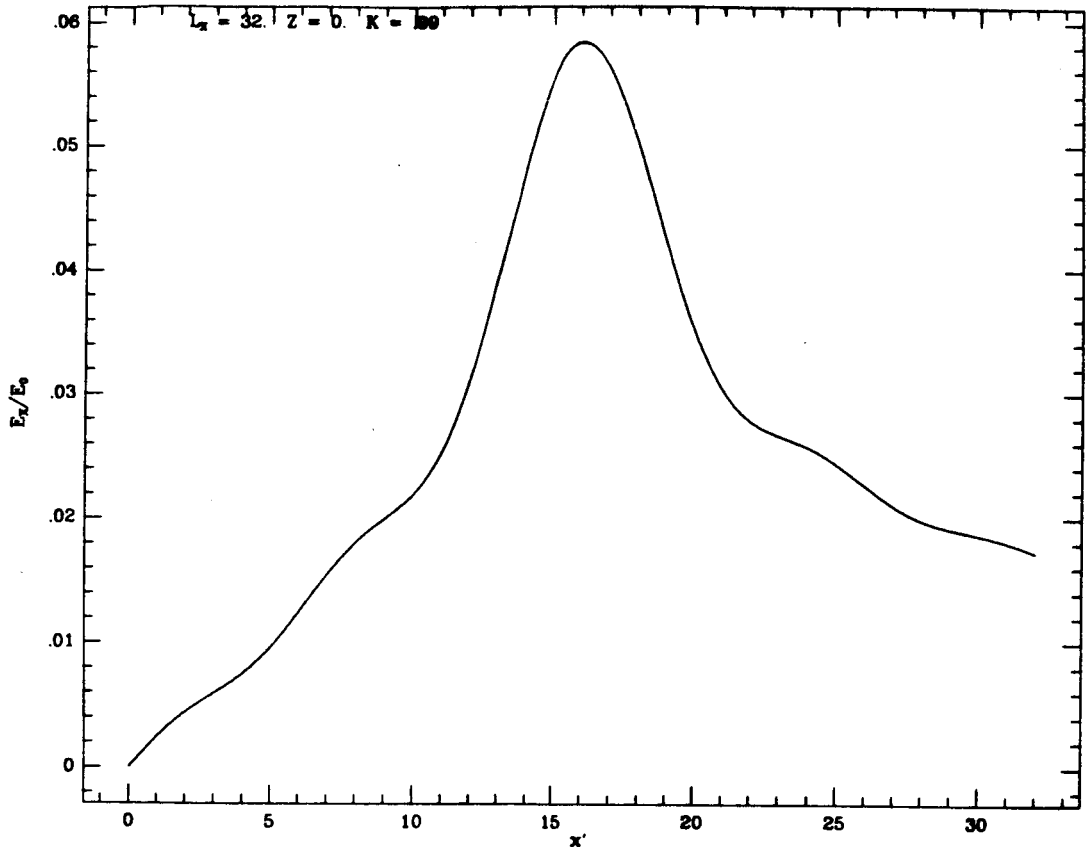

Figure 2.12. E_x in units of $(E_o/\bar{L}_z)$ ($E_o \simeq 2.4\text{x}10^{-3}$ V/m per A of tether current at F-region maximum) for $\bar{L}_z = 32$ and $\tilde{z} = 0$.

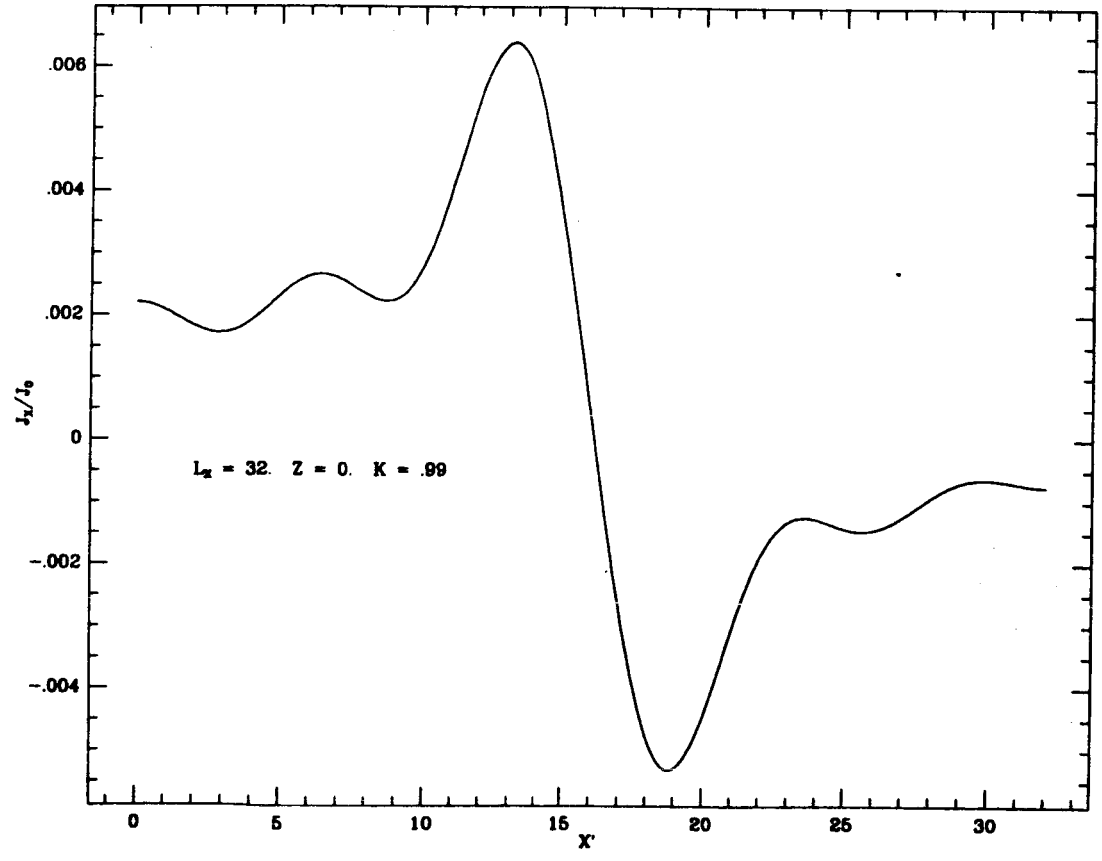

Figure 2.13. J_x in units of $(J_o/\bar{L}_z)$ ($J_o \simeq 6.4\text{x}10^{-6}$ A/m^2 per A of tether current at F-region maximum) for $\bar{L}_z = 32$ and $\tilde{z} = 0$.

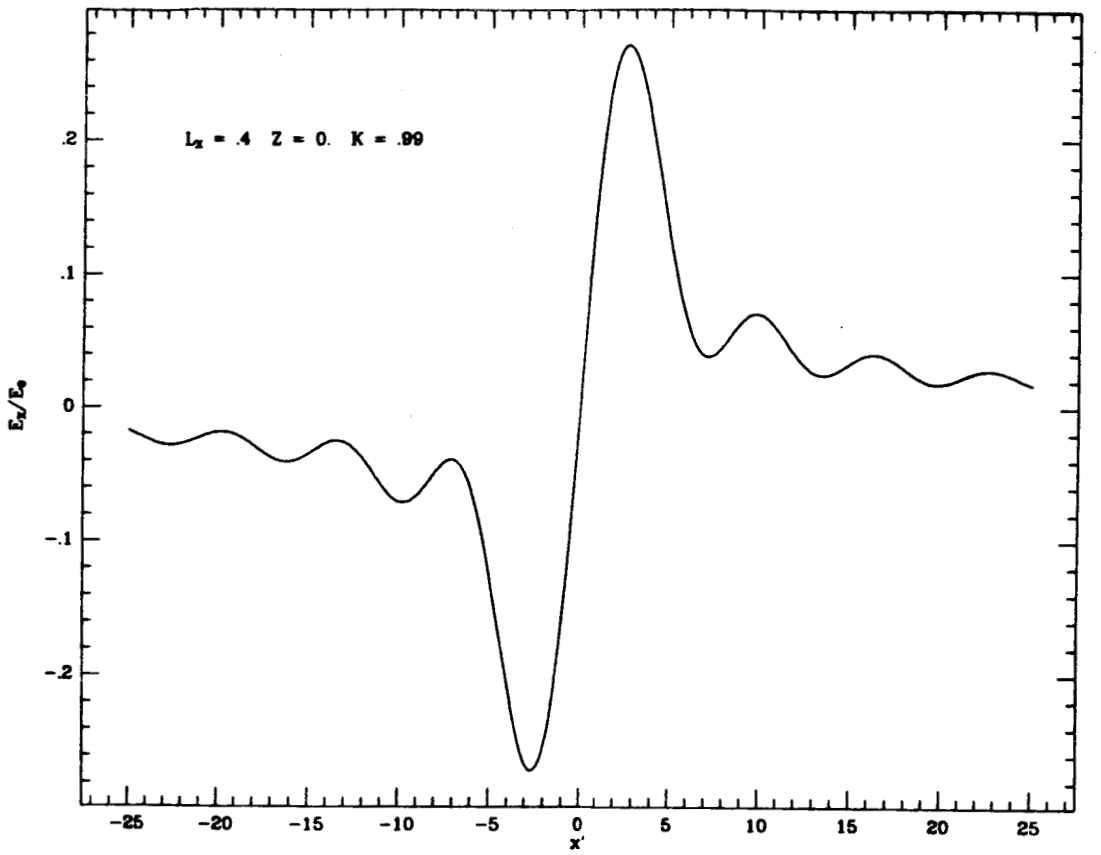

Figure 2.14. $E_x\overline{L}_x/E_o$ for $\overline{L}_x = 0.4$ and $z = 0$.

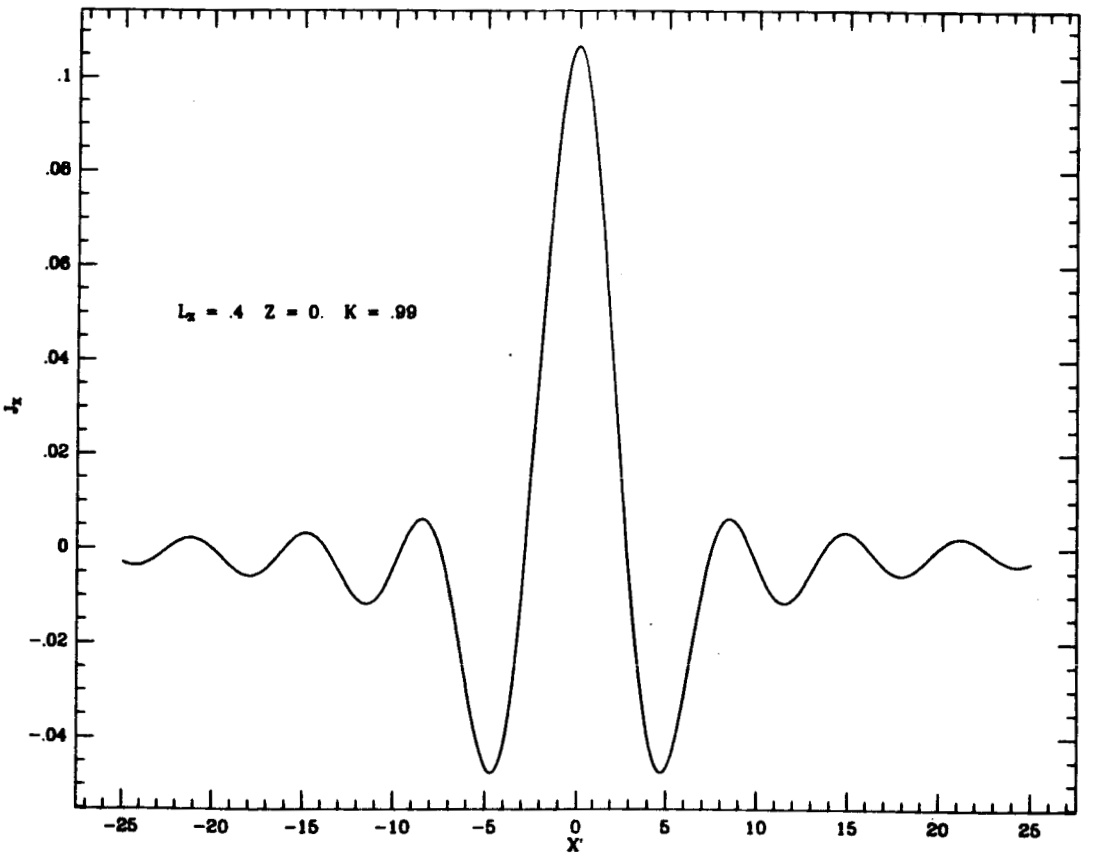

Figure 2.15. $J_x\overline{L}_x/J_o$ for $\overline{L}_x = 2$ and $z = 0$.

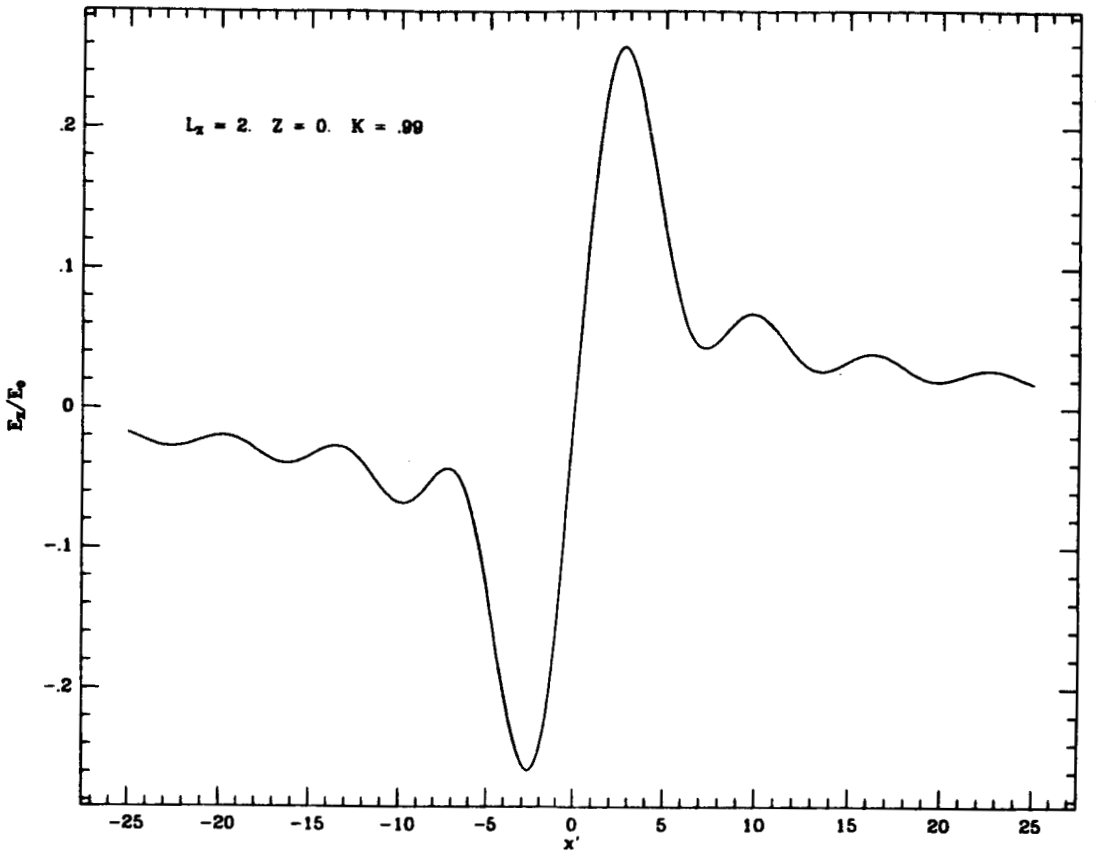

Figure 2.16. $E_z\overline{L}_z/E_o$ for $\overline{L}_z = 2$ and $z = 0$.

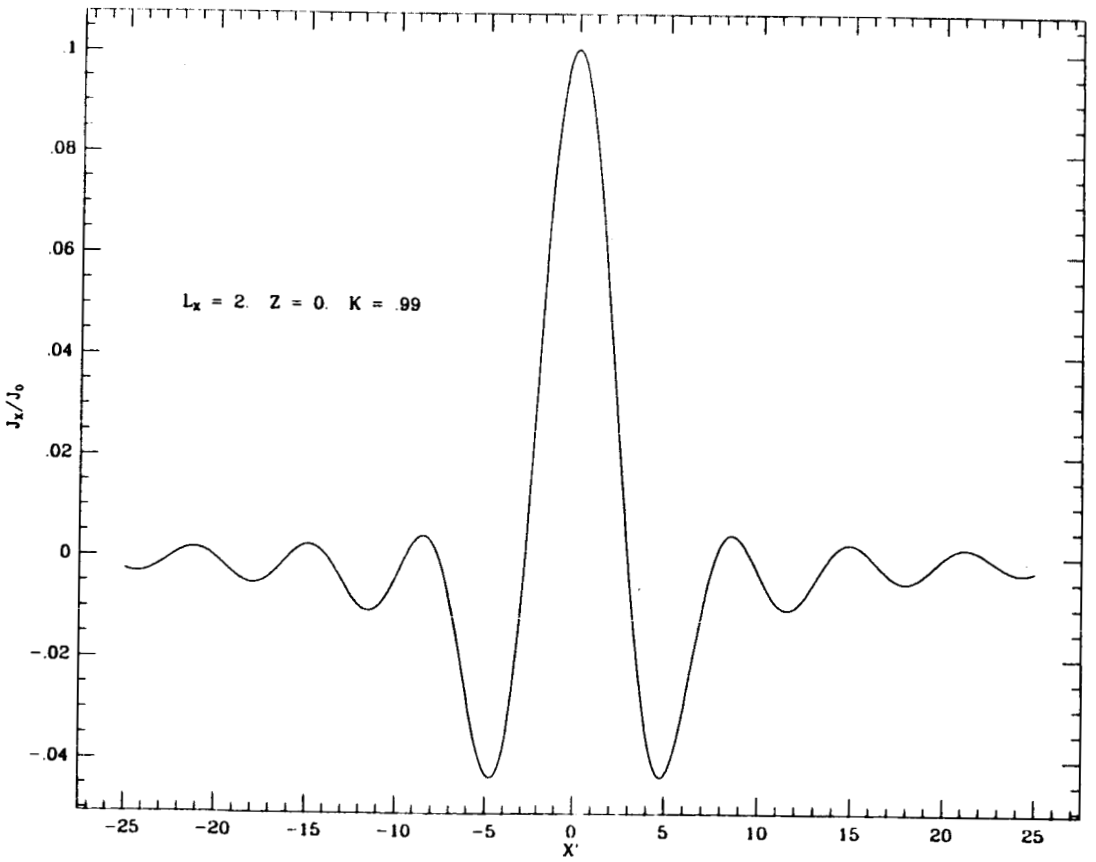

Figure 2.17. $J_z\overline{L}_z/J_o$ for $\overline{L}_z = 2$ and $z = 0$.

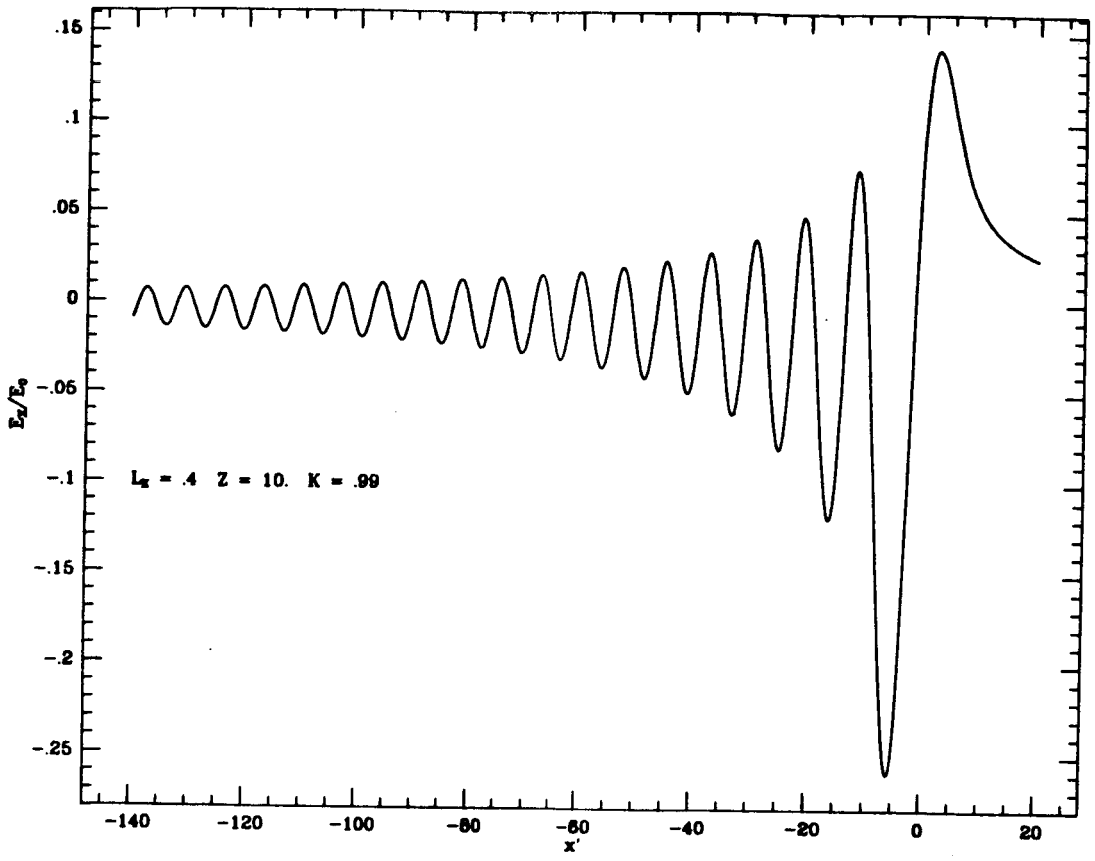

Figure 2.18. $E_x\overline{L}_x/E_o$ for $\overline{L}_x = 0.4$ and $\widetilde{z} = 10$: (a) $\Omega_{\max} = .99\Omega_{ci}$

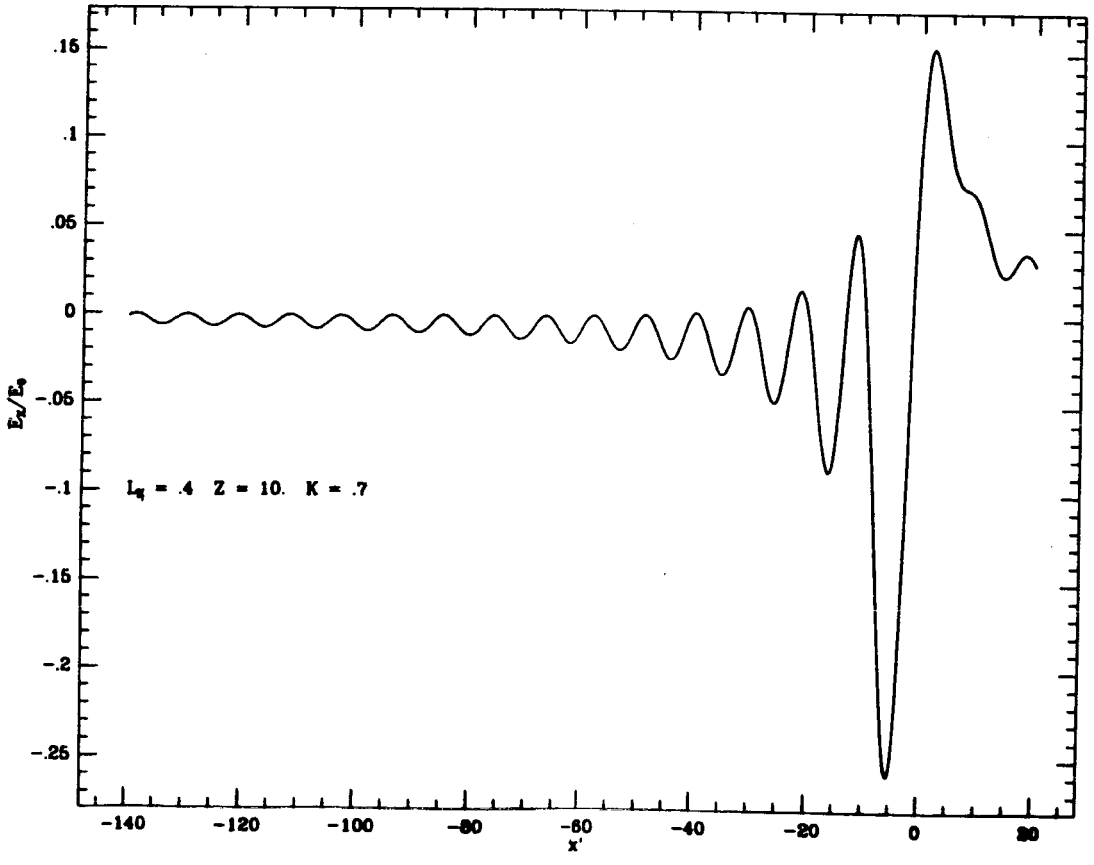

Figure 2.18. $E_x\overline{L}_x/E_o$ for $\overline{L}_x = 0.4$ and $\widetilde{z} = 10$: (b) $\Omega_{\max} = .7\Omega_{ci}$

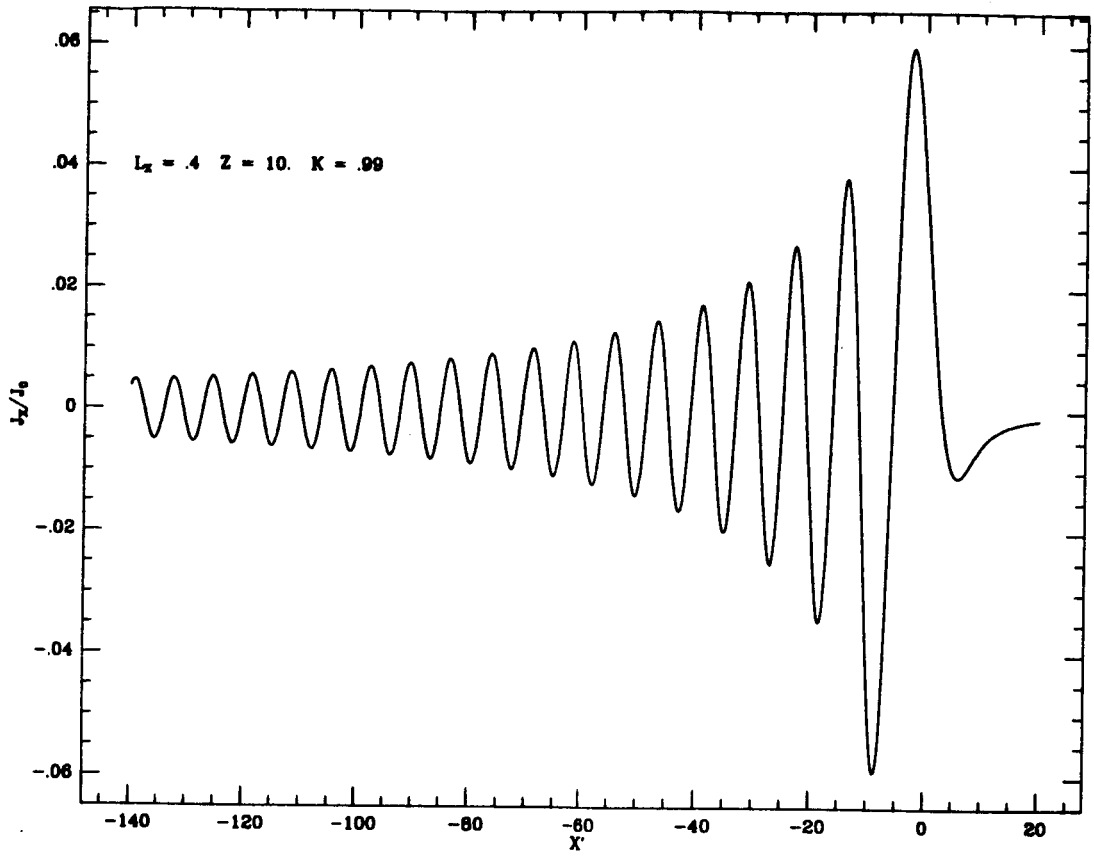

Figure 2.19. $J_x\overline{L}_x/E_o$ for $\overline{L}_x = 0.4$ and $\widetilde{z} = 10$: (a) $\Omega_o = .99\Omega_{ci}$

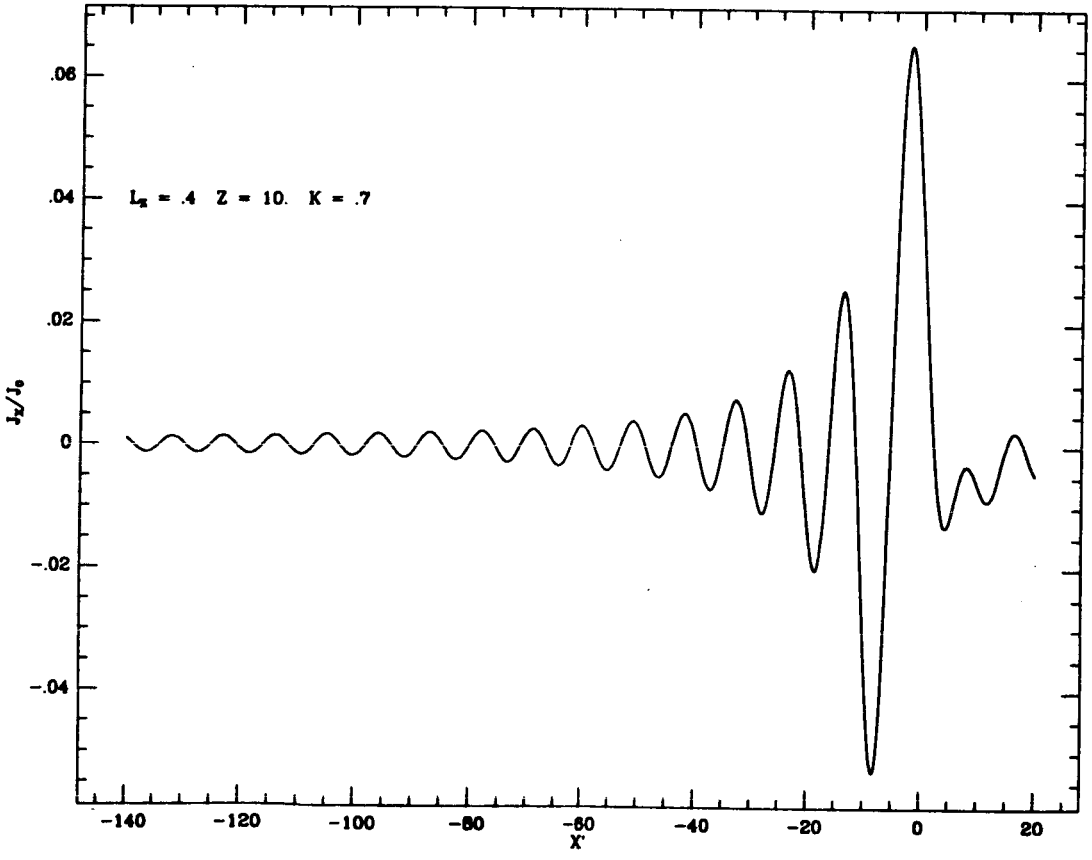

Figure 2.19. $J_x\overline{L}_x/E_o$ for $\overline{L}_x = 0.4$ and $\widetilde{z} = 10$: (b) $\Omega_o = .7\Omega_{ci}$

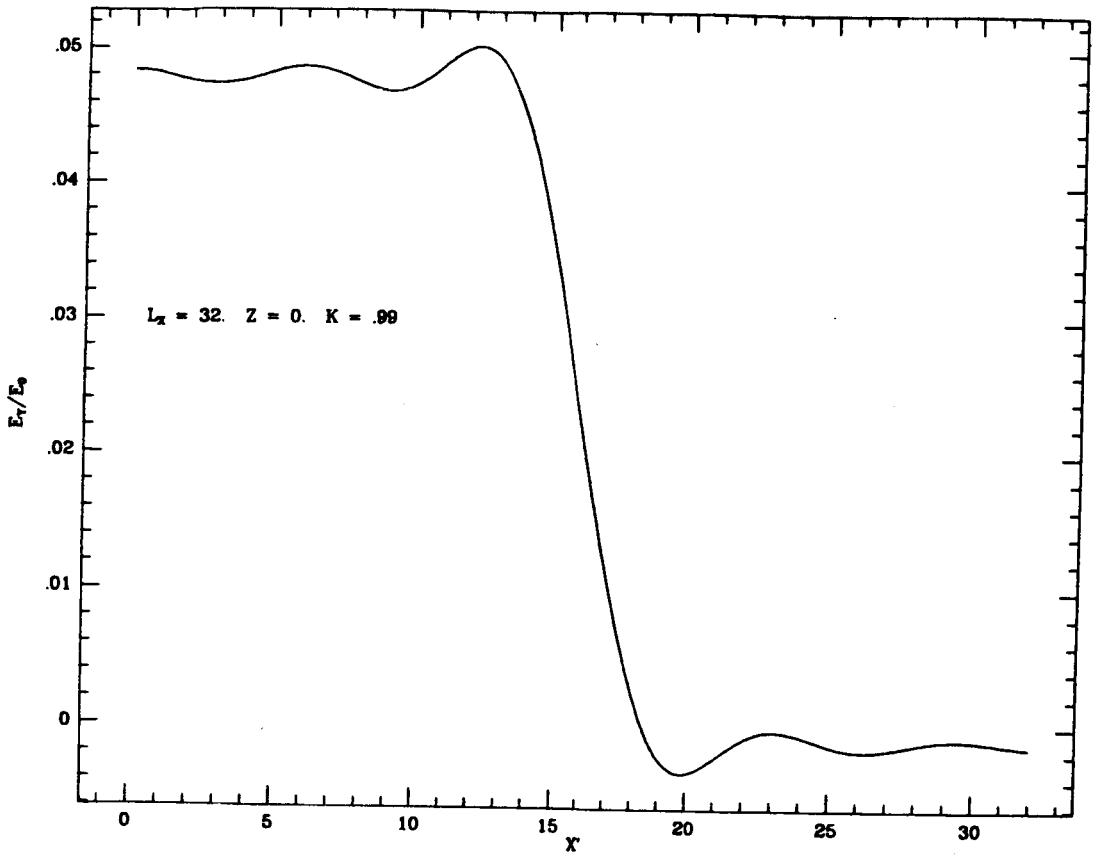

Figure 2.20. $E_y\overline{L}_x/E_o$ for $\overline{L}_x = 32$ and $\widetilde{z} = 0$

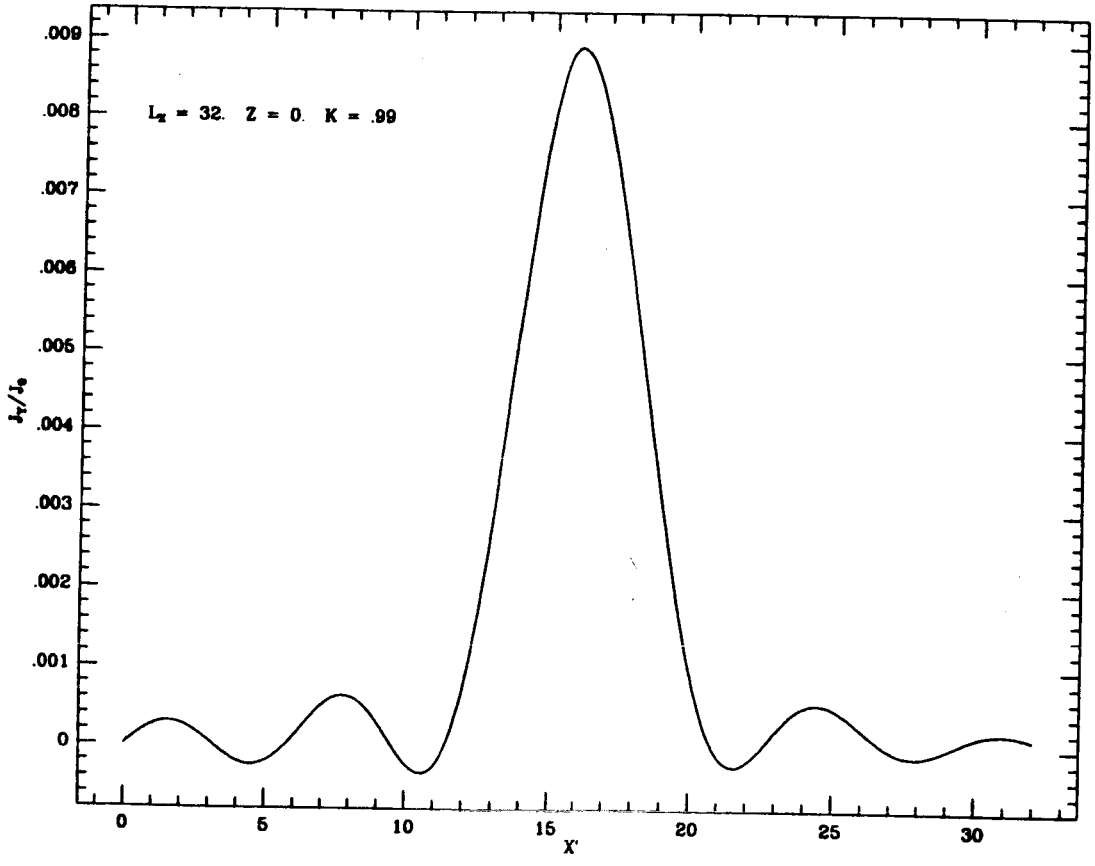

Figure 2.21. $J_y\overline{L}_x/E_o$ for $\overline{L}_x = 21$ and $\widetilde{z} = 0$

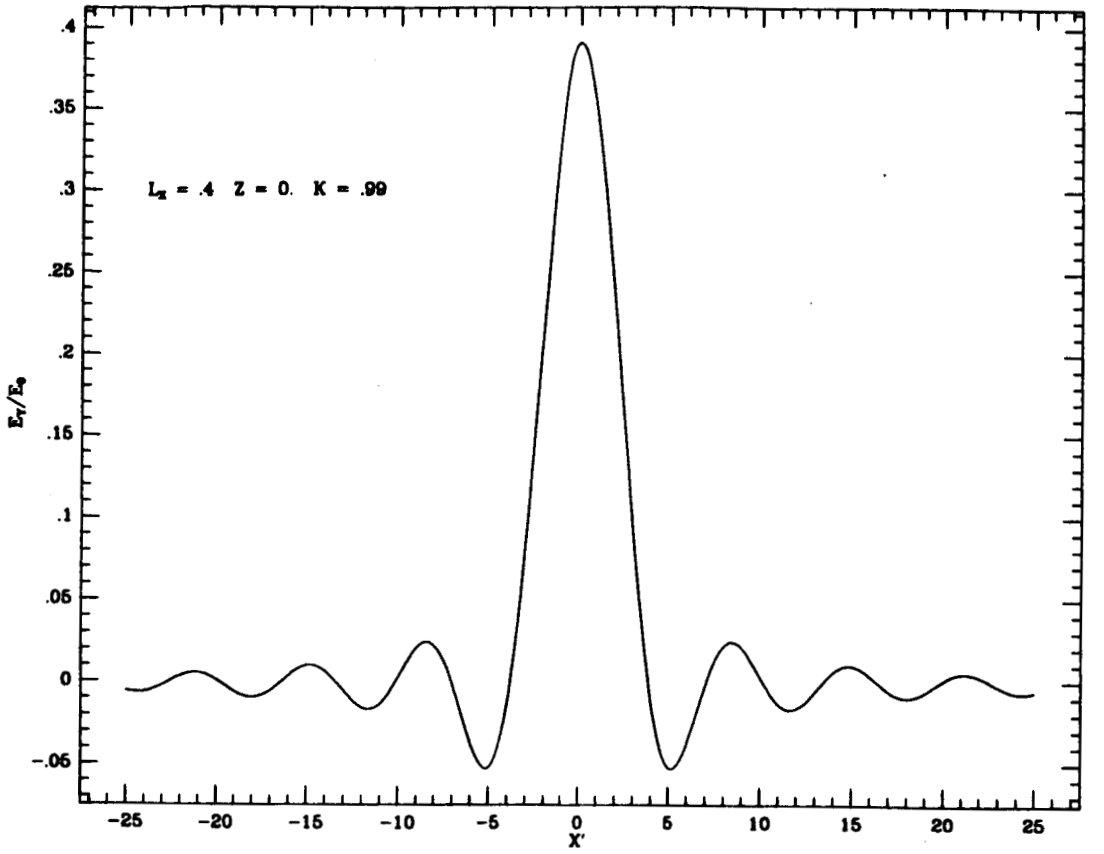

Figure 2.22. $E_y\overline{L}_z/E_o$ for $\overline{L}_z = 0.4$ and $z = 0$.

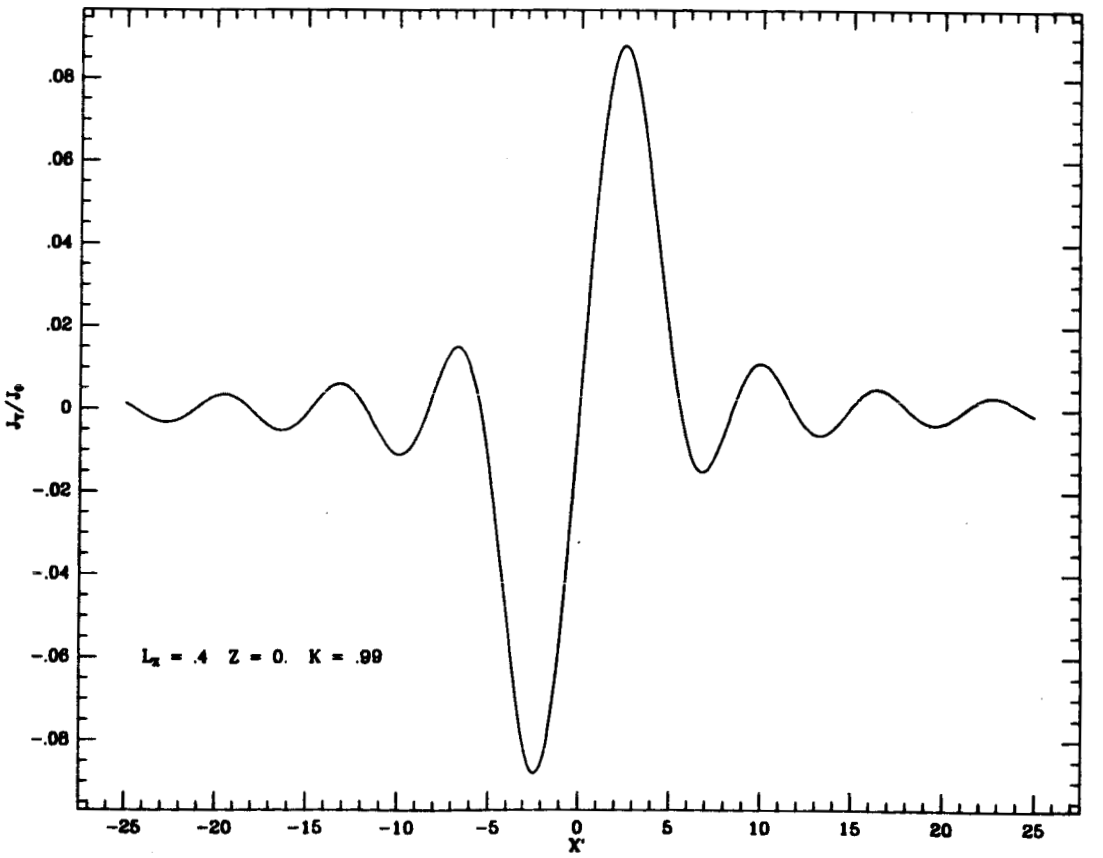

Figure 2.23. $J_y\overline{L}_z/J_o$ for $\overline{L}_z = 2.0$ and $z = 0$.

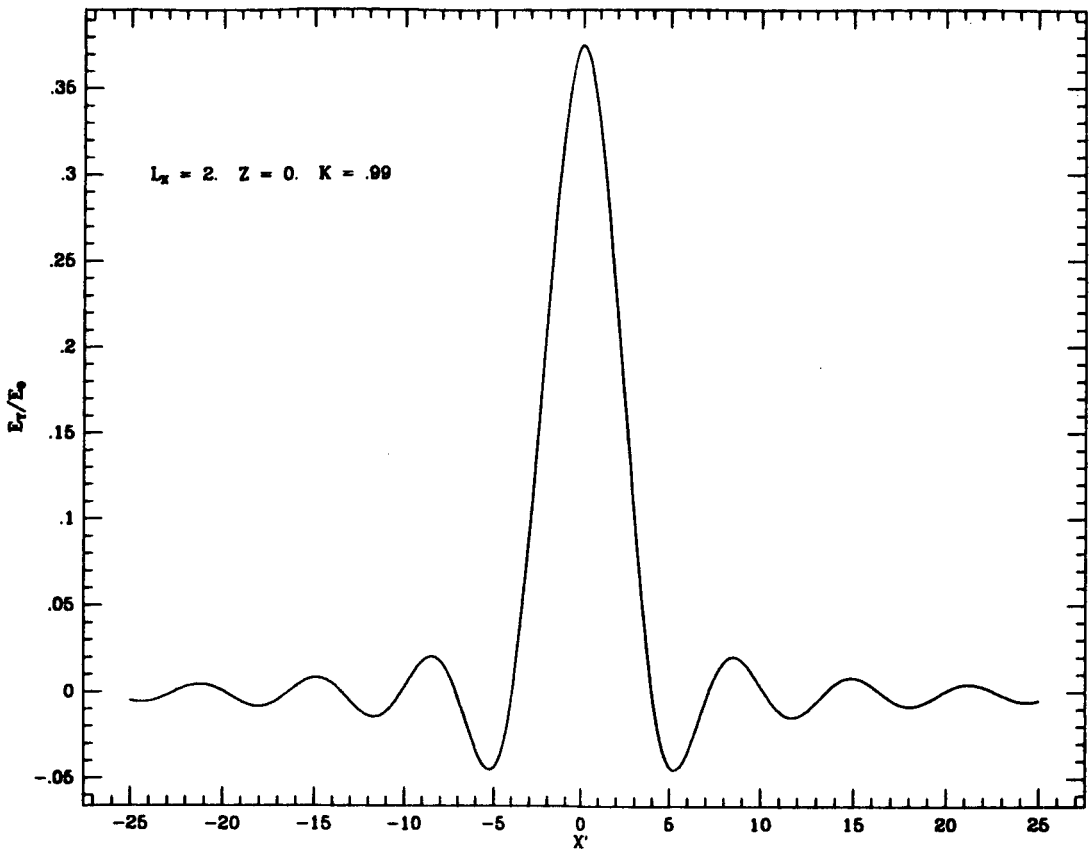

Figure 2.24. $E_y\overline{L}_x/E_o$ for $\overline{L}_x = 2.0$ and $z = 0$.

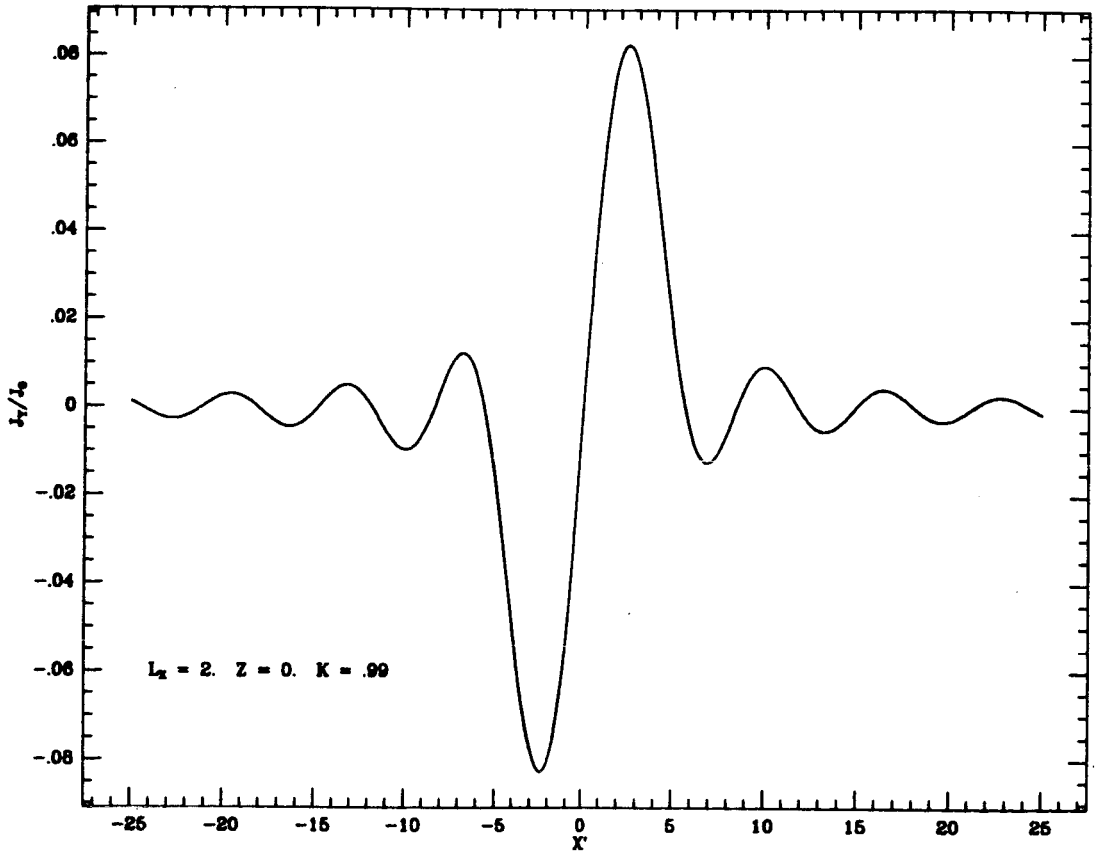

Figure 2.25. $J_y\overline{L}_x/J_o$ for $\overline{L}_x = 2.0$ and $z = 0$.

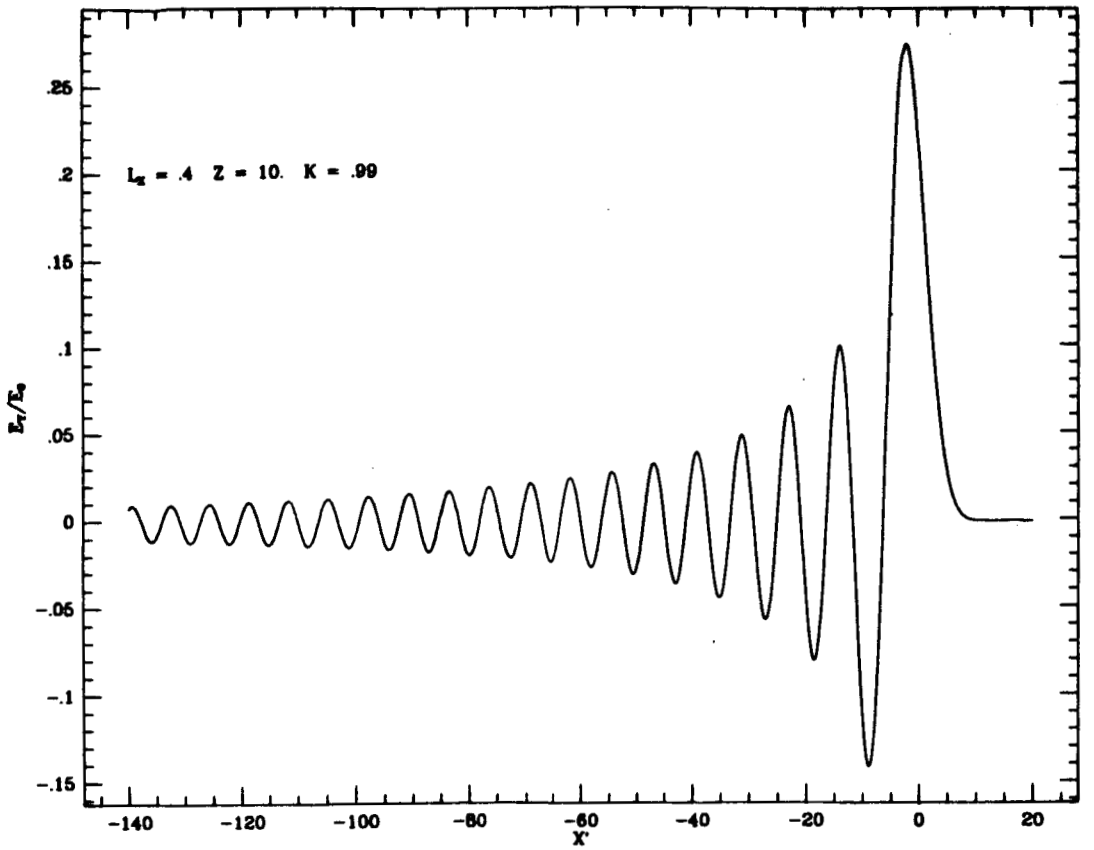

Figure 2.26. $E_y\overline{L}_z/J_o$ for $\overline{L}_z = 0.4$ and $\widetilde{z} = 10$: (a) $\Omega_o = .99\Omega_{ci}$

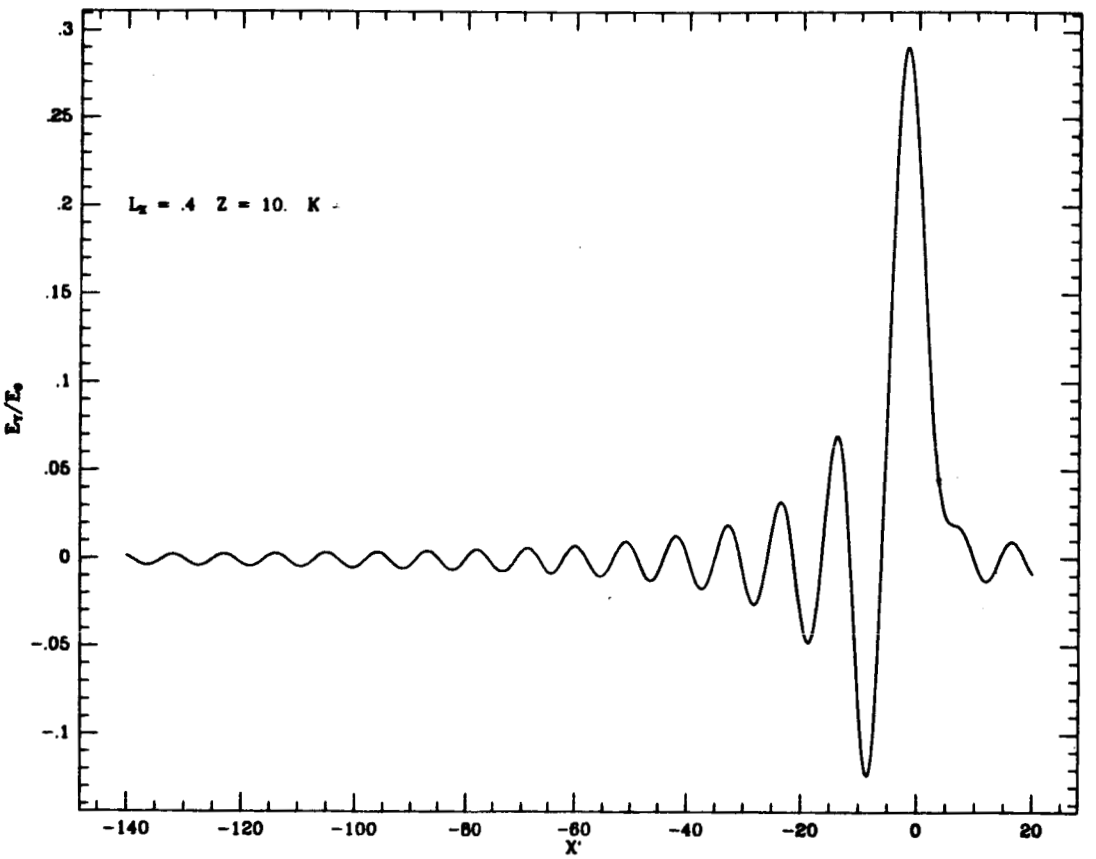

Figure 2.26. $E_y\overline{L}_z/J_o$ for $\overline{L}_z = 0.4$ and $\widetilde{z} = 10$: (b) $\Omega_o = .7\Omega_{ci}$

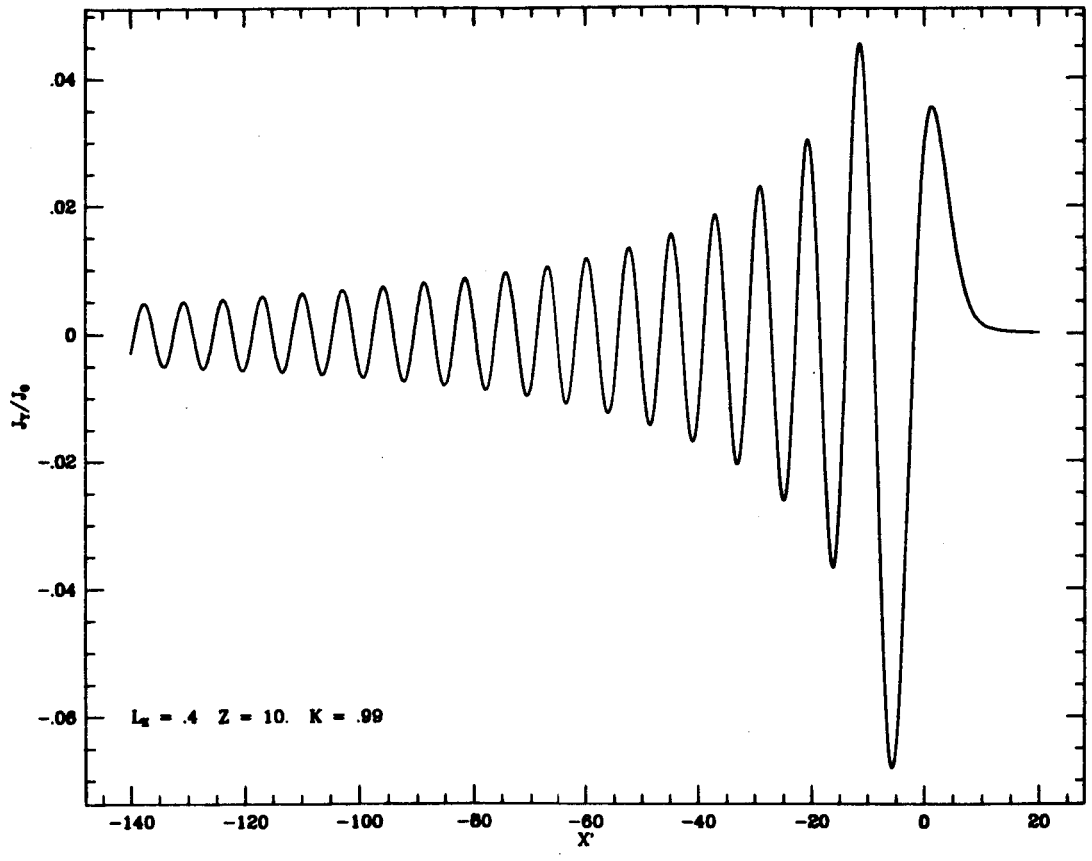

Figure 2.27. $J_y\overline{L}_z/J_o$ for $\overline{L}_z = 0.4$ and $\widetilde{z} = 10$: (a) $\Omega_o = .99\Omega_{ci}$;

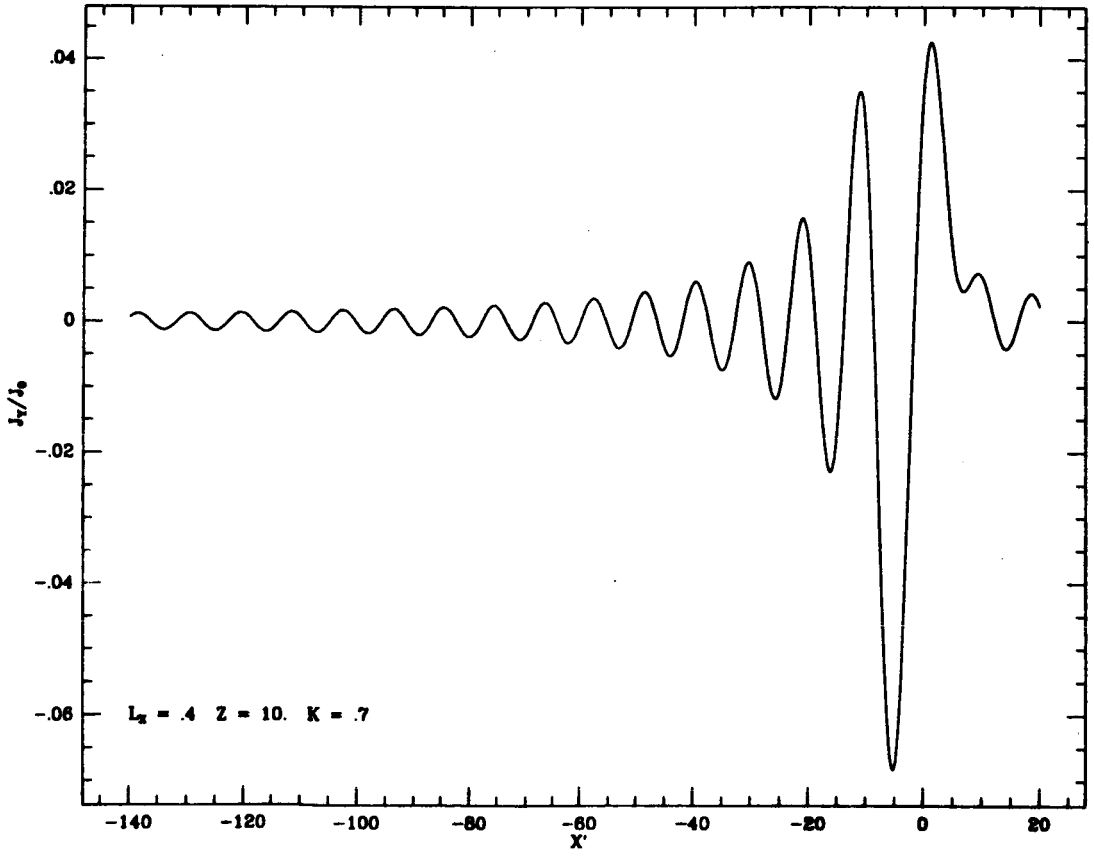

Figure 2.27. $J_y\overline{L}_z/J_o$ for $\overline{L}_z = 0.4$ and $\widetilde{z} = 10$: (b) $\Omega_o = .7\Omega_{ci}$

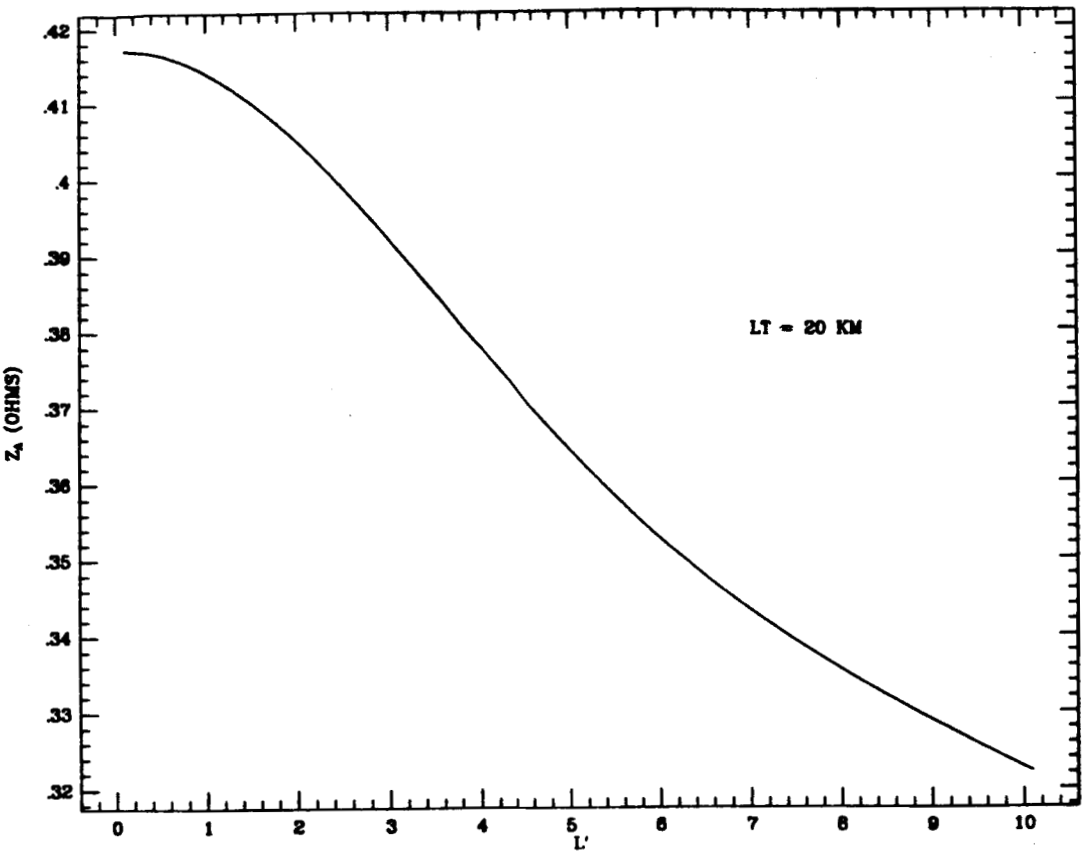

Figure 2.28. Wave impedance as a function of $\overline{L}_z$ for $\overline{L}$ = 800 (L = 20 km at F-region maximum).

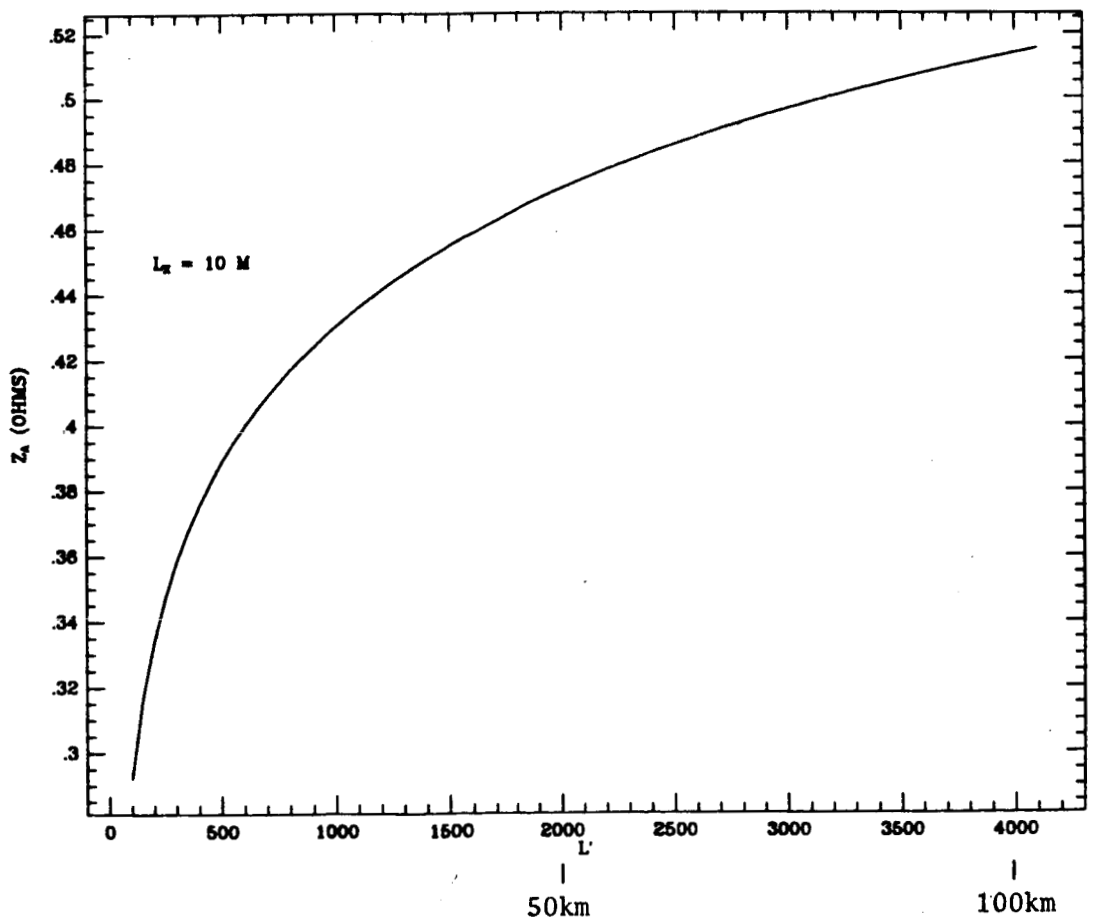

Figure 2.29. Wave impedance as a function of $\overline{L}$ (one unit $\simeq$ 25m) for $\overline{L}_z$ = 0.2.

3.0 SYSTEM APPLICATION STUDY*

3.1 Introductory Remarks

To search for and to identify a variety of system applications of the spaceborne tether (that NASA is developing at present at a substantial level of funding) is a focus of activity for NASA's Advanced Programs Office in Code M, and for the NASA-Intercenter "Tether Application Working Group," chaired by Georg F. von Tiesenhausen, of MSFC. This search is, undoubtedly, a good strategy to assure adequate return on the R&D investment being now made.

An application of orbiting tethers that has the potential of providing the U.S. Navy with a new option to implement ELF/ULF strategic communications with deeply-submerged submarines ("bell rings" function) is the use of the tether as a self-powered generator/radiator of electromagnetic waves in the ULF/ELF band (Grossi, 1981, 1984).

The designers of suitable radiators have limited thus far their efforts to the ELF band and have considered solely ground-based configurations. The unusually large radiators that are required have been the object of a long-lasting controversy: their societal acceptability has proved to be problematic, mostly because of their environmental impact. These problems have held back, in fact, their full scale development for more than two decades.

Some historical background may be of interest. The large ELF ground antenna proposed in the mid '60s for Project SANGUINE was supposed to be installed in Wisconsin and to cover there an area of 13,750 km^2 of low

*Contributed by M.D. Grossi

conductivity soil. It was designed to use a total wire length of about 1,000 km, with the wire cut in 10 segments, each about 100 km long, with all segments parallel and spaced 10 km apart. A total of 100 transmitter modules would have required a primary power of 25 Megawatt. Current in the wire was supposed to reach 77.1 A, with a total electric moment of 7.71 10^8 Am.

Of the smaller SEAFARER antenna, also in the ELF band, two versions were designed in the mid '70s, one for installation in Wisconsin and one in Michigan. The Wisconsin antenna was supposed to have a total wire length of 750 km and to cover an area of 3,368,75 km^2. All wire segments were supposed to be parallel and spaced about 1 km apart, with a total of 40 terminal grounds. A set of four transmitters required a 5 MW primary power line. The Michigan antenna was designed to use a total length of 649.37 km buried wire and to cover a 4,550 km^2 area. Wire segments were supposed to be all parallel and spaced 8.37 km apart, with a total of 66 terminal grounds. The required level of primary power was 5 MW.

Because of societal opposition against the large ELF antennas above, "Austere ELF" antenna concepts were elaborated upon, in the late '70s. A proposed scheme would use the ELF antenna that exists at Clam Lake, Wisconsin. It is a center-driven, end-grounded, telephone-pole-mounted wire configuration, with a limit of 300 A wire current imposed by environmental constraints. The plan was to feed this antenna with a transmitter that was phase-locked, via telephone line, to a similar transmitter at a planned ELF installation of K.I. Sawyer AFB, Michigan, that is 265 km away. The latter's design would have consisted of three arms, with length 48.5 up to 64.5 km, and with a total wire length of 210 km. This second installation, however, was never built, because of the opposition of the environmentalists. Only a very modest effort at ELF is at

present carried out by the U.S. Navy. It uses the so-called Propagation Validation System (PVS), with the transmitting terminal consisting of the ground-based antenna/radiator of the Clam Lake, Wisconsin Test Facility (WTF) mentioned above.

The ecological problems virtually vanish when the radiator is spaceborne. The closest point on the Earth surface would be illuminated with a signal that under the most favorable conditions of propagation, would still be weak enough to be of no ecological concern whatsoever.

However, considering now the obvious limitations in size and mass of an orbiting system (particularly severe, when we take into consideration how large the ground-based ELF mechanizations are), we must now make sure that we radiate from orbit enough power to provide a signal intensity of practical interest on the Earth surface, at ELF/ULF (we add here the ULF frequencies because we expect that there will be a substantial amount of energy that is radiated in that band by the orbiting system).

We have also to make sure that the lifetime of the orbiting system is six months at least, in order to meet U.S. Navy operational requirements. We must recognize that in the case of spaceborne ELF/ULF, performance and lifetime are related. The reasoning behind this statement is as follows. It would be impractical, if not outright impossible, to install in the spaceborne terminal: a) an antenna; b) a transmitter; and c) a primary power plant, all of the necessary size and mass. To save mass and volume, we are therefore compelled to use the antenna (a vertical wire, 20 to 100 km long) as a self-powered generator capable, in principle, of producing primary power levels in the hundreds of kilowatts. This is, however, at the expense of the orbital energy of the vehicle, thus at the

expense of its orbital height. The self-generated tether current could also be modulated so that the electromagnetic emissions of the tether could carry information, to be conveyed downward to the Earth surface and received by underwater terminals. This way, the tether-antenna (item a above) would also perform the function of the spaceborne transmitter (item b) and of the primary power plant (item c), with considerable saving in equipment.

However, if no special provisions are taken, the orbiting vehicle that carries the ELF/ULF transmitting terminal would deorbit in a few hours owing to the severe electrodynamic drag that accompanies the self-powered operation of the system. We could deploy in orbit vehicles with the long tether antennas stored in their drums, keeping them dormant during peace time and deploying the long tethers only when a situation of emergency arises (this is the concept of the "orbiting cocoons"). However, even in this case, U.S. Navy operational requirements impose a lifetime of at least six months counting from the moment that the antenna is deployed. This lifetime is well beyond the few hours that would result from the "self-powered" operation of the antenna, if we do not perform any attempt at drag compensation.

A focus of our investigation has been on this essential point: to find a way of associating long orbital life with a self-powered operation of the tether. Once that a possible solution was identified, we proceeded to work-out the detailed configuration of the system. Concerning the level of <u>required</u> electric (DC) primary power to be generated by means of the $v \times B \cdot L$ mechanism and the level of <u>required</u> e.m. wave power to be radiated in the ionosphere by the tether-antenna, we have performed preliminary estimates in Section 3.2. Other areas of concentrations of our effort have been the conceptual design of a suitable signalling scheme for "bell rings" transmission, a preliminary analysis of the effects that

3.2 Basic Design Criteria

At ULF and ELF, the ionosphere performs as a refractive medium with an index of refraction that is about 100 at night and about 1000 in the daytime. Consequently, the wavelengths at the two extremes of the band under consideration are:

at 1 Hz	at 100 Hz
Wavelength = 3000 km by night 300 km by day	Wavelength = 30 km by night 3 km by day

The tremendous shortening of the wavelength from free-space conditions, imposes serious limitations to the validity of radiation models that could be otherwise effective in describing the e.m. performance of large metal structures in space, such as the electrodynamic tether, the two-dimensional structures that are under investigation at our Observatory, etc.

For instance, in the case of a vertical electrodynamic tether, the phantom loop model of Figure 3.1 could be considered as suggestive of an equivalent magnetic dipole of large magnitude, $I \times A \simeq I \times 4 \times 10^{10}$ Amp.m^2, corresponding to a 4×10^{11} Amp.m^2 moment for a tether current of 10 A.

However, the radiation diagram of a magnetic dipole, for a radiator to be of practical use, must be characterized by the presence of no more than two maxima and two minima. In order to achieve this, the circumference of the area A of the loop must be $\leq \lambda/4$. For the frequency of 1 Hz, and for a night time ionosphere, the phantom loop of Figure 3.1 does meet these conditions (barely), while it does not satisfy them in the day time ionosphere. Then, for frequencies

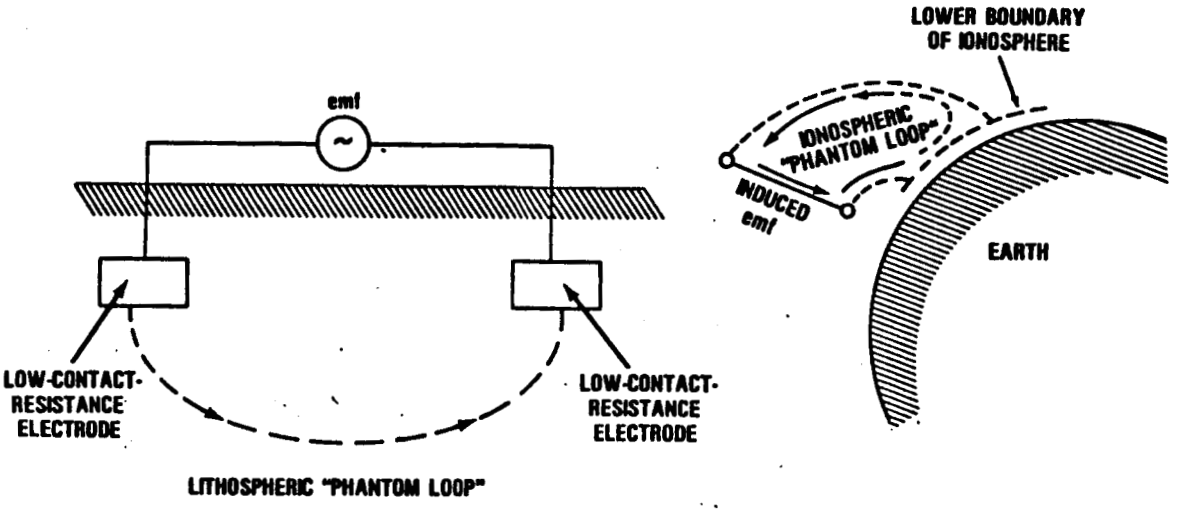

(A) Ground-based antenna

(B) Spaceborne antenna (using a vertical tether)

Figure 3.1 - "Phantom Loop" Antenna Concept

However, the radiation diagram of a magnetic dipole, for a radiator to be of practical use, must be characterized by the presence of no more than two maxima and two minima. In order to achieve this, the circumference of the area A of the loop must be $\leq \lambda/4$. For the frequency of 1 Hz, and for a night time ionosphere, the phantom loop of Figure 3.1 does meet these conditions (barely), while it does not satisfy them in the day time ionosphere. Then, for frequencies larger than a few hertz, the condition above is not met neither by night, nor by day. Because the most useful frequencies in potential system applications to communications are the frequencies of a few tens Hertz, a reliable estimate of the equivalent magnetic dipole moment can be performed only for two-dimensional structures made with wire, such as the tethered structures under study at our Observatory, under the terms of another contract from NASA/MSFC. Figure 3.2 and 3.3 depict two examples of such structures, one rectangular in shape, and one elliptical, both stabilized by electrodynamic forces (interaction with the geomagnetic field of a DC current in the wire, with the plane of the structure perpendicular to the line of force). We must still meet the condition that the circumference be smaller than 1/4 of the wavelength. At 75 Hz, the radius r of the loop must be such that

$$
\begin{aligned}
r &\leq \frac{\lambda}{4} \quad \frac{1}{2\pi} \\
&\leq \frac{4 \ km}{4} \quad \frac{1}{2\pi} \quad (by \ day) \\
&\leq 159 \ m \ (by \ day)
\end{aligned}
$$

In order to accomplish this, a large loop such as the one of Figure 3.3 must be subdivided in elementary loops, each one meeting the conditions above (see Figure 3.4, for a possible scheme). Each elementary loop must then be fed with

the appropriate amplitude and phase, in order to achieve the desired radiation diagram. By assuming (pessimistically) that we do not achieve any antenna gain by the phasing of the elementary loops, the 75 Hz signal intensity that is achievable at the Earth surface is shown in Figure 3.5. By adopting for the background noise the values indicated in Figure 3.6, we will achieve threshold conditions (SNR=1) at a distance along the Earth surface of about 5 Megameters from the point of maximum illumination (roughly, from the vertical of the ionospheric exit point of the e.m. waves). Tether current is assumed here to be 20 A (curve (b)). More realistically, the gain achievable at 75 Hz with the arrangement of Figure 3.4, when the number of elementary loops is 177, is 45 dB. This provides a hefty SNR in 1 Hz bandwidth, the latter being quite adequate for the communications application. There is also another consideration to make, concerning the background noise of Figure 3.6. Recent results of noise abatement with the least-squares liner predictor developed at DREP, Victoria, Canada (Barrodale and Erickson, 1980 (a) (b)) are indicative of the strong possibility of a noise reduction of at least 20 dB, thus further improving the outlook of the expected value of SNR. One of the possible ways to utilize this extra margin is to reduce the tether current, or to increase the area of Earth surface illumination of a single orbiting source, or both.

(The tethers are all aluminum and have the same diameter)

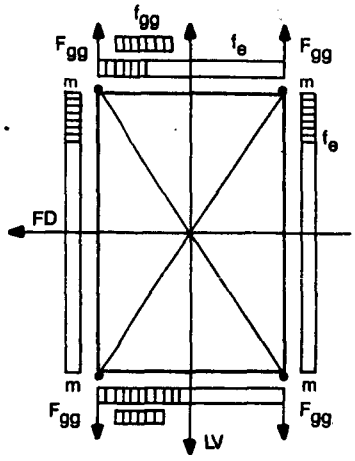

*T(N)	V = Electro Motive Force (kV)	h(km)	l (km)	Diameter Conductive Tether (mm)	Current (Amp)	Power (kW)	Solar Panel Area (m^2)	**Orbit Decay (km/day)
0.06	13.80	10	20	0.21	0.2	2.76	20.0	1.61×10^{-2}
0.1	13.80	10	20	0.27	0.33	4.55	32.5	1.83×10^{-2}
0.2	13.80	10	20	0.38	0.67	9.23	66.0	2.39×10^{-2}
0.3	13.80	10	20	0.47	1.01	13.80	98.6	2.93×10^{-2}
0.6	13.80	10	20	0.67	2.03	27.98	199.9	4.55×10^{-2}

Figure 3.2 - A first example of two-dimensional structure in orbit, using tethers. Stabilization is achieved by electrodynamic forces. Loop usable as magnetic dipole antenna.

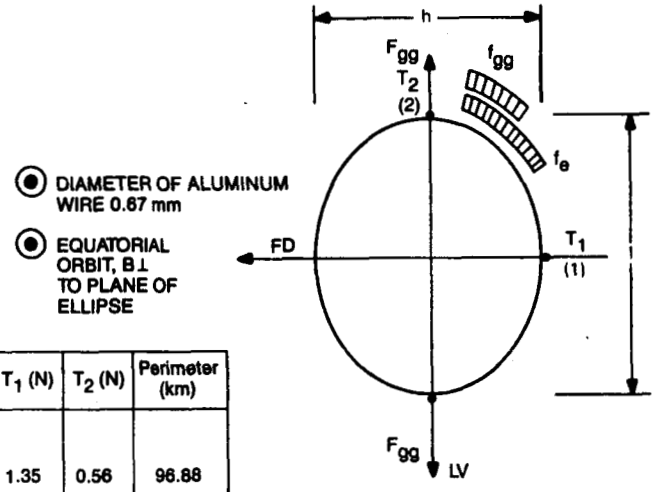

	Current (Amp)	Voltage (kV)	T_1 (N)	T_2 (N)	Perimeter (km)
Case 1 h = 20 km ℓ = 40 km)	1.130	12.4	1.35	0.56	96.88
Case 2 h = 10 km ℓ = 20 km	0.565	3.10	0.339	0.141	48.44

Figure 3.3 - A second example of two dimensional structure in orbit, using a wire deployed in a pseudo-elliptical loop. Stabilization is achieved by electrodynamic forces. Loop usable as a magnetic dipole antenna.

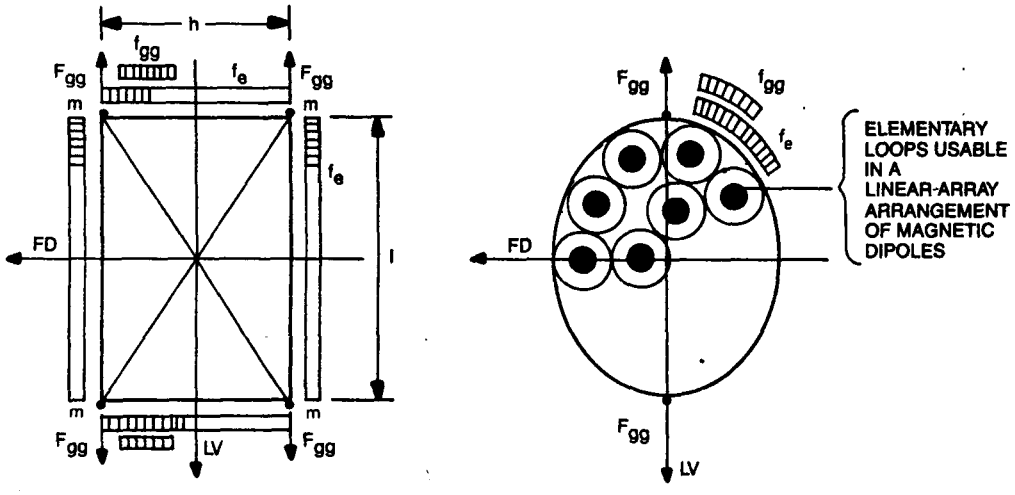

Figure 3.4 - Two-dimensional tethered structure (where shape stability is provided by electrodynamic forces), with area subdivided in elementary loops, usable (when fed with appropriate amplitude and phase) in a linear-array arrangement of magnetic dipoles.

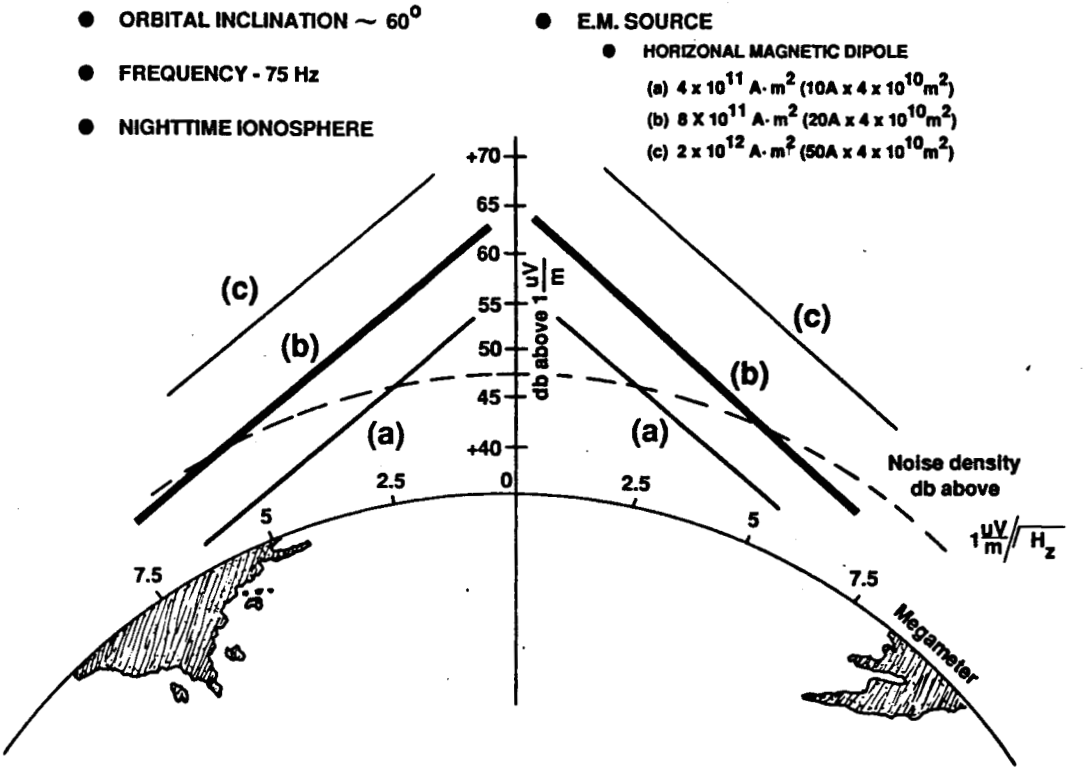

Figure 3.5 - Signal intensity at ELF as a function of distance from vertical of maximum illumination.

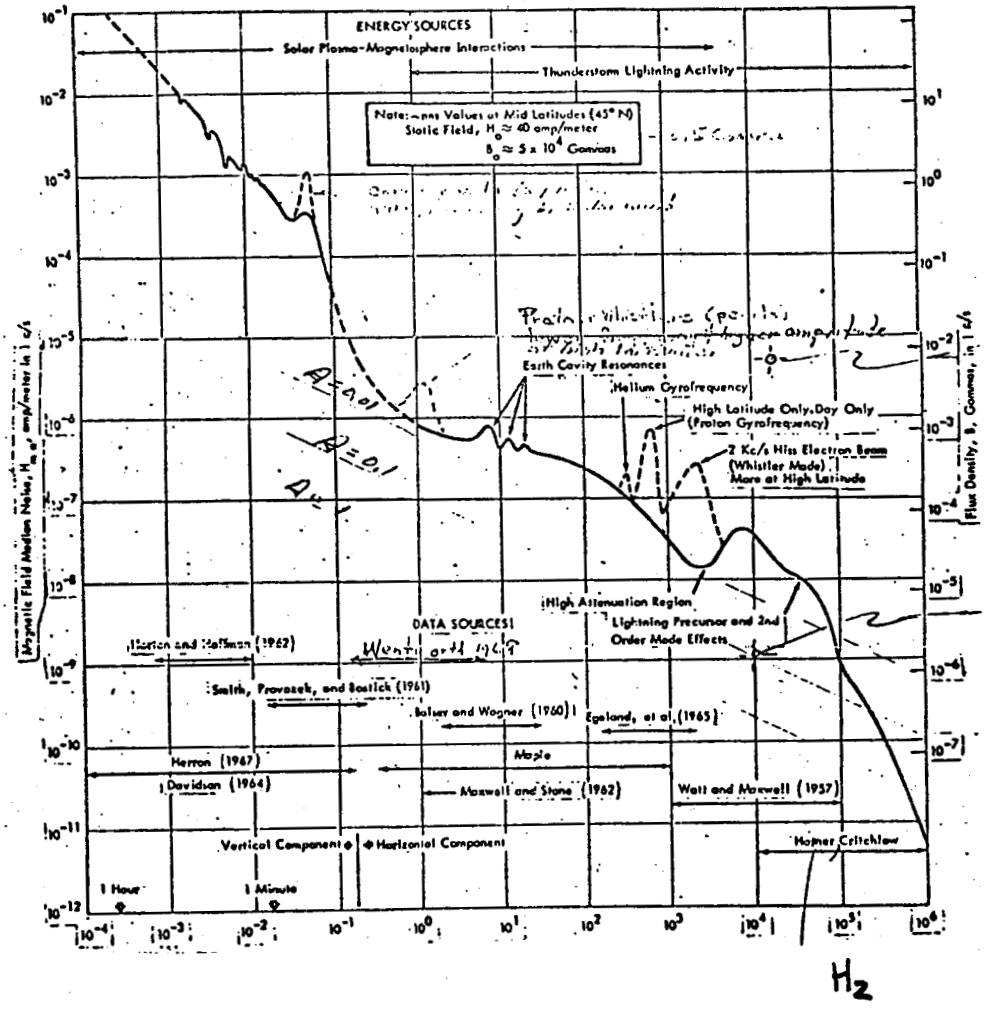

Figure 3.6 - Spectral density curve of geophysical noise from 10^{-4} Hz to 10^{6} Hz. On the left-side y-axis, the units are At/m/$\sqrt{\text{Hz}}$. On the right-side y-axis, the units are Gamma/$\sqrt{\text{Hz}}$.

Note: We remind that 1 gamma = 10^{-5} gauss = 10^{-9} Weber/m^2. Also: 1 gamma = -62 db with respect to 1 At/m = 7.9433 10^{-4} At/m

The SNR outlook is less favorable when considering as generator a vertical electrodynamic tether. Figure 3.7 shows the expected signal intensity, at the Earth surface, for a 100 km tether used at 75 Hz as a vertical antenna in a 500 km orbit, and with a tether current of 31.8 Amp. Even at a distance from the vertical of maximum illumination of only 500 km, the signal is less than $6\mu V/m$ (15 dB above 1 μV/m), and this corresponds to a e.m. wave magnetic field of $6\times10^{-6}/377 = 1.5\times10^{-8}$ At/m, while Figure 3.6 shows that the background noise at 75 Hz is about 5×10^{-7} At/m, or a factor of 30 dB higher!!! Therefore, while a vertical electrodynamic tether is adequate for a feasibility experiment in which the bandwidth of the receiver can be narrowed adequately, it could not be used in a link with a bandwidth of about 1 Hz, as it is at present practiced in strategic communications. Adequacy of the vertical electrodynamic tether must be therefore predicated on the feasibility of adopting a noise abatement scheme and of achieving a processing gain larger than 30 dB. This is not totally out of the question; in fact, an upper limit of 40 dB in noise reduction is under active consideration by the DREP group mentioned before.

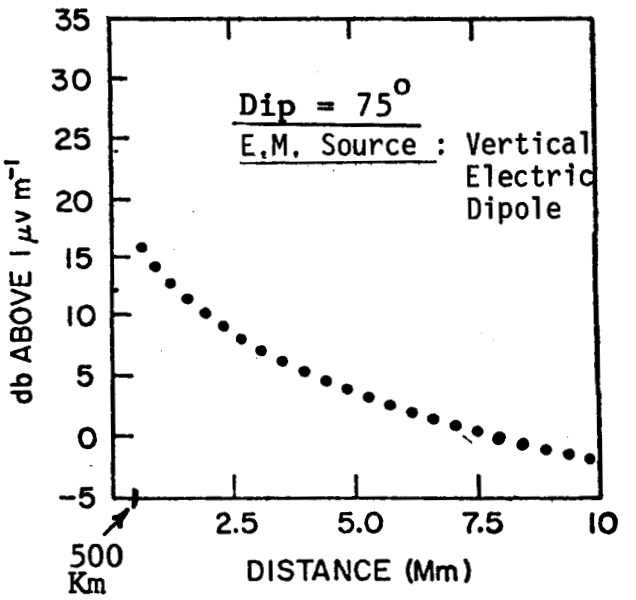

Note: Dip is 0° at magnetic equator

Figure 3.7 - Signal intensity as a function of distance from vertical of maximum illumination, on the Earth surface; Frequency = 75 Hz; 100 km vertical tether in a 500 km orbit; Tether current = 31.8 Amp; Moment = 3.18×10^6 A.m. (Pappert, 1973).

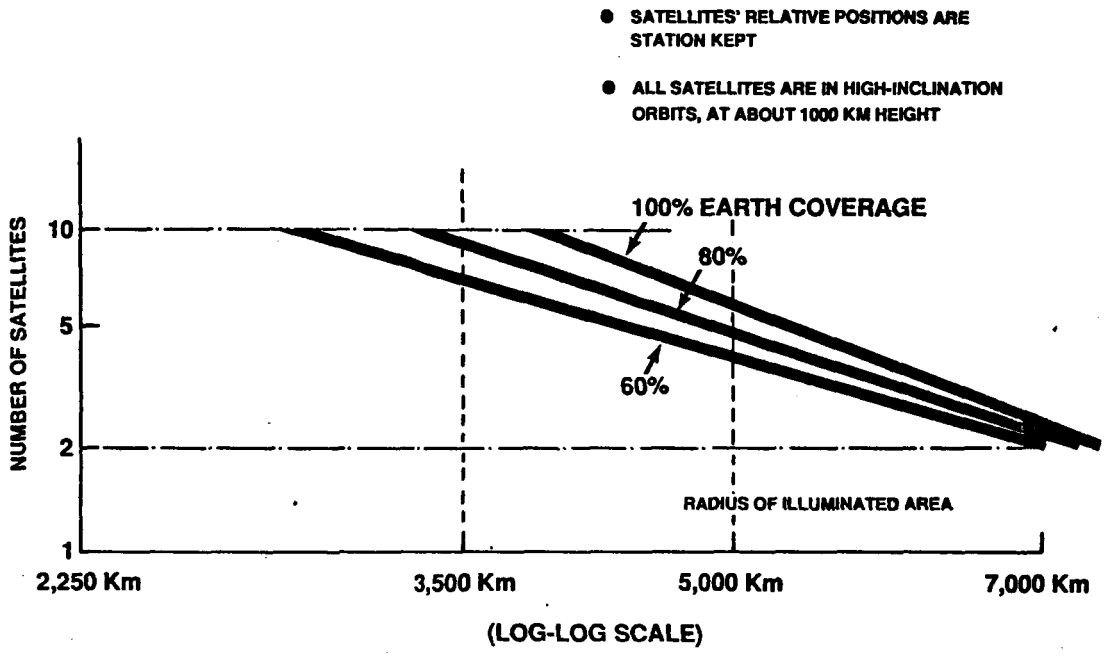

Figure 3.8 - Number of satellites required to cover the Earth surface, as a function of the area illuminated by each satellite.

1st Example Orbital altitude H = 220 km, M = 2×10^3 kg

$B \simeq 0.3\times10^{-4}$ Weber/m^2

$\Omega = 1.178\ 10^{-3}$ rad/sec, $\ell = 5\times10^4$m, I = 4A

$F = B\ I\ \ell = 6$ Newtons ; $\frac{da}{dt} \simeq 440$ km/day

2nd Example Orbital altitude H = 500 km, M = 2×10^3 kg

$B \simeq 0.25\times10^{-4}$ Weber/m^2

$\Omega = 1.107\ 10^{-3}$ rad/sec, $\ell = 5\times10^4$m, I = 4A

$F = B\ I\ \ell = 5$ Newtons

$\frac{da}{dt} \simeq 390$ km/day

From the two examples above, it can be seen that in both cases, the lifetime is going to be of only very few hours. Therefore, it was essential for our project to conceive and adopt some form of electrodynamic drag compensation. This is what we did, as it will be illustrated in Section 3.2, by using the tether, sequentially in time, as a generator and as a motor. Figure 3.9 summarizes the results of our calculations for the orbital lifetime, with and without drag compensation. It can be seen that with the drag compensation approach that was initially proposed by Ivan Bekey of NASA Headquarters, the orbital decay for a fully deployed tethered satellite system is practically reduced to zero.

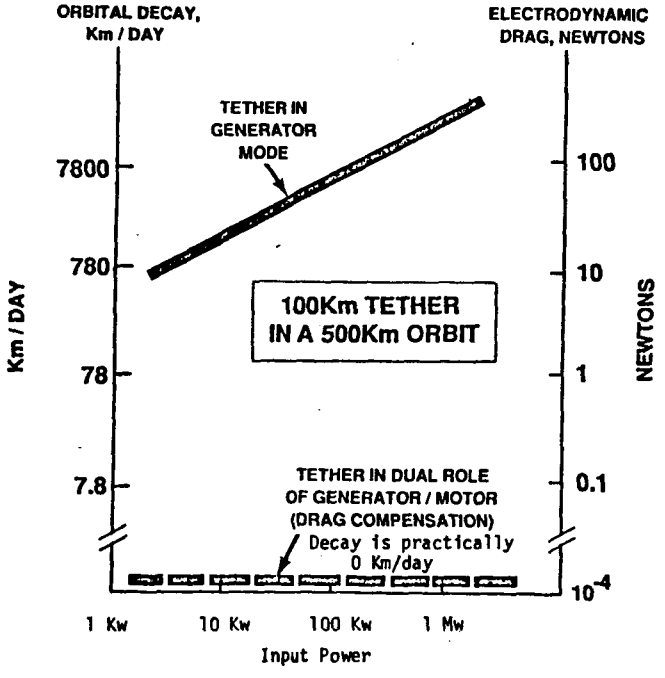

Figure 3.9 - Effect on orbital decay of drag compensation, by using, in time sequence, the electrodynamic tether as a generator and as a motor.

3.3 A Highlight Of The System Study: The Drag-Compensation Method

We approach the problem from the energetic standpoint, which gives us results that are independent of the specific type of energy storage or power transfer system that is used. This analytical approach has been conceived by SAO's David A. Arnold (1985).

We first consider the tethered system in its "natural" current drawing mode, i.e. in the phase for which current flows strictly due to the emf induced by the system's orbital motion across the terrestrial magnetic field. This is illustrated in Figure 3.10, where we assume an eastward motion and upward deployment. For simplicity of illustration, we show the case for which the tether (connecting satellite S and S_1), the magnetic field $\vec{B}$, and the orbital velocity $\vec{v}$ are mutually perpendicular. The results we obtain are completely general, however. A current i flows up the tether (electrons flowing down the tether). Current also flows through the ionosphere along magnetic field lines. We show this current as being evenly divided between the two directions along the field lines in Figure 3.10.

In the tether rest frame, the equivalent circuit is conveniently represented by Figure 3.11(a). The motion induced emf is shown as $V_B = vB\ell$, where ℓ is the tether length. R_t is the tether resistance, R_{ion} is the radiation resistance of the ionosphere, and Z_L is the load impedance of the system being used for energy storage on satellite S. We assume the contact resistances between the satellite S_1 and the ionosphere and between satellite S and the ionosphere are kept at negligible levels by the use of plasma contactors. This simplifying assumption is not essential. The D-C resistance R_t of the tether can be considered constant. For current levels below some critical value, at least, the radiation resistance should

also be nearly constant over a time interval short enough to maintain nearly constant values of plasma density and temperature. We assume that the time period T during which we draw the current in the "natural" mode satisfies this criterion.

In this case, the current i flowing in the tether-ionosphere current loop varies depending on the value of Z_L, the load impedance, since

$$i = \frac{V_B}{R_t + R_{ion} + Z_L} \tag{1}$$

This is the current that would flow due to a voltage

$$V' = V_B - i Z_L \tag{2}$$

if only the tether and ionosphere were considered, as shown in Figure 3.11(b). This, then, is the voltage we have to obtain in the reverse sense if we want to have the current reversed, but with the same absolute value, in the second phase of operation.

We desire this in order to gain an electrodynamic thrust that makes up for the drag experienced in the "natural" current phase of operation and to radiate electromagnetic waves from the tether functioning as an antenna.

The power into the load is $i^2 Z_L$. Assuming for the moment 100% efficiency, the total energy that is stored in the natural current phase is given by:

$$E_{STORED} = i^2 Z_L T \tag{3}$$

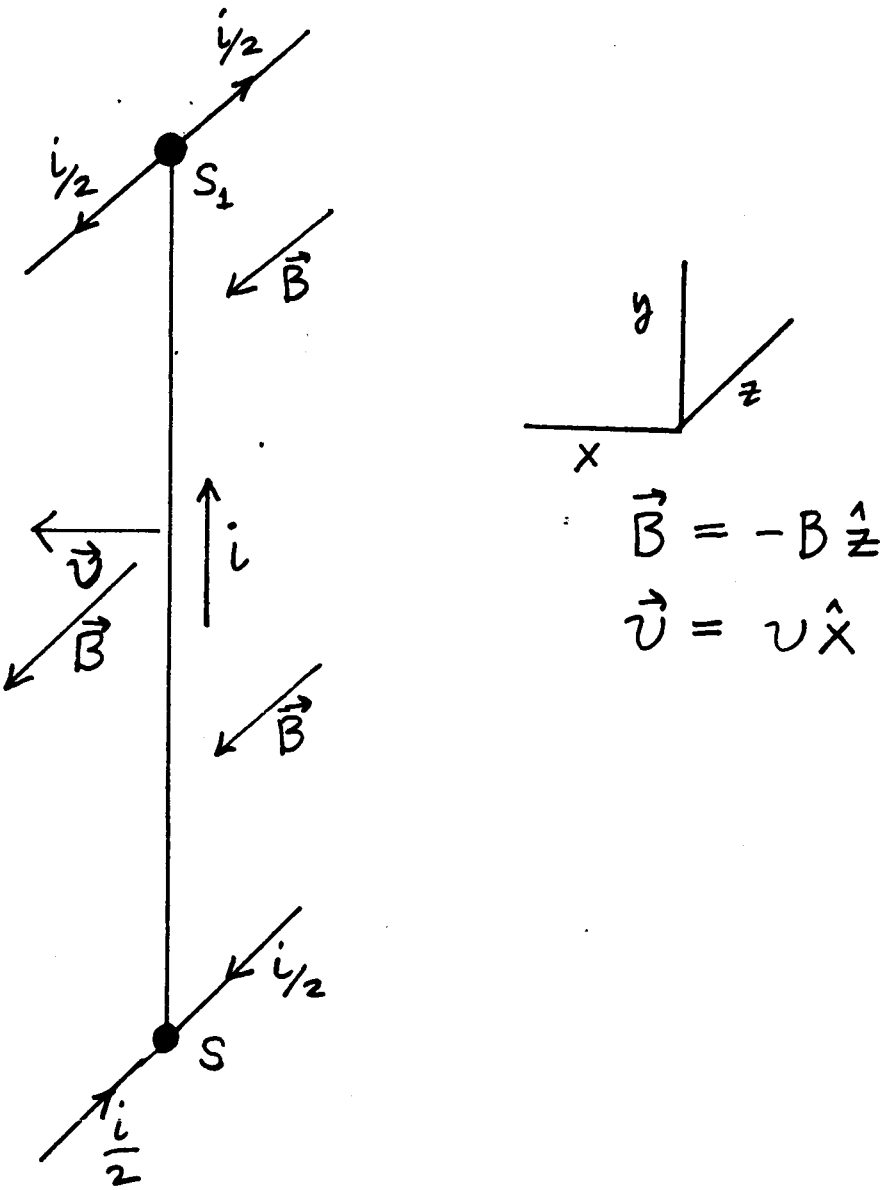

Figure 3.10 - System Configuration and Currents

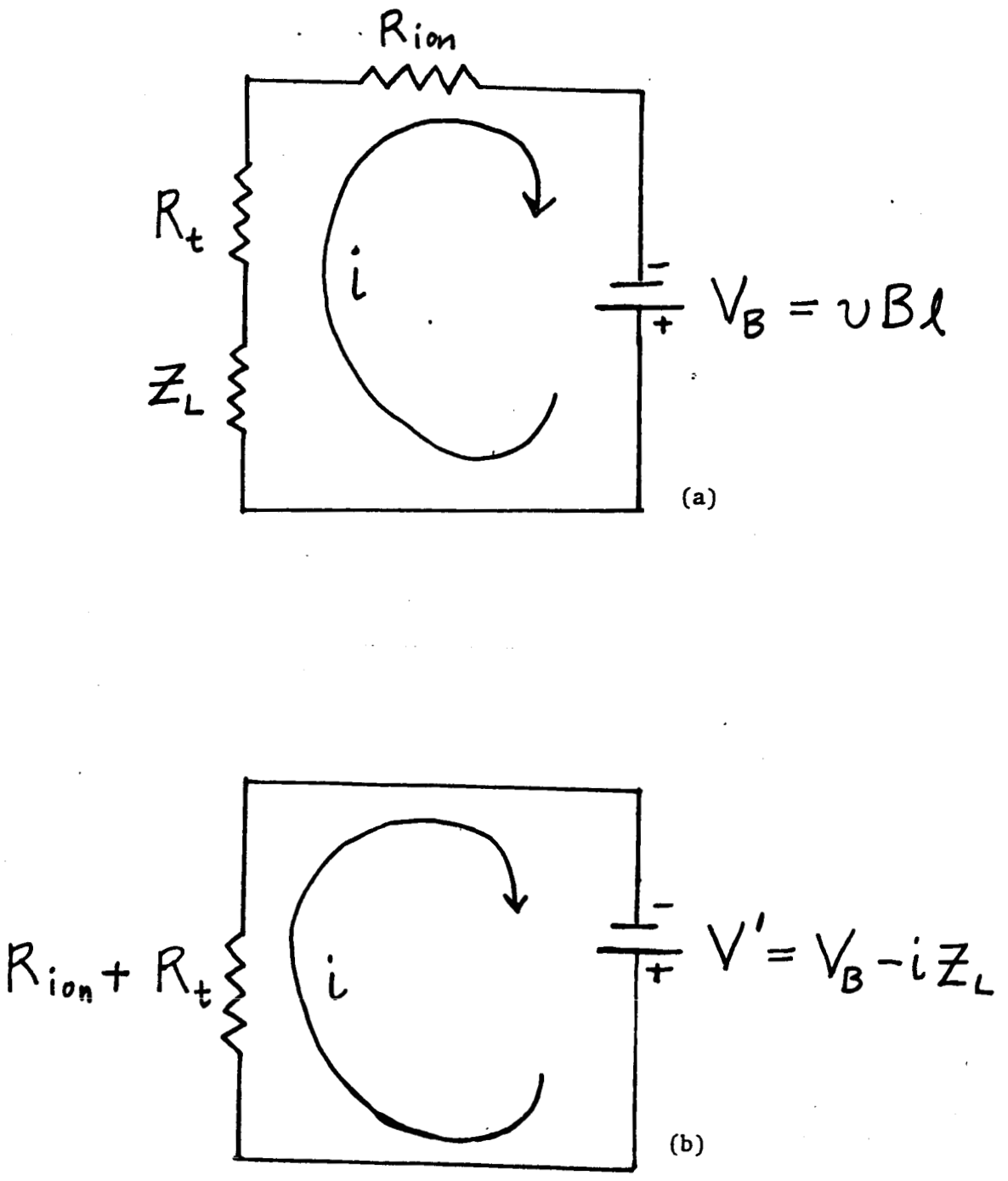

Figure 3.11 - Equivalent Circuits for Tether/Ionospheric "Natural" Current Mode.

where T is the period of the natural current phase.

This energy is available for a contribution to the reversed current mode operation.

Figure 3.12 illustrates the equivalent circuit for the reversed current mode. The motion induced emf V_B is still part of the circuit. There is now an applied voltage V_R which acts in the direction opposite to V_B and which drives the current in the opposite direction. We assume that this current is being driven through the same tether as in Figure 3.10 or that, if the current is driven through a tether connecting satellite S to a lower satellite S_2 (as in Figure 3.13), the second tether is identical to the first.

From equation (2) we see that the voltage V_R necessary to drive the current i in the reversed sense is given by:

$$V_R = V' + V_B = 2V_B - iZ_L \tag{4}$$

To sustain this reversed current for a period of time T equal to that of the natural current phase requires an energy $E_R = i\ V_R\ T$.

Combining equations (1) and (4) gives:

$$E_R = \left[2\ i^2\ \left(R_t + R_{ion}\right) + i^2\ Z_L\right]T \tag{5}$$

The last term in this expression is $i^2\ Z_L\ T$, which is just the energy stored of equation (3).

Thus the energy that must be supplied from an external power service, i.e. by solar cells or batteries is seen to be:

$$E_{ext} = 2i^2 \left(R_t + R_{ion}\right)T \tag{6}$$

the amount of energy dissipated in the two phases of operation.

The average external power required is given by:

$$\overline{P}_{ext} = i^2 \left(R_t + R_{ion}\right) \tag{7}$$

This result — its functional dependence on i, R_t, and R_{ion}, that is — is independent of Z_L. It depends on V_B and Z_L through equation (1). The average external power required in expression (7) represents the thermodynamic minimum. Dissipated energy represents an unrecoverable loss. There would be an additional amount of external power required to make up for conversion losses, which we have taken thus far to be zero.

We have driven the current in the reversed sense for a time T equal to the time of "natural" current flow. Thus, always assuming constant $\vec{B}$ and $\delta v \ll v$, where δv is the change in orbital velocity due to the electrodynamic drag, we have made up in the second (reversed current) part of our cycle for the orbital energy lost in the first part.

Having derived the simple basic equations (1) and (7), we are now in a position to examine their consequences for a partially self-powered radiating tethered satellite system.

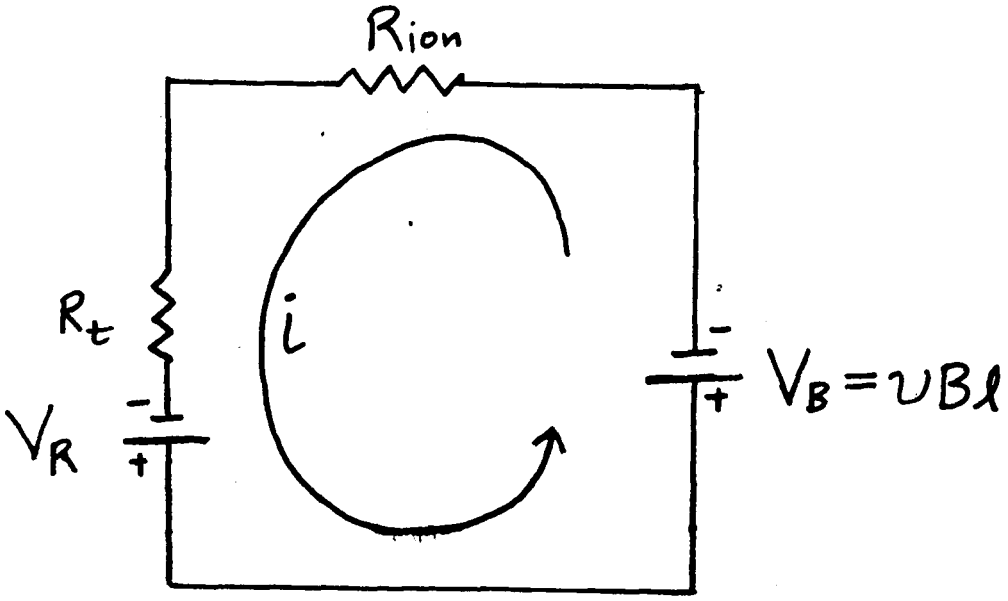

Figure 3.12 - Equivalent Circuit for Tether Reversed Current Mode

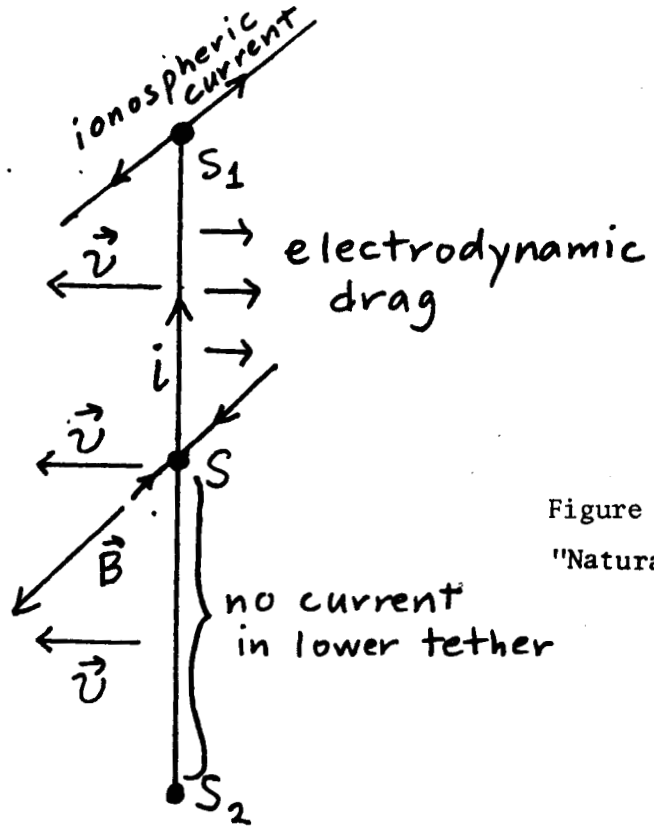

Figure 3.13(a)

"Natural" Current Phase

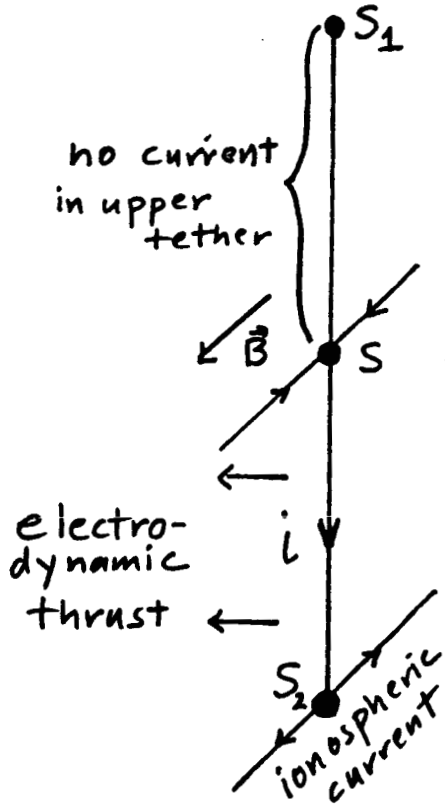

Figure 3.13(b)

"Reversed" Current Phase

Figure 3.13 - The Dual Tether System

It is immediately apparent from equation (7) that, whatever the current value, the required external power will be reduced if the tether resistance R_t is reduced. We can maintain a given current level while reducing R_t (maintaining the same tether length ℓ) by increasing Z_L, and hence increasing the energy stored in the first part of the cycle. This is seen from equation (1).

Thus there is a premium on using tethers with low resistance values per unit length. For now we are assuming that tether length is not one of the parameters we can vary. We assume it to be fixed by the desired radiation resistance and the wavelength of our radiation.

We also assume that there is a certain current level below which we do not want to go because of the radiated power levels we require. By making some estimates of what tether lengths and current values might be used in an actual system we are able to clearly demonstrate the feasibility and advantages of maintaining radiating tethered systems in orbit for long periods of time by the use of the "self-driven" reverse current thrust mode of operation. A number of cases are summarized in the tables that follow (Table 3.2.I through Table 3.2.IV). The required average external power is well within the reach of solar cells of reasonable size for a number of the parameter combinations.

Table 3.2-I

	ℓ (km)	R_t (Ω)	R_{ion} (Ω)	i (A)	V_B (kV)	Z_L (Ω)	i^2Z_L (kW)	P_{rad} (kw)	P_{ext} (kw)
(a)	20	650	50	5.0	3.5	0	0.0	1.25	17.5
(b)	20	303	10	11.2	3.5	0	0.0	1.25	39.1
(c)	20	690	10	5.0	3.5	0	0.0	0.25	17.5
(d)	20	311	2	11.2	3.5	0	0.0	0.25	39.1
(e)	20	698	2	5.0	3.5	0	0.0	0.05	17.5

Table 3.2-I. - 20 km tether, no energy storage in natural current phase.

Table 3.2-II

	ℓ (km)	R_t (Ω)	R_{ion} (Ω)	i (A)	V_B (V)	Z_L (Ω)	i^2Z_L (kW)	P_{rad} (kw)	P_{ext} (kw)
(a)	5	125	50	5.0	875	0	0.0	1.25	4.4
(b)	5	68	10	11.2	875	0	0.0	1.25	9.8
(c)	5	165	10	5.0	875	0	0.0	0.25	4.4
(d)	5	76	2	11.2	875	0	0.0	0.25	9.8
(e)	5	173	2	5.0	875	0	0.0	0.05	4.4

Table 3.2-II - 5 km tether, no energy storage in natural current phase.

Table 3.2-III

	ℓ (km)	R_t (Ω)	R_{ion} (Ω)	i (A)	V_B (kV)	Z_L (Ω)	i^2Z_L (kW)	P_{rad} (kw)	P_{ext} (kw)
(a)	20	100	50	5.0	3.5	550	13.8	1.25	3.75
(b)	20	100	10	11.2	3.5	203	25.4	1.25	13.75
(c)	20	100	10	5.0	3.5	590	14.8	0.25	2.75
(d)	20	100	2	11.2	3.5	211	26.4	0.25	12.75
(e)	20	100	2	5.0	3.5	598	15.0	0.05	2.55
(f)	20	303	10	5.0	3.5	387	9.7	0.25	7.83
(g)	20	650	50	2.2	3.5	865	4.3	0.25	3.50

Table 3.2-III - 20 km tether, energy stored in natural current phase; low resistance (R_t/ℓ = 5Ω/km) for columns (a) through (e).

Table 3.2-IV

	ℓ (km)	R_t (Ω)	R_{ion} (Ω)	i (A)	V_B (V)	Z_L (Ω)	i^2Z_L (kW)	P_{rad} (kw)	P_{ext} (kw)
(a)	5	25	50	5.0	875	100	2.5	1.25	1.88
(b)	5	25	10	11.2	875	43	5.4	1.25	4.38
(c)	5	25	10	5.0	875	140	3.5	0.25	0.88
(d)	5	25	2	11.2	875	51	6.4	0.25	3.38
(e)	5	25	2	5.0	875	148	3.7	0.05	0.68
(f)	5	68	10	5.0	875	97	2.4	0.25	1.96
(g)	5	125	50	2.2	875	216	1.1	0.25	0.88

Table 3.2-IV- 5 km tether, energy stored in natural current phase; low resistance (R_t/ℓ = 5Ω/km) for columns (a) through (e).

These Tables display for a number of system parameter combinations the on-board power requirements to operate an electrodynamic tethered system as ULF/ELF radiator. This important quantity - the on-board power required - is given in the last column of each table as $\overline{P}_{ext}$ the average external power, calculated from equation (6).

Concerning the values chosen for R_{ion} (which is also the radiation resistance), we have considered cases of R_{ion} = 2Ω, 10Ω, and 50Ω. R_{ion} may in fact vary considerably with the frequency of tether current oscillation. Barnett and Olbert (1986) obtained values ranging from less than 1Ω (ULF) to tens of thousands of ohms (for frequencies greater than the lower hybrid frequency $f_{LH} \approx$ 7kHz at 300 km). The values of radiation resistance we have chosen do lie within a range that is reasonable to consider for purposes of illustration and comparison. At the upper end (50Ω) the radiation resistance becomes comparable to or larger than the resistance of the tether in some of the cases considered.

Tables 3.2-I and 3.2-II are for tether lengths of 20 km and 5 km, respectively, in the case where none of the motion-generated power of the natural current phase of operation is utilized to drive the reverse current of the second phase.

Tables 3.2-III and 3.2-IV may be compared row by row with Tables 3.2-I and 3.2-II for rows (a) - (e) to show the effect of reducing tether resistance (per unit length) and at the same time maintaining constant current and radiated power values by utilizing some of the motion-induced electrical power (an amount $i^2 Z_L$) to provide a portion of the power necessary to run the system in the reversed current mode of operation, as described in the next section.

Furthermore, the two additional rows (f) and (g) of Tables 3.2-III and 3.2-IV demonstrate the effect of this kind of power utilization for cases where the tether resistance is maintained at a fixed value and the current and power radiated values necessarily drop. A comparison of rows (f) and (g) of Tables 3.2-III and 3.2-IV with rows (b) and (a) of Tables 3.2-I and 3.2-II demonstrates a general fact: for constant R_t and R_{ion}, the ratio of the radiated power to the average external power required $P_{rad}/\overline{P}_{ext}$ is a constant, independent of Z_L.

The results indicate an optimization process that consists of two parts, which are not necessarily independent of each other. The first step is to determine the minimum tether length compatible with wave transmission at the desired frequency and at sufficient power levels. Then, at this minimum length, utilize a tether with the lowest practical resistance value consistent with tether flexibility, mass constraints, etc., in conjunction with an electrical energy storage system and the reversed current mechanism.

3.4 Discussion Of The Effects On The Propagation Path Of High-Altitude Nuclear Debris Patches

There are several advantages in favor of the spaceborne location (as opposed to a location on the Earth surface) for the ULF/ELF transmitting facility of a strategic communications link. These are: (a) the minimization of the environmental impact (it was because of the opposition of the environmentalists to the ground-based location of the transmitter, that an operational strategic communications system has been never built); (b) the coverage of the entire surface of the Earth with high-illumination intensity, making it possible to reach corners of the globe that would be out of reach for a CONUS-based transmitting facility;

(c) the ability of the "Orbiting Cocoons" to hide in orbit, because of their small radar cross-section during their dormant phase, when the tether is still wound on the winch housed inside the satellites; etc.

However, there are also disadvantages, one of which is represented by the fact that the propagation paths in our case are required to cross the bottom boundary of the ionosphere in order to reach from orbital heights the receiving terminal on the Earth surface. The bottom of the ionosphere, at about 65 km height (the so-called D-layer of the ionosphere), is strongly affected in its electron content and in its e.m. wave absorption properties by high-altitude nuclear detonations, that cause the appearance of debris patches at that height. When the transmitting facility of the strategic communications link is located on the Earth surface, propagation to the receiving terminal takes place exclusively in the atmosphere. If there are debris patches in the D-layer, the propagation paths do not cross them, because now transmitter and receiver are on the same side of the patches. Hence, the disadvantage for our spaceborne scheme, on this score.

The study of the detailed interaction of e.m. waves in the ULF/ELF band with the debris patches above requires access to classified information, and is outside the charter of our Observatory. This is why in the SAO 1985 proposal that led to grant NAG8-551, we remarked that, should NASA be interested in such a study, the Agency should assign this task to another Contractor with access to the classified literature. What we could do, and we did, was to formulate preliminary conclusions on the effect on our propagation paths of high-altitude nuclear debris patches, based on information that is available in the unclassified, public-domain, technical literature. We do believe, however, that our conclusions would not be altered in their essence, if the classified literature would be brought to bear on this discussion.

Here are our conclusions for this study task. For a high-altitude detonation (meaning at an altitude of 65 km and higher), the locations of the beta and gamma ionization regions associated with the debris resulting from an explosion are shown in Figure 3.14 (Glasstone and Dolan, 1977). They cause increased ionization in the local D-region, while the beta particles travel also to the magneto-conjugate point and cause ionization there too. Two other sources of enhanced ionization are also active: Compton electrons and neutrons. However, the ionization levels produced by these two sources are lower than the ionization produced by the primary sources: delayed gamma rays and beta particles. Debris patches height, radius of the patches versus time, characteristic time of the changes, etc. are illustrated in Figure 3.15 for three yields: 10 Kton, 100 Kton and 1 Megaton. The Figure shows that the patches have a radius of about 1 Megameter (inclusive of expansion due to atmospheric winds), and they reach this size in a few hours after the detonation. Absorption for ULF/ELF propagation paths impinging on the patch is total. We conclude therefore that there will be a communications blackout of about 5 minutes every time that the tethered satellite overflies the patch. However, this does not mean that a receiver on the Earth surface located in the shadow of the patch will never receive the messages broadcasted by the tethered satellite. These messages are continually repeated and will be able of reaching such a receiver by guided propagation, along the surface of the Earth (see Figure 3.5 and Figure 3.7). This will occur when the tethered satellite, in its orbital motion, will overfly totally the debris patch and the e.m. waves that it radiates will now be able of leaking through to the Earth surface, and will propagate back, along the surface, to the locations that are directly underneath the absorbing patch, and that were unable of receiving the emissions from the tethered satellite via direct downcoming propagation.

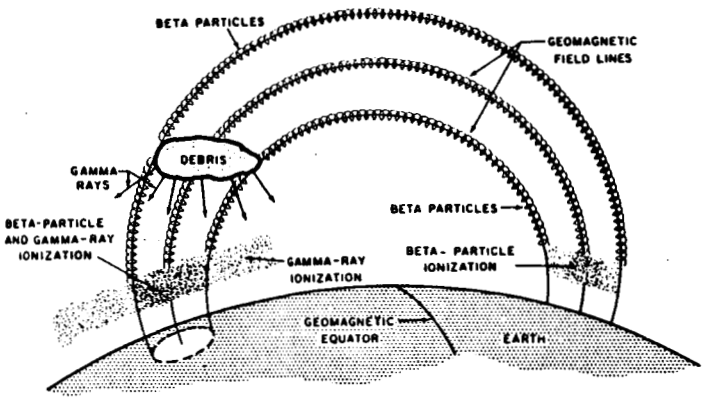

Figure 3.14 - Location of beta and gamma ionization regions when the debris from an explosion in the northern hemisphere is above 65 km altitude (Glasstone and Dolan, 1977).

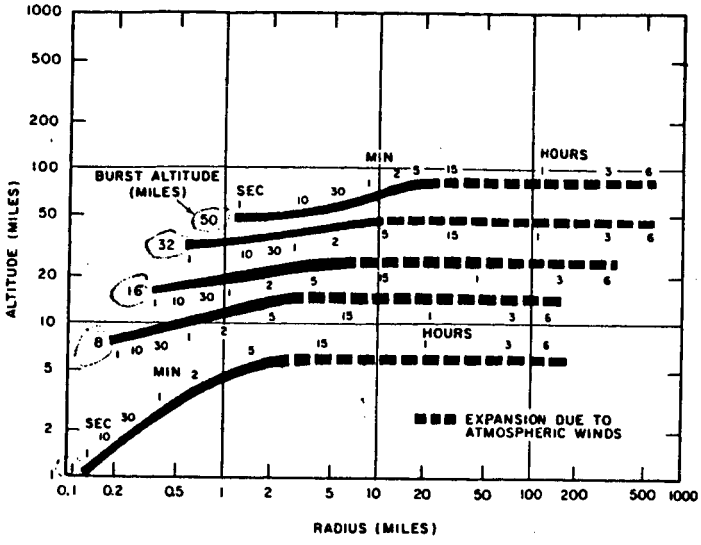

10-kiloton explosion

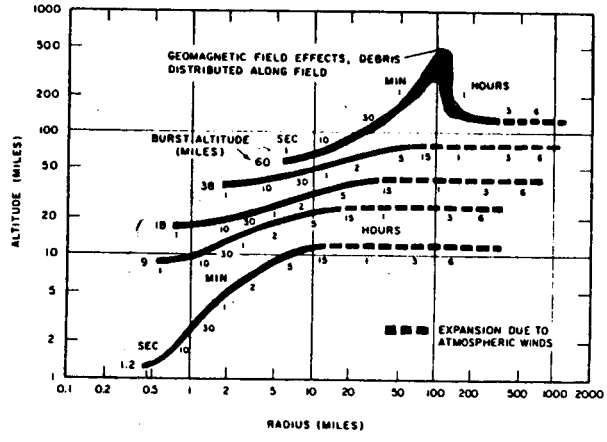

100-kiloton explosion

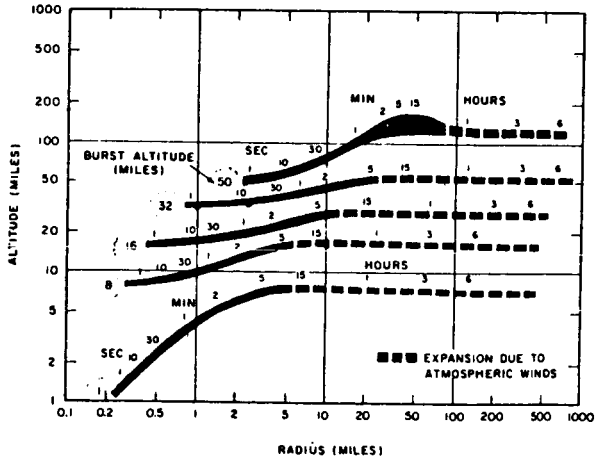

1-Megaton explosion

Figure 3.15 - Fireball/debris altitude and horizontal radius, for explosions at various heights of three different yields (Glasstone and Dolan, 1977).

3.5 The Proposed System Configuration

3.5.1 General -

Figure 3.16 provides a simplified block diagram of a possible system mechanization. It consists of a single tether that is used in the dual mode of generator and thruster (in order to generate, in time sequence, the first and second half of the radiated waveform shown in Figure 3.17 and in addition, in order to provide drag compensation). When the commutator in Figure 3.16 is in position "1", the electromotive force generated by the tether (now working as a high voltage DC generator) causes a current to flow in the system. The power that is generated goes partly into radiation (semiwaveform A of Figure 3.17), partly into ohmic losses, and in part is stored in rechargeable batteries, or equivalent on-board storage system. When the commutator is in position "2", a high-voltage on-board power supply feeds the tether, and causes a reverse flow of current in it. The power spent in this operation goes into radiation (semi-waveform B of Figure 3.16), into ohmic losses, and into doing work against the $\vec{v} \times \vec{B}$ force. An on-board primary power plant such as the array of solar cells of Figure 3.16 provides for the compensation of the ohmic losses and radiative losses incurred in generating both semiwaveforms A and B and for energy lost in the conversion processes. Under the circumstances, the loss of orbital height due to the electrodynamic drag associated with the generation of semiwaveform A is compensated by the thruster action of the tether that is associated with the generation of semiwaveform B. In the latter case, the tether must be fed with a voltage that is high enough, not only to cancel the induced electromotive force, but also to cause a current (of identical intensity to the one that flows by the $\vec{v} \times \vec{B} \cdot \vec{\ell}$ mechanism in generating semiwaveform A) to flow in the opposite direction.

Modulation can be achieved, for instance, by changing the time position of the negative-going zero crossing that separates semiwaveform *A* from semiwaveform *B*. In reception, the waveform can be differentiated, thus resulting in a negative-going pulse modulated in position. This reduces to a case of pulse-position-modulation (PPM). The relative-time reference is provided by the positive-going zero-crossing that immediately precedes (or that follows) the time modulated negative-going zero-crossing. The positive pulse obtained by differentiating the received waveform is the "sync" of the link. The radiated waveform's nominal frequency (carrier frequency) is kept constant, with adequate stability, by means of the commutator control of Figure 3.16. Modulation would arrive via a communication receiver, possibly operating at millimeter waves. The satellite before tether deployment, is 3-axis stabilized by an on-board platform, so that its base S1 (see Figure 3.16), where the receiver antenna is mounted, looks always toward the Earth. When the tether is deployed, gravity gradient stabilization could replace (or operate in association with) this 3-axis platform, and keep the satellite on the same basic orientation.

3.5.2 Possible Modulation Schemes -

In Section 3.5.1 we introduced a PPM (Pulse Position Modulation) approach as a suitable scheme for the modulation of the tether-generated e.m. waves. PPM is particularly simple to visualize, and is an effective conceptual example. However, the efficiency of the scheme, in terms of required SNR and bandwidth is rather poor. In fact, the approach is strongly susceptible to noise: the latter causes the wandering of the position-modulated pulse, that, we saw in the previous section, is obtained by differentiating (or by equivalent operation performed on) the downgoing transition between semi-waveform A and B of Figure 3.17.

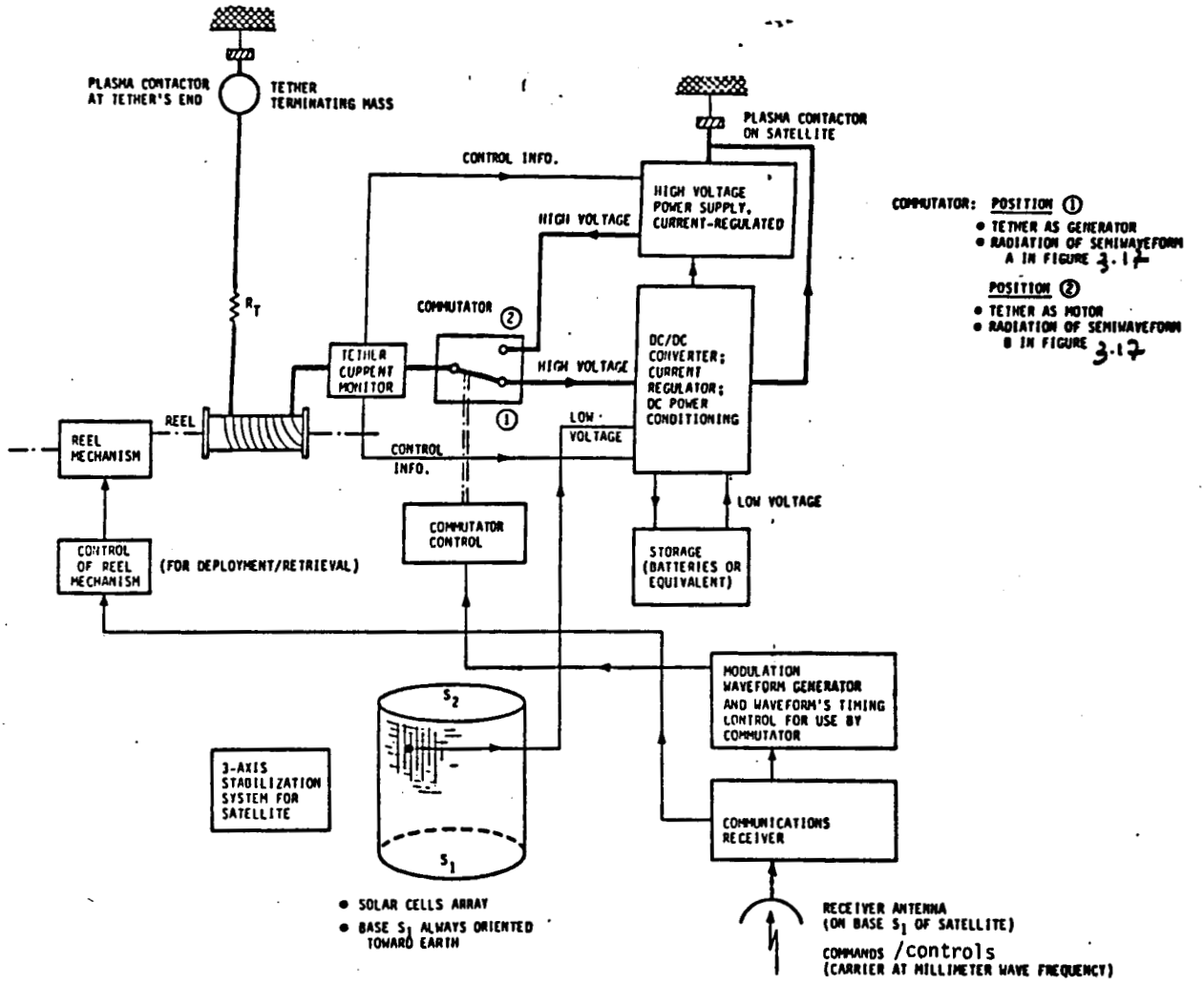

Figure 3.16 - Block diagram of ULF/ELF generator.

C-2

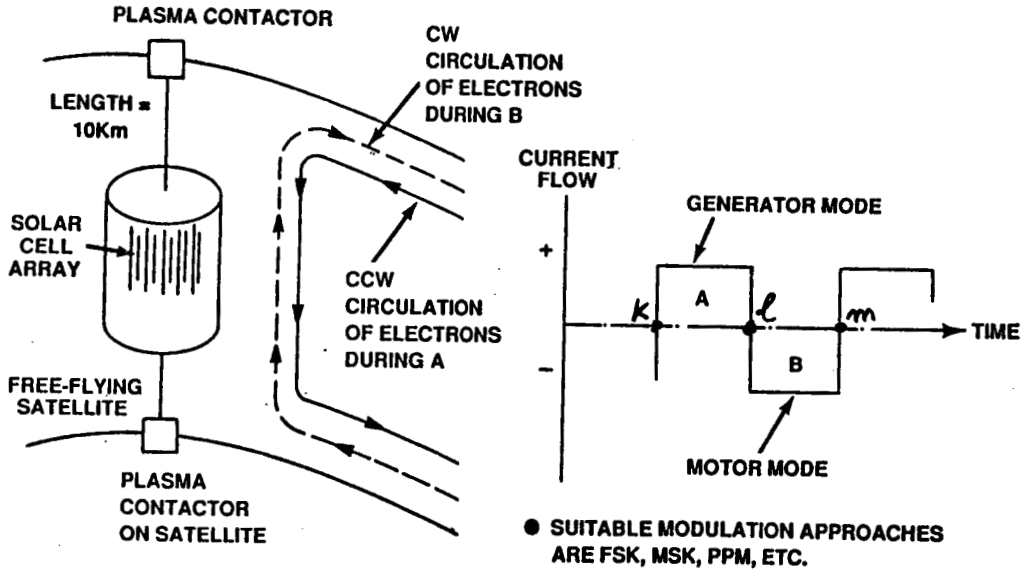

Figure 3.17 - Generation of the radiated carrier by sequentially using the tether in its generator mode and in its motor mode (thus providing drag compensation).

Let's continue the PPM example. If the frequency of the carrier is, for instance, 75 Hz, the period is 13.33 milliseconds. If there is no modulation, the downgoing transition between A and B is at a time 13.33/2 from the inception of waveform A. Suppose now that we have a binary transmission and that "1" (we can realistically assume that every baseband bit lasts 1 second) is represented by a shift of the transition line above of 3.33 milliseconds to the left, while a "0" is represented by the same transition of 3.33 milliseconds to the right. Of course, there will be 75 cycles of the carrier affected the same way for the "1" and equal number of cycles affected for the "0." This will allow integration, with improvement in SNR. In reception, we differentiate the downgoing transition between A and B, each cycle for 75 cycles. This corresponds to high-pass filtering and to the broadening of the required bandwidth. PPM had found extensive applications in the early day of telemetry for space probes and missiles. However, its use has substantially declined in the recent years.

Modulation schemes that are more suitable for our application are the FSK and the PSK approaches (the latter in its DPSK embodiment), where FSK = Frequency Shift Keying; PSK = Phase Shift Keying; DPSK = Differential Phase Shift Keying.

In FSK, we choose two frequencies, one to represent a "1" and the other a "0." For instance, if the nominal frequency of the link is 75 Hz, we could adopt 70 Hz for "1" and 80 Hz for a "0." In reception, a band-pass filter selects each one of the two tones (see Figure 3.18). The filter's output is undergoing square-law detection, then goes to an integrator.

The performance of the scheme depends upon the multipath structure and the doppler spread of the channel, quantities that have not been measured thus far

for our space-to-ground propagation paths at ULF/ELF (they must be measured at the earliest convenience). Severe conditions of multipath and doppler spread might require the use of some diversity in our space-to-ground link, such as transmitting for instance two simultaneous frequencies for "1" and two different ones for the "0." In reception (see Figure 3.19) the signal would be processed to yield a "1" or a "0," according to the energy content of the sum of f_1 and f_3, as compared to the content of the other pair f_2 and f_0. Calculations of achievable error rates, required SNR, required bandwidth can be performed with routine design formulas, as long as the multipath spread and the doppler spread of the channel are known.

In the PSK scheme, the frequency stays at the nominal value, say 75 Hz, but the e.m. wave phase is reversed (with respect to a reference) for the duration of 1 second (assumed duration of a bit), in order to transmit a "1" (for instance). For transmitting a "0," the phase is, on the contrary, kept again for 1 second, equal to the reference's. In reception, we need a reference, to decide whether the phase shift was 0 or π. As in the previous schemes, 75 cycles of the carrier are affected the same way by the modulation, thus providing the possibility of integration.

As embodiment of PSK that does not require the need for a coherent reference at the receiver is the Differentially Coherent PSK signalling scheme, also known as DPSK. We will describe this interesting scheme in some detail, based on the analysis of Shanmugan (1979).

In the DPSK scheme, the phase reference for demodulation is derived from the phase of the carrier during the preceding signalling interval, and the receiver decodes the digital information based on the differential phase. If the channel perturbations and other disturbances are slowly varying compared to the bit rate,

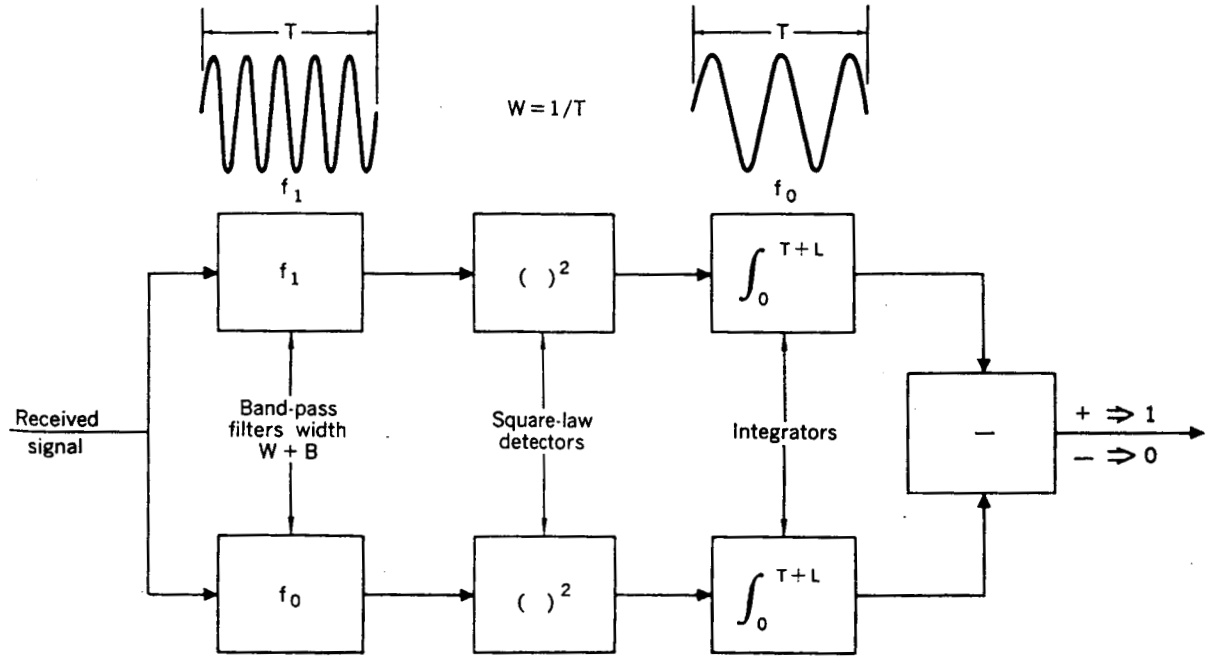

Figure 3.18 - Basic FSK signaling and detecting technique - A receiver for a binary signal.

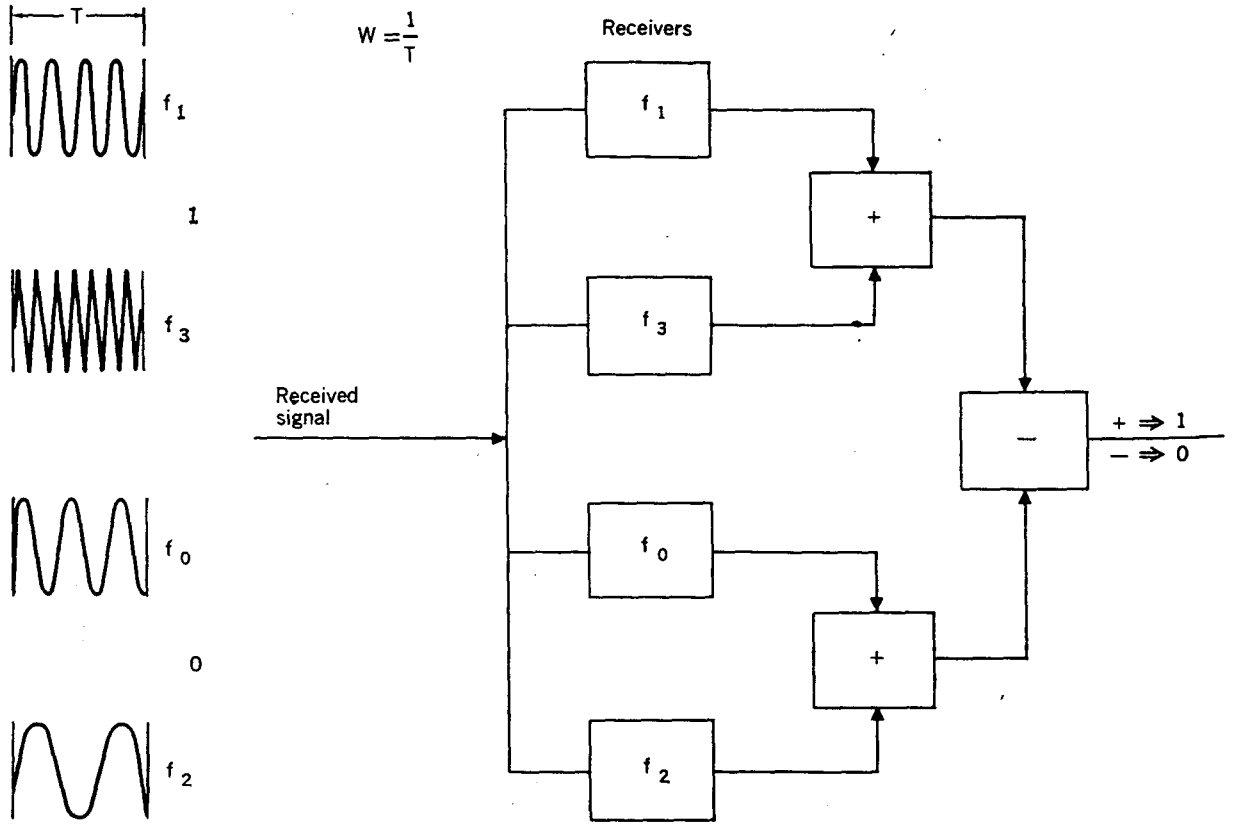

Figure 3.19 - Block diagram of a FSK receiver for the transmission of two simultaneous frequencies. Each pulse contains one half of the energy of the pulses in the previous figure.

then the phase of the RF pulses $s(t)$ and $s(t - T_b)$ are affected by the same manner, thus preserving the information contained in the phase difference. If the digital information had been differentially encoded in the carrier phase at the transmitter, the decoding at the receiver can be accomplished without a coherent local oscillator signal. The DPSK scheme may be thought of as the noncoherent version of the PSK scheme.

Block diagrams of a DPSK modulator and demodulator are shown in Figures 3.20(a) and 3.20(b), respectively. The differential encoding operation performed by the modulator is explained in Table 3-I. The encoding process starts with an arbitrary first bit, say 1, and thereafter the encoded bit stream d_k is generated by

$$d_k = d_{k-1} b_k \oplus \overline{d}_{k-1} \overline{b}_k$$

Table 3-I

Table 3-I Differential Encoding and Decoding

Input Sequence (b_k)		1	1	0	1	0	0	0	1	1
Encoded Sequence (d_k)	1[a]	1	1	0	0	1	0	1	1	1
Transmitted Phase	0	0	0	π	π	0	π	0	0	0
Phase Comparison Output		+	+	-	+	-	-	-	+	+
Output Bit Sequence		1	1	0	1	0	0	0	1	1

[a] Arbitrary Starting Reference Bit.

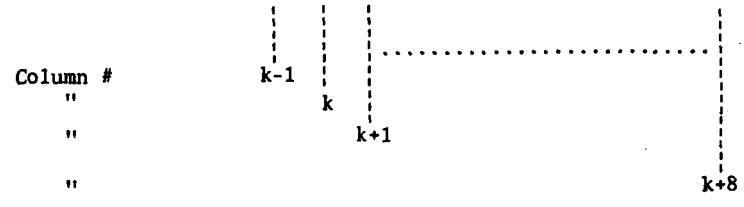

where $\oplus$ means modulo-2 sum and where $\overline{d}_{k-1}$ and $\overline{b}_k$ are the conjugate of d_{k-1} and b_k (in other words $\overline{d}_{k-1}$ is a 0 if d_{k-1} is a 1 and vice versa; the same applies to $\overline{b}_k$).

Let's see now how the processing (encoding and decoding) works:

- We start with an arbitrary starting reference bit. In Table 3-I, we call this d_{k-1} and we take it equal to 1 (just as an example). We have:

$$d_{k-1} = 1 \qquad , \ \overline{d}_{k-1} = 0$$

$$b_k = 1 \qquad , \ \overline{b}_k = 0$$

- We remind that a modulo-2 sum is performed by adding the addenda as in a regular (arithmetic) sum. However, we do not stop there; we continue the operation by dividing by 2 the sum normally obtained, and by taking (as the modulo-2 result) the remainder of the division. Therefore:

$$d_k = d_{k-1}b_k \oplus \overline{d}_{k-1}\overline{b}_k$$

$$= 1 \cdot 1 \oplus 0 \cdot 0 = 1$$

- We go ahead with the same rule and we get (see Table 3-1):

$$d_{k+1} = 1 \cdot 1 \oplus 0 \cdot 0 = 1$$

$$d_{k+2} = 1 \cdot 1 \oplus 0 \cdot 1 = 1$$

.
.
.
.

The differential sequence d_k then phase-shift keys a carrier with the phases 0 and π, as shown in Table 3-I.

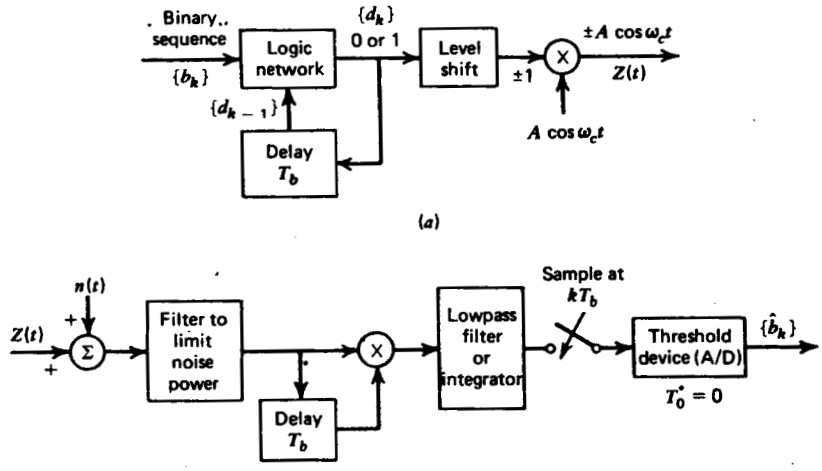

Figure 3.20 - (a) DPSK modulator; (b) DPSK demodulator (Shanmugan, 1979).

The DPSK receiver correlates the received signal plus noise with a delayed version (delay = 1 bit duration) of the signal plus noise. The output of the correlator is compared with zero and a decision is made in favor of 1 or 0 depending on whether the correlator output is + or -, respectively. We can easily verify that the receiver recovers the bit sequence $[b_k]$ correctly, in the absence of noise, by assuring ourselves that the receiver essentially checks to see if the phase angles of the received carrier during two successive bit intervals are the same or different. With an initial angle of 0 (for the reference bit), the receiver output is 1 at the end of the k th signaling interval if the carrier phase is the same during the $(k-1)st$ and the k th signaling intervals. If the phase angles are different, then the receiver output is 0. The last two rows in Table 3-I illustrate that phase comparison detection at the receiver works correctly.

Taking into account such aspects as the required SNR, the required bandwidth and the complexity in equipment implementation, our conclusion is that FSK represents the best approach at this point, for our link, not knowing too much as yet about the channel properties.

3.5.3 System Block Diagram And Satellite Mechanization -

We have worked out an example of system configuration that uses a simple electrodynamic tether suitable for a demonstration flight. Tether length has been assumed to be 10 km, and tether current 10 A. Therefore, the electric dipole moment will be 10^5 A.m. Although this configuration would not provide a SNR large enough to be of use in strategic communications, it would be adequate for a feasibility check in orbit of the ability of the electrodynamic tether to generate and radiate, in a self-powered, drag-compensated, mode of operation, e.m. waves at ULF and ELF.

Figure 3.21 provides a simplified block diagram of the system, while Figure 3.22 shows a possible mechanization of the satellite.

The system illustrated in these two Figures would provide a dipole moment substantially larger, of about 20 dB, with respect to the TSS-1 mission, expected to fly in the time frame 1990-1991.

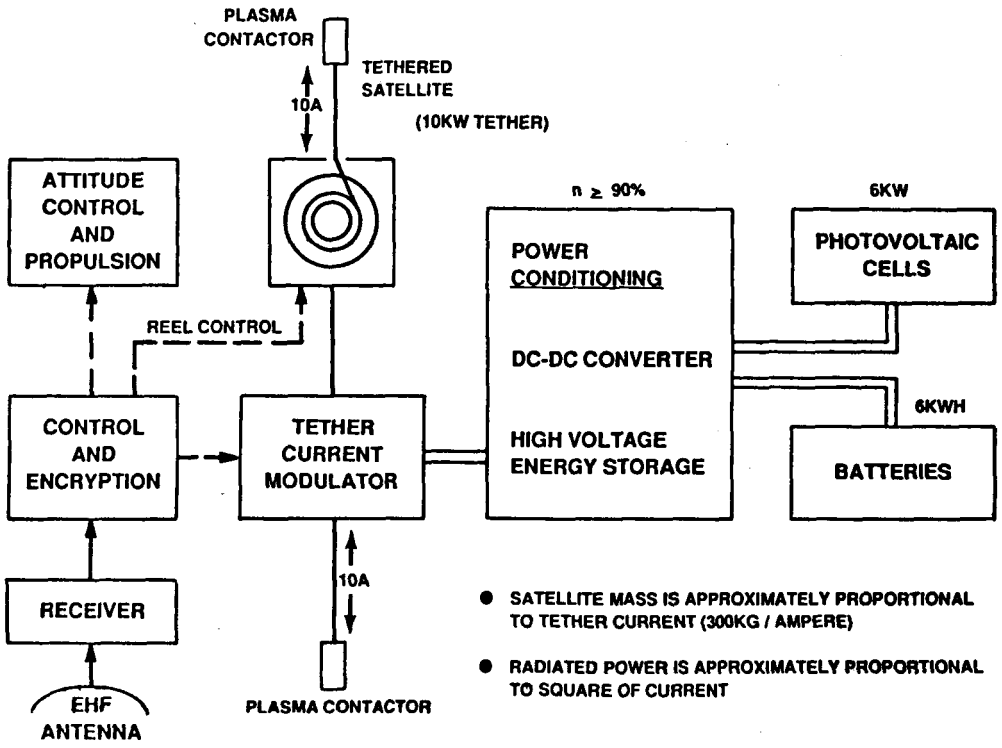

Figure 3.21 - Simplified block diagram of the spaceborne terminal (NASA/TRW).

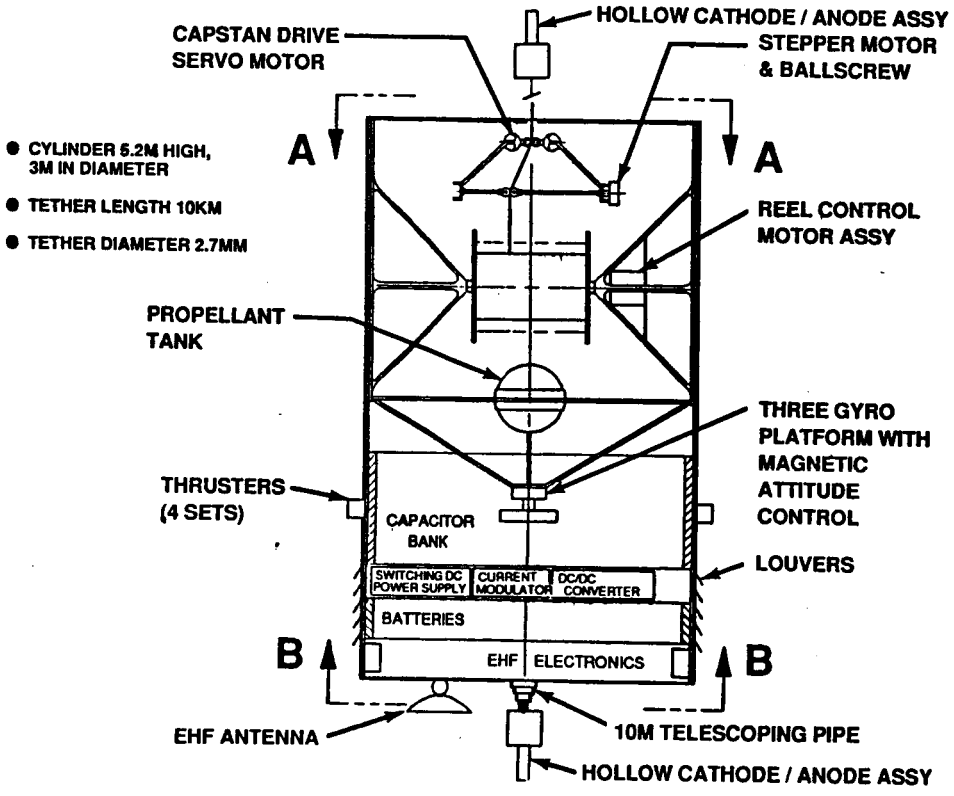

Figure 3.22 - A possible configuration of the orbiting cocoon, for a 10 km tether length (NASA/TRW).

3.5.4 First-Cut Breakdown Of Subsystems -

A first-cut breakdown of the various subsystems is as follows:

(A) Tether reel (with 20 km tether wound around it); tether reel mechanism; control of tether reel; tether current monitor.

Estimated total mass: 2,000 kg

Size of tether reel (with 20 km tether wound around it): a cylinder with 1 m length and 0.3 m diameter

Size of tether reel mechanism: a box 0.75m x 0.3m x 0.2m

Size of control of tether reel: a box 0.3m x 0.2m x 0.1m

Size of tether control monitor: 0.1m x 0.05m x 0.05m

(B) Commutator and Commutator Control

Estimated total mass: 25 kg

Size of commutator: a box 0.3m x 0.1m x 0.1m

Size of commutator control: a box 0.1m x 0.05m x 0.05m

(C) Three axis stabilization system (3-gyro platform and long-life magnetic attitude control, or equivalent)

Estimated total mass: 300 kg

Size of platform (for reference): a box 0.3m x 0.2m x 0.1m

Size of magnetic attitude control (coils, power supplies, etc.): two boxes, each with dimensions 0.1m x 0.1m x 0.5m

(D) High-voltage power supply

Estimated total mass: 100 kg

Size of power supply: a box 0.3m x 0.3m x 0.2m

(E) DC/DC converter; current regulator; DC power conditioning

Estimated total mass: 75 kg

Size: a single box 0.25m x 0.2m x 0.2m

(F) Storage batteries or equivalent

Total estimated mass: 560 kg

Size: a single box 0.2m x 0.1m x 0.1m

(G) Modulation waveform generator; waveform timing control

Total estimated mass: 8 kg

Size: a single box 0.2m x 0.1m x 0.1m

(H) EHF communications receiver

Estimated total mass: 2 kg

Size: a box 0.2m x 0.1m x 0.05m

(I) EHF communications antenna

Estimated total mass: 5 kg

Size: a dish with 1 m diameter

(J) Plasma contactors (with accessories)

Two plasma contactors, each with a 10 kg mass (20 kg total)

Size: two cylinders, 0.5m long, 0.2m diameter

(K) Satellite structure (a cylinder with 5.2m height and 3m diameter, with reinforcement beams and other support structures): 500 kg

Grand Total Masses: 3,600 kg

3.6 References For Section 3

1. Arnold, D.A., 1985, Efficiency of a Self-Powered Spaceborne ELF/ULF Radiator, SAO Technical Note TP85-007, November.

2. Barrodale I., and R.E. Erickson, 1980(a), Geophysics, Vol. 45, #3, pp. 420-432, March.

3. Barrodale I. and R.E. Erickson, 1980(b), Geophysics, Vol. 45, #3, pp. 433-446, March.

4. Glasstone S. and P.J. Dolan, 1977, The effects of nuclear weapons, 3rd Edition, a Book published by DOD and DOE, Washington, D.C.

5. Grossi M.D., 1981, New Technology for ELF radiators: A review of Airborne, Rocket-borne, and Spaceborne ELF Antennas, Proceedings of NATO-AGARD 29th Symposium on E.M. Wave Propagation Panel, Brussels, Belgium, September 21-25, pp. 41.1 to 41.32.

6. Grossi M.D., 1984, Spaceborne Long Vertical Wire as a Self-Powered ULF/ELF Radiator, IEEE Journal of Oceanic Engineering, Vol. OE-9, No. 3, pp. 211-213, July.

7. Pappert R.A., 1973, Excitation of the Earth-ionosphere Waveguide by Point Dipoles at Satellite Heights, Radio Science, 8, No. 6, pp. 535-545.

8. Shanmugan K.S., 1979, Digital and Analog Communications Systems, Publisher: John Wiley & Sons, New York, NY.

4.0 CONCLUSIONS AND RECOMMENDATIONS

The investigation of the self-powered, drag-compensated tethered satellite as an orbiting transmitter at ULF/ELF is in its initial phase. There are still several fundamental issues that must be studied thoroughly (and experimented with) before a system can be configured in engineering detail, and on this basis, a rigorous assessment of feasibility and practicality can be formulated. There is no question, however, that from our initial study effort the potential clearly emerges of a novel option for ULF/ELF communications characterized by the avoidance of the potential environmental threat posed by traditional ELF ground-based placements, and that could therefore gain that societal acceptability that has eluded thus far the conventional sitings.

Of fundamental importance in establishing feasibility is conducting experiments with an orbiting system that is as close to the operational configuration as possible. To this end, it appears advisable to consider the possibility of performing orbital tests with a prototype ULF/ELF tethered satellite launched by a rocket. A refurbished Titan II rocket could, in fact, place in a 1000 km orbit a 2000 kg prototype of a simplified "orbiting cocoon" with a launch that could be scheduled for a date 4 to 5 years from today, thus adding no extra delay to the time that is required anyhow to design and construct the prototype itself.

Concerning the analytical effort, we recommend that the following tasks be performed, in a follow-on contract:

Task #1 Formulate comprehensive theory of e.m. wave generation by an electrodynamic tethered satellite system operating in a motion-induced mode.

(A) Account for discrepancies in previous analyses.

(B) Resolve question of high radiation impedances in lower hybrid band of Barnett and Olbert (1986).

(C) Obtain expressions for wave impedances as a function of system and plasma parameters.

Task #2 Perform an analysis of the transmission of ULF/ELF wave packets through the lower ionosphere.

(A) Use a model for the ionosphere that takes into account seasonal, diurnal, latitudinal, and solar activity variations in collision frequencies, electrical conductivities, etc.

(B) Consider waves with arbitrary angle with respect to the horizontal plane.

(C) Investigate possibility of surface waves at the lower boundary of the ionosphere.

(D) Estimate signal intensity on earth surface and earth ionosphere waveguide attenuation.

Task #3 Apply results of Task #2 above to alternating polarity Alfvén wings pulses and make determination of their suitability as signal carriers.

Task #4 Based on results of the above tasks, provide input into system design — i.e. determine optimal tether lengths, orbital parameters, and modulation frequencies (from transmission standpoint).